CHAPTER 3

BALANCING OF RIGID AND FLEXIBLE ROTORS

Dr. Edgar J. Gunter
Professor of Mechanical and Aerospace Engineering
University of Virginia

Charles Jackson, P.E.
Turbomachinery Consultant

3.1 BACKGROUND AND INTRODUCTION TO BALANCING

3.1.1 Introduction

Rotor balancing is a fundamental requirement for the smooth operation of turbomachinery. Ideally, in the operation of all rotating machinery, the inertia axis of the rotor lies along the rotor spin axis. In actuality, this does not occur, and centrifugal forces and moments are generated which can result in high forces transmitted to the bearings and the supporting structure. Excessive rotor unbalance may lead to large amplitudes of motion or even failure of the shaft, bearings, and the foundation. Unbalance and shaft misalignment are recognized as two of the major factors that can lead to machinery malfunction and even catastrophic failure.

The unbalance in a machine may result from its initial manufacturing process or may occur as a result of various operating factors such as machine erosion, thermal effects, and unbalance buildup of process material on impellers and surfaces of the rotor. A rotor will experience some residual unbalance during manufacturing because of machine tolerances and material inhomogeneity. Multistage turborotors such as compressors, pumps, and turbines are susceptible to unbalance due to the assembly of multiple components. In the initial manufacturing of most rotors ranging from simple motors to elaborate pumps, compressors, and aircraft engines, the manufacturers generally employ elaborate procedures to ensure the initial balance of their machinery. The balancing may involve individual balancing of all the components and a final balance of the assembly. These balancing procedures usually involve commercial balancing machines based on either the soft hearing or the hard bearing support concept. These rotors are balanced in two planes to extremely high accuracies. For very flexible rotors, the manufacturer may even employ a high-speed spin pit facility to apply final trim balance.

Once the rotor is placed in service, however, unbalance may occur in the system due to any number of situations. Table 3.1 by Rieger (1986) shows

TABLE 3.1 Possible Causes and Signs of Rotor Unbalance (Rieger, 1986)

Cause of unbalance	Observable signs*
Disk or component eccentric on shaft	Detectable runout on slow rotation (center of gravity runs to bottom on knife-edges)
Dimensional inaccuracies	Measurable lack of symmetry
Eccentric machining or forming inaccuracies	Detectable runout
Oblique-angled component	Detectable angular runout; measured with dial gauge on knife-edges
Bent shaft; distorted assembly; stress relaxation with time	Detectable runout on slow rotation, often heavy vibration during rotation
Section of blade or vane broken off	Visually observable; bearing vibration during operation; possible process pulsations
Eccentric accumulation of process dirt on blade	Bearing vibration
Differential thermal expansion	Shaft bends and throws out center of gravity; source of heavy vibration
Nonhomogeneous component structure; subsurface voids in casting	Rotor machined concentric, bearing vibration during operation; center of gravity runs to bottom on knife-edges
Nonuniform process erosion	Bearing vibration
Loose bolt or component slip	Vibration reappears after balancing because of component angular movement; possible vibration magnitude and phase changes
Trapped fluid inside rotor, possible condensing or vaporizing with process cycle	Vibration reappears after balancing; apparent angular movement of center of gravity occurs; possible vibration magnitude and phase changes
Ball-bearing wear	Bearing vibration; eccentric orbit with possible multi-loops; frequency of vibration is 1, 2, or more per revolution

* Unless otherwise indicated, the frequency of vibration is once per revolution.

3.2

possible causes and signs of rotor unbalance. After a rotor is placed in service, the procedure for correction balance may be considerably different from the initial process employed by the manufacturer. It may be very expensive and time-consuming to remove the rotor to return to the manufacturer for reworking and balancing.

In many cases, it is necessary to apply an in situ or field balance on the machine in place. The object of the field balancing is to add correction weights in one or more axial planes along the rotor to maintain permissible levels of vibration. Some of these various methods of field balancing are discussed in detail in later sections.

The subject of balancing has been of interest to users of rotating machinery for over 100 years. The literature on the field is extensive, and thousands of references concerning rigid and flexible rotor balancing have been written as well as balancing standards developed by various organizations. Rieger's (1986) authoritative work will be of interest to those who wish to further study the theory and practice of balancing and standards in extensive detail.

3.1.2 Classification of Rotors

The International Standards Organization (ISO) (1973) has issued documentation on rotor classification and balance quality of rotating rigid bodies which are also discussed by Rieger (1986).

Rotors may be classified as either rigid or flexible systems according to their dynamic behavior at operating speeds. The classification of a rotor may be readily determined by performing a critical speed analysis on the system. If the strain or potential energy in the bearings is over 80 percent of the system's total strain energy, then the rotor may be generally classified as rigid. A rigid-body rotor is one which may be balanced in two arbitrary planes. The rotor will appear to maintain balance throughout its operating speed range.

On the other hand, if the strain energy of the shaft begins to exceed 20 percent of the system strain energy and the rotor is operating through one or more critical speeds, then it may be considered a flexible or quasi-flexible rotor. Under these circumstances, a two-plane rigid-body balance may not be adequate, and additional trim weights may have to be placed along the shaft to minimize the vibration amplitude at speed.

The ISO has classified rotors to describe the type and quality of balance needed for each particular instance. Table 3.2 presents the ISO classification of rotors as presented by Rieger (1986). Five basic classifications are presented by the ISO:

Class 1: Rigid rotors: These rotors may be balanced in any two arbitrary axial planes and will remain in balance throughout the operating speed range.

Class 2: Quasi-flexible rotors: These rotors are not perfectly rigid but may be adequately balanced in a low-speed balancing machine and will maintain smooth operation throughout the speed range.

Class 3: Flexible rotors: These rotors cannot be balanced in a low-speed balancing machine and require one or more high-speed trim plane corrections.

Class 4: Flexible-attachment rotors: These rotors can be categorized as class 1, class 2, or class 3 rotors but have components within themselves or flexibly attached.

Class 5: Single-speed flexible rotors: These rotors could be classified as class 3 flexible rotors but are balanced for operation at one speed only.

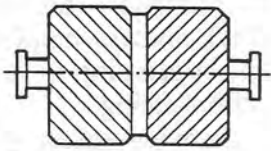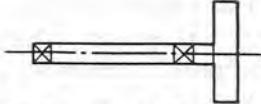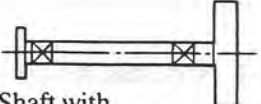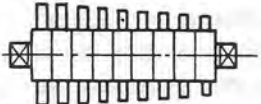**TABLE 3.2** ISO Classification of Rotors (ISO, 1973)
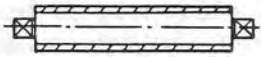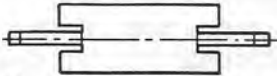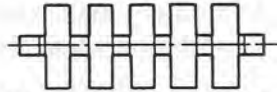
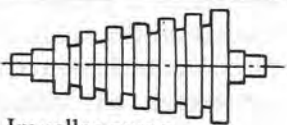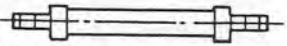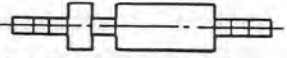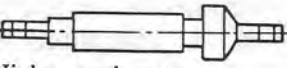| Class	Description	Example
1	Rigid rotor. Unbalance can be corrected in any two (arbitrarily selected) planes, and after that correction, unbalance does not significantly change at any speed up to maximum service speed.	(a) Gear wheel
2	Quasi-flexible rotors: rotors that cannot be considered rigid but can be balanced in a low-speed balancing machine	
2A*	A rotor with a single transverse plane of unbalance (e.g., single mass on a light shaft whose unbalance can be neglected)	(b) Shaft with grinding wheel
2B*	A rotor with two axial planes of unbalance (e.g., two masses on a light shaft whose unbalance can be neglected)	(c) Shaft with grinding wheel and pulley
2C*	A rotor with more than two transverse planes of unbalance	(d) Jet-engine compressor rotor
2D*	A rotor with uniformly distributed unbalance	(e) Printing-press roller
2E*	A rotor consisting of a rigid mass of significant axial length supported by a flexible shaft whose unbalance can be neglected	(f) Computer memory drum
2F†	A symmetric rotor, with two end correction planes, whose maximum speed does not significantly approach second critical speed, whose service speed range does not contain first critical speed, and with a controlled initial unbalance	(g) Five-stage centrifugal pump
2G†	A symmetric rotor with two end correction planes and a central correction plane whose maximum speed does not significantly approach second critical speed and with a controlled initial unbalance	(h) Multistage pump impeller

TABLE 3.2 (*Continued.*)

Class	Description	Example
2H†	An asymmetric rotor with controlled initial unbalance treated in a similar manner as class 2F rotors	(i) Impeller pump. Steam turbine rotor
3	Flexible rotors: rotors that cannot be balanced in a low-speed balancing machine and require high-speed balancing	(j) Generator rotor
4	Special flexible rotors: rotors that could fall into classes 1, 2, or 3 but have in addition one or more components that are themselves flexible or are flexibly attached	(k) Rotor with centrifugal switch
5	Single-speed flexible rotors: rotors that could fall into class 3 but for some reason (e.g., economy) are balanced only for a single service speed	(l) High-speed motor

* Rotors where the axial distribution of unbalance is known.
† Rotors where the axial distribution of unbalance is not known.

Single- and two-plane constant-speed balancing is usually adequate for class 1 and class 2 rotors. For class 3 and 4 flexible rotors, a least-squared-error influence coefficient or combined modal technique is preferred.

3.1.3 Types of Balancing

Balancing of rotating machinery may be generally classified in two broad areas. The first general area is balancing in the factory done on either hard or soft bearing balancing machines. This procedure is done at the manufacturer, and components may be individually balanced as well as the final assembly balanced as a rigid rotor. If the components are individually balanced before final assembly as well as at final assembly, then even extremely long flexible rotors may operate very successfully without further adjustments in the field. For certain classes of rotors such as generators in particular, it may be necessary to further balance the rotor in a spin pit facility. This is usually only done with class 3 rotors that must operate through a number of critical speeds. This balancing procedure is very expensive and time-consuming. The facilities available to do this type of balancing are very limited.

The second broad area of balancing is field or in situ balancing in which the rotor is balanced in place. In field balancing, the turborotor is balanced in its own bearings, and suitable instrumentation is placed on the shaft, bearing housing, or foundation to monitor motion. We now give a brief summary of the type of field balancing procedures that may be employed.

Single-Plane Balancing by the Influence Coefficient Method

The single-plane single-speed influence coefficient method of balancing is the simplest of all procedures. Phase-angle conventions are different between displacement probe measurements and phase angles obtained directly with strobe lights. Also some balancing instruments will have different conventions as to the initiation of phase measurement. In this method, a trial or calibration weight is placed on the shaft. The new vibration response of the rotor is recorded after the placement of the trial weight. The change in vibration divided by the trial weight represents an influence coefficient. The influence coefficient represents the response of the rotor due to the placement of a unit trial weight at a particular speed. It is important to realize that this influence coefficient is a vector quantity which represents an amplitude and a phase angle. The phase angle represents the relative phase relationship between the forcing function and the vibration measurement.

In field balancing by the influence coefficient method, it is imperative that one fully understand the phase measurements employed. The phase measurements may be made with direct-reading noncontact or displacement probes, velocity pickups, or accelerometers. Phase may be determined by an electronic key phasor or by means of a strobe light to measure the phase angle on the shaft. One should be fully acquainted with the phase measurement procedure to be employed before attempting single- or multiplane balancing.

In single-plane balancing by the influence coefficient method, the system is assumed to be linear and a single correction weight is placed on the shaft based on the computed influence coefficient. This procedure is referred to as *trim balancing* and is the method generally used in 90 percent of the balancing situations encountered in the field. The application of the single-plane balance correction may theoretically reduce the rotor amplitude to zero at that particular speed. The major problem with the single-plane single-speed influence coefficient method of balancing is that even though the rotor amplitude may be reduced to small vibrations at that particular location and speed, other points along the rotor may exhibit higher vibrations. At other speeds, the rotor may appear not be in balance.

The advantage of the single-plane method is that it may be performed rapidly in the field, and the influence coefficient may be calculated by a graphical procedure. Once the influence coefficient is computed for a particular rotor, the machine may be rebalanced without the necessity of adding a trial weight. This method of balancing is often referred to as the "one-shot" method of balancing and is based on a predetermined value of the influence coefficient.

Two-Plane Balancing by the Influence Coefficient Method

There are many rotors in which a single phase of unbalance will not suffice. The application of a balance correction at one plane may cause an excessive amount of vibration at another location. Under these circumstances, a simultaneous two-plane influence coefficient balancing procedure must be employed.

The father of modern field balancing is Thearle (1934), who presented the general two-plane influence coefficient balancing procedure in 1934. The procedure developed by Thearle was a semigraphical method to determine the shaft influence coefficients and the two-plane balance corrections. This procedure is very popular and is still currently used by industry. The procedure is very simple to program on a hand calculator.

In the two-plane balancing procedure, a trial weight is placed on the first or near plane, and the responses at the near and far planes are recorded. From these

measurements, two influence coefficients are computed. Next the weight is removed and placed at the second or far plane. The procedure is repeated to generate two more influence coefficients. This then forms a 2×2 matrix of complex influence coefficients which must be inverted to solve for the balancing. The 2×2 matrix of complex influence coefficients is equivalent to a 4×4 matrix of real numbers. Thus, two-plane balancing is equivalent to inverting a 4×4 matrix in order to determine four quantities which represent the respective rotor balancing magnitudes and relative phase-angle locations. This method is tedious to compute by hand, but fairly simple to perform on a calculator or desktop computer.

Single-Plane Balancing Using Static and Dynamic Components

This method is a variation of the single-plane influence coefficient procedure, except that vibration measurements are recorded at both ends of the shaft. The two vibration recordings are vectorially added and subtracted to determine the static and/or dynamic components. If the average static component appears to be highest, then either one or two weights are placed on the rotor in phase. If the dynamic or out-of-phase components of vibration appear to be highest, then two weights are placed 180° out of phase. This method is, in essence, a simplified modal procedure using the influence coefficient method.

Single-Plane Balancing by the Influence Coefficient Method Using Linear Regression

In the single-plane influence coefficient balancing method at one speed, it is possible to overbalance the rotor at the one speed and have extremely high vibrations at other speeds. The linear regression method of balancing is the simplest of the least-squared error methods of rotor balancing. Instead of measuring the rotor response at one speed, the vibration characteristics are measured over a speed range. The linear regression procedure produces a balancing magnitude which will not cause a large excitation at the other speeds. Balancing magnitudes computed by this procedure are always smaller than the magnitude computed from the single-plane influence coefficient method. This procedure ensures that one does not overcorrect by the application of too large a balance weight. This method is useful for balancing rotors with shaft bows and large initial runouts.

Generalized Influence Coefficient Method Using Pseudoinversion

The generalized influence coefficient method of balancing using two or more planes and multiple speed measurements is referred to as the *generalized influence coefficient method*. This method is also referred to as the *pseudoinverse method* or *least-squared-error method* of balancing. Unlike the two-plane method which is referred to as the *exact-speed point method* of balancing, more speed measurements may be used than balancing planes. This method leads to a best fit of the balancing data and is the preferred method for balancing large turbine-generators. The generalized least-squared-error method of balancing was initially presented by Goodman (1964) and has been improved upon by Lund and Tonnesen (1972), Badgley (1974), Thomson (1965), and Palazzola and Gunter (1977). The advantage of the generalized least-squared-error method of balancing is that it requires no prior rotordynamic knowledge of the system. It has been successfully used in multiplane balancing of turbine-generators through five critical speeds. Several variations of this procedure have been developed such as

the weighted least-squared-error method which places emphasis on a weighting function on particular vibrations to minimize or ignore.

If the balance planes are improperly chosen, then it is possible that the least-squared-error method will generate extremely large balance magnitudes in adjacent planes, 180° out of phase, which are impossible to incorporate into the rotor. The least-squared-error method cannot limit the magnitude of balance weights predicted for a particular plane.

Multiplane Balancing Using Linear Programming Techniques

Multiplane balancing procedure using linear programming theory proceeds in a fashion similar to the least-squared-error method of balancing in obtaining the influence coefficients; however, in linear programming, a constraint or upward bound may be placed on the magnitude of the computed balancing weights at a particular station. This method was reported on by Little (1971), and a practical linear programming approach has been developed for the microcomputer by Foiles and Gunter (1982). In most well-behaved systems, however, the results from linear programming and the generalized least-squared-error balance theory are very similar.

Modal Balancing

Flexible rotors operating through multiple critical speeds such as generators are best balanced by a modal method. In the modal method, the critical speed mode shapes of the rotor must be known from either theoretical or experimental measurements. The weights placed on the rotor are proportional to the rotor mode shape. Each modal distribution is used to individually balance one mode at a time. The object of modal balancing is to balance rotors with high amplification factors without upsetting the balance at other modes. The modal balance corrections to apply on a rotor are best computed by using the influence coefficient method to measure the rotor response and predict the modal influence balancing coefficients. M. Darlow (1989) has presented considerable material on the combined modal and influence coefficient method referred to as the *unified method of rotor balancing*. The accuracy of the method depended on the knowledge of the rotor mode shapes, which may become quite complex for modes higher than the second critical speed. This method has been applied with great success to generators and long, flexible centrifuges.

Three-Trial-Weight Method of Balancing

There are many instances in which it is not possible to obtain an accurate phase measurement. Blake (1967) pioneered a method referred to as the *three-trial-weight or four-run method*. By applying a trial weight at three different locations, a locus of balancing points may be generated to determine the magnitude of the unbalance and the balance location. This method has been very successfully applied to fans in which the speed is unsteady or beating is encountered. It is extremely accurate and compensates for nonlinearities. This method of computation is graphical and does not require the use of a computer to perform the calculations.

Multiplane Balancing without Phase

The three-trial-weight method has been extended to balance flexible rotors through multiple critical speeds by Foiles and Gunter (1982). In this extension, a modal distribution of weights is placed on the rotor. The amplitude of the rotor is measured at the critical speed by using a fast Fourier transform (FFT) analyzer or

using the peak hold data acquisition system to record the maximum amplitude at a particular critical speed. Each mode then may be separately balanced without exciting the previous critical speed modes.

This method has the advantage of balancing flexible rotors which have extremely high amplification factors and are difficult or impossible to balance by either the least-squared error or the linear programming method. It also has the advantage that it will accurately balance shafts with substantial shaft bow.

The disadvantage of this method is that the rotor mode shapes must be known and that three runs must be performed for each critical speed to be balanced. After this method has been performed, one may initiate a two-run method using the rotor modal sensitivity derived in the initial exercise.

Rotor Balancing without Trial Weights

Rotor balancing without trial weights is referred to as a *one-shot method* of balancing. Once the influence coefficients for a particular rotor are determined, a balance may be predicted by using the current vibration measurements with the influence coefficients.

A modal method of balancing without trial weights was developed by Palazzolo and Gunter (1982). In this procedure, the Nyquist plot of rotor amplitude is used to determine the rotor amplification factor at a particular mode. By computing the rotor amplification factor, the modal unbalance eccentricity for a particular critical speed may be determined. From the polar or Nyquist plot, the phase locations of the modal weight distribution may be determined to balance a particular critical speed.

The disadvantage of this method is that the rotor modal mass and critical speed mode shape must be known. The advantage of this method is that the balance predictions may be used as the initial trial run for further refinement by the influence coefficient method of balancing.

Coupling Trim Balancing

There are many instances in which two machines are perfectly balanced but, when interconnected with a coupling, appear to have high vibrations. Since the two rotors are initially well balanced, it is undesirable to attempt to rebalance the units. In the coupling method of balancing developed by Winkler (1983), the coupling is rotated 180°. From the new resulting vibration measurements, the optimum position of the coupling may be computed for trim balancing.

3.1.4 Instrumentation and Vibration Measurement Techniques for Balancing

When a rotor is balanced at low speed as a component, the procedure will generally take place in an integrated general-purpose balancing machine with built-in transducers, signal conditioning, and often a highly automated data reduction and presentation facility. On the other hand, when rotor balancing is performed in situ at operating speed in the factory or the field, the instrumentation and data systems, whether removable or permanently installed, must be tailored to the specific design and to its operating environment and circumstances. It is therefore appropriate and most efficient that any vibration measurement systems included for such other functions as condition monitoring, performance verification, fault diagnosis, and/or parameter identification be specified to include the data acquisition requirements of the selected balancing procedure—

typically, the amplitude and phase of that portion of the signal which is synchronous with the rotor speed at the specified number of locations and at the specified rotor speeds. A general discussion of such general-purpose vibration instrumentation can be found in Sec. 4.2.

3.1.5 Nomenclature

A = amplification factor, dim

A_c = amplification factor at critical speed

a = influence coefficient

a = acceleration vector, in/s^2 (m/s^2)

a_t = tangential acceleration, in/s^2 (m/s^2)

a_n = normal acceleration, in/s^2 (m/s^2)

C_c = critical damping, lb · s/in^2 (N · s/m)

D = shaft diameter, in (m)

$\mathbf{e}_u$ = unbalance eccentricity vector, in (m)

$\mathbf{e}_r$ = unit vector in radial direction, rotating with angular velocity ω

$\mathbf{e}_t$ = unit vector in tangential direction, rotating with angular ω

F_b = bearing reaction, lb (N)

F_u = rotating unbalance force, lb (N)

f = frequency ratio, dim

g = gravity, in/s^2 (m/s^2)

I = shaft second moment of area, in^4 (m^4)

I_{ij} = moment-of-inertia matrix

I_p = polar moment of inertia, lb · in · s^2 (kg · m^2)

I_t = transverse moment of inertia, lb · in · s^2 (kg · m^2)

$[\mathbf{I}]$ = moment-of-inertia matrix

K = bearing or shaft spring rate, lb/in (N/m)

L = length, in (m)

L_b = bearing span, in (m)

M = rotor mass, lb · s^2/in (kg)

m_b = small rotor balancing mass, lb · s^2/in (kg)

m_i = unbalance masses, lb · s^2/in (kg)

m_u = effective unbalance mass, lb · s^2/in (kg)

$\mathbf{M}_u$ = unbalance moment, lb · in (N · m)

n = number of unbalance weights

N = rotor speed, rpm

N = number of balance planes

$\mathbf{P}$ = position vector

R = shaft radius or radius of motion

t = disk thickness, in (m)

$\mathbf{U}$ = unbalance vector, g · in, oz · in, lb · s^2 (kg · m, g · mm)

U_b = rotor radial balance correction, g · in, oz · in, lb · s^2 (kg · m, g · mm)

$\mathbf{V}$ = velocity vector, in/s (m/s)

V = velocity of motion, in/s (m/s)

W = total rotor weight, lb (kg)

w_u = unbalance weight, lb (kg)

X, Y = absolute cartesian coordinates of rotor motion

x_i, y_i = relative cartesian locations of unbalance weight W_i

x, y, z = cartesian coordinate system fixed in shaft with z along spin axis Z

X', Y', Z' = principal coordinates fixed in disk or cylinder

Z = rotor spin axis or axial distance, in (m)

$\mathbf{Z}$ = complex displacement

α = angular acceleration, rad/s^2

α_{ij} = influence coefficient matrix

β = relative mass-displacement phase angle, deg

δ = shaft deflection, in (m)

ϕ = phase angle, deg

ρ = material density, lb · s^2/in^4 (kg/m)

θ = cylindrical coordinate, deg

τ = disk skew, deg or rad

ω = angular velocity, rad/s

ω_{cr} = rotor critical speed on rigid supports, rad/s

3.2 RIGID ROTOR BALANCING

3.2.1 Introduction to Rigid-Body Balancing

The concept of rigid-body balancing is fundamental to the balancing of all rotating machinery. In reality, no rotor or equipment is truly rigid. The term *rigid body* may be applied to specific rotors which are operating substantially below their flexible critical speeds. An ideal rigid-body rotor may be accurately balanced in any two arbitrary planes.

A rigid body may be described by its mass, location of the center of gravity, and inertia properties. For the case of an idealized rotor represented only by a point mass, the rotor may be balanced by the application of a single balancing correction weight. In a more generalized rigid body such as an electric motor or a gyroscope, the body must be described by an inertia matrix as well as by the rotor mass and location of the center of gravity. The body has three principal orthogonal axes about which there are no products of inertia. An arbitrary free-spinning body will rotate in a stable condition about either its minimum or its maximum principal moment of inertia axis.

For the case of rotating machinery, such as an idealized rigid-body motor, the rotor or motor is constrained to spin about a fixed axis because of the action of the bearings. Balancing is required when the spin axis of the rotor does not correspond to either the maximum or the minimum principal inertia axis. If the mass center of the rigid body is displaced from the spin axis, then the rotor is said to have *static unbalance*. If the mass center lies along the spin axis of the shaft, but the minimum or maximum inertia axis does not coincide with the spin axis, then the rotor is said to have *dynamic unbalance*.

In the first case, a single correction plane is required for static balancing. In the second case, two weights of equal magnitude but 180° out of phase are required for the dynamic correction. An example is the old procedure of balancing automobile tires by means of a bubble balance. The wheel may be accurately balanced for static unbalance by a single-plane correction, but may be severely dynamically unbalanced due to the action of unbalance couples. After the wheel is statically balanced, two additional weights are required on opposite

sides of the wheel and 180° out of phase to each other to provide dynamic balance.

In general, a combination of static and dynamic unbalance will exist simultaneously in a rotor. Thus rigid-body balancing, in general, will require two distinct balancing planes situated normal to the spin axis of the rotor. The object of rigid-body balancing, therefore, is to make the maximum or minimum rigid-body inertia axis correspond identically with the rotor spin axis. When this occurs, the rotor is said to have rigid-body balance.

The theoretical conditions for rigid-body balancing are independent of machine speed provided that the rotor speed is well below the rotor flexible critical speed. Various types of low-speed rigid-body balancing machines have been developed to utilize the concept of rigid-body balancing in which the inertia axis corresponds with the rotor spin axis. In one set of balancing machines, called *soft bearing balancing* machines, the rotor is supported by bearings with very low spring rates. This causes the rotor to spin about its inertia axis. The displacement, magnitude, and phase are recorded at each end of the rotor. Weights are placed on the rotor until the runouts (displacements) are corrected to a minimal value. By this means, the rotor principal inertia axis is made to correspond to the spin axis.

In another class of balancing machine, the rotor is supported by very stiff bearings (Schenck Jrebel, 1980). The bearing supports are calibrated, and the bearing forces and phase angles are recorded at a given speed. This type of balancing machine is referred to as a *hard bearing balancing* machine. From the magnitude and phase of the recorded forces, the unbalance corrections may be determined for the rotor regardless of the rotor size.

A rotor is said to be a rigid rotor if it may be perfectly balanced by the application of suitable correction balance weights in any two arbitrary planes. The assumption of a rigid-body rotor is reasonable for electric motors but not for large turbine-generators due to shaft flexibility effects. A rotor, therefore, may be perfectly balanced as a rigid rotor in a balancing machine but may exhibit high unbalance characteristics at high speeds due to rotor flexibility effects when operating near a bending critical speed.

The process of rigid-body balancing is the application of suitable balance weights at two separate balancing planes along the rotor. The rotor is in static balance when the rotor mass center lies on the spin axis of the rotor. The rotor is in dynamic balance when the principal inertia axis coincides with the rotor spin axis. Dynamic balancing is equivalent to the condition that the product of inertia terms corresponding to the rotor spin axis and any other orthogonal axis acting through the rotor mass center be zero.

3.2.2 Single-Plane Balancing

Single-plane rotor balancing represents the most fundamental procedure in rotor balancing. With single-plane balancing, the rotor mass center is assumed to be offset from the spin axis of the shaft. The amount of radial offset is often referred to as the *rotor unbalance eccentricity* e_u or unbalance eccentricity vector $\mathbf{e}_u$.

In single-plane balancing, the suitable small balance correction weights are placed on the rotor to shift the mass center of the system to lie along the rotor spin axis. This process is static balancing.

Forces Caused by Single-Plane Rotating Unbalance
Consider the rotating mass M which is displaced from the origin point 0 by a fixed radius R, as shown in Fig. 3.1. The mass is rotating about the Z axis and is
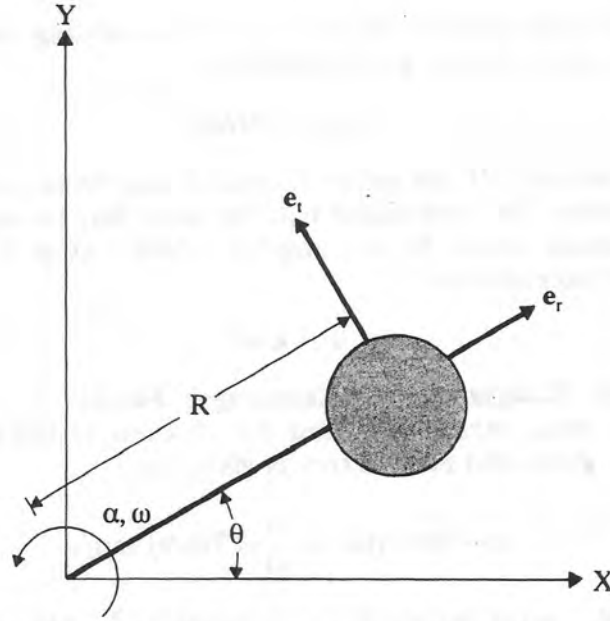
FIGURE 3.1 Schematic diagram of rigid-body point mass moving in XY plane.

moving in a circle of radius R in the XY plane. A position vector to the mass M from the origin 0 is given by

$$\mathbf{R} = R\mathbf{e}_r \tag{3.1}$$

The velocity of the mass is given by

$$\mathbf{V} = \dot{\mathbf{R}} = \dot{R}\mathbf{e}_r + R\dot{\mathbf{e}}_r = R\omega\mathbf{e}_t \qquad [\text{since } R \neq R(t), |R| \text{ is constant}]$$

The acceleration of the mass center is given by

$$\mathbf{a} = R\alpha\mathbf{e}_t - R\omega^2\mathbf{e}_r = a_t\mathbf{e}_t + a_n\mathbf{e}_r \tag{3.2}$$

where

$$a_t = R\alpha = \text{tangential acceleration}$$

$$a_n = -R\omega^2 = \text{centripetal acceleration}$$

The forces generated in the bar are given by Newton's second law of motion:

$$\mathbf{F} = M\mathbf{a} = M(R\alpha\mathbf{e}_t - R\omega^2\mathbf{e}_r) = F_r\mathbf{e}_r + F_t\mathbf{e}_t \tag{3.3}$$

The reaction forces acting on the bar at point 0 are equal and opposite to the forces generated in the bar and are given by

$$F_r = MR\omega^2$$
$$F_t = -MR\alpha \tag{3.4}$$

The radial reaction force F_r is often referred to as the *centrifugal force* caused by the centripetal acceleration $-R\omega^2$.

The total reaction is given by

$$F_{\text{reaction}} = MR\omega^2\left(1 + \frac{\alpha^2}{\omega^2}\right)^{1/2} \tag{3.5}$$

For acceleration rates normally encountered with rotating machinery, the rigid rotor bearing reaction force is approximated by

$$F_{\text{reaction}} = MR\omega^2 \tag{3.6}$$

The product of the mass M and radial distance R may be expressed as $\mathbf{U}$, which is the *radial unbalance*. The generalized reaction force may be expressed in terms of the radial unbalance vector $\mathbf{U}$ and angular velocity ω as follows (considering negligible system acceleration):

$$\mathbf{F} = \mathbf{U}\omega^2 \tag{3.7}$$

Example 3.1: Calculation of Centrifugal Force. A rotor of 45.36 kg (100 lb) has its mass center displaced by 25.4 μm (0.001 in, or 1 mil). The centrifugal force generated at 3600 rpm is given by

$$\omega = 3600 \text{ rpm} \times \frac{2\pi}{60} = 376.91 \text{ rad/s}$$

$$F_{3600} = (45.36 \text{ kg})(25.4 \times 10^{-6})(376.91)^2 = 163.68 \text{ N}$$

or

$$F_{3600} = \left(\frac{100 \text{ lb}}{386 \text{ in/s}^2}\right)(0.001)(376.91)^2 = 36.8 \text{ lb}$$

At 10,000 rpm the rotating force is

$$F_{10,000} = 36.8\left(\frac{10,000}{3600}\right)^2 = 284 \text{ lb}$$

The rotating weight of 100 lb (0.259 lb · s/in) displaced from the center of rotation by 1 mil (0.001 in) produces a rotating force of 37 lb at 3600 rpm. At 10,000 rpm, this rotating load has increased almost eightfold to 284 lb. Therefore, small displacement of the mass center of a rotor can lead to large rotating loads at high speeds.

The product of mass and radial distance, or eccentricity, may be expressed in metric units, U.S. Customary System (USCS) units, or as a product of the two systems. Typical units of unbalance $\mathbf{U}$ may be gram-micrometers, gram-inches, or ounce-inches.

Example 3.2. Express the equivalent unbalance $\mathbf{U}$ of Example 3.1 in terms of gram-inches and ounce-inches.

$$\mathbf{U}_{\text{oz} \cdot \text{in}} = (100 \text{ lb} \times 16 \text{ oz/lb})(0.001 \text{ in}) = 1.6 \text{ oz} \cdot \text{in}$$

or

$$\mathbf{U}_{\text{g} \cdot \text{in}} = \frac{100 \text{ lb} \times 1000 \text{ g/kg}}{2.2046 \text{ lb/kg}} \times 0.001 \text{ in} = 45.4 \text{ g} \cdot \text{in}$$

The rotating force generated by unbalance U expressed in terms of ounce-inches and gram-inches, respectively, is given by

$$F_{\text{lb}} = 1.775 \times 10^{-6} U_{\text{oz} \cdot \text{in}} \times (N \text{ rpm})^2 \tag{3.8}$$

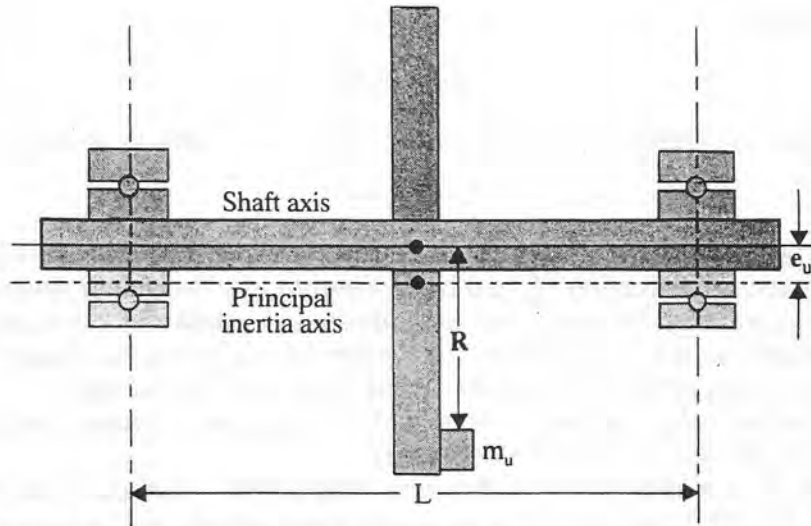$$F_{\text{lb}} = 6.26 \times 10^{-8} U_{\text{g} \cdot \text{in}} \times (N \text{ rpm})^2 \tag{3.9}$$

FIGURE 3.2 Single-mass disk with radial unbalance.

Relationship between Rotor Unbalance Eccentricity e_u and Unbalance U

Figure 3.2 represents a single-mass disk of mass M with a small unbalance mass of m_u placed at a radial distance $\mathbf{R}$ from the disk shaft axis. The effective mass center of the system is shifted radially by a small magnitude of e_u from the original axis of rotation. The amount of the shift e_u is given by

$$\mathbf{e}_u = \frac{\mathbf{R}m_u}{M + m_u} = \frac{\mathbf{U}}{M + m_u} \approx \frac{\mathbf{U}}{M} \qquad (3.10)$$

The small radial unbalance mass m_u at radius $\mathbf{R}$ causes a translation of the principal inertia axis from the shaft neutral axis by the vector magnitude e_u.

The unbalance weight is assumed to be much smaller than the total rotor weight, and the radius at which the weight is placed is much larger than the rotor unbalance eccentricity. If these conditions are not met, then the balancing and the rotordynamics may not be described by linear equations of motion. The unbalance eccentricity vector e_u thus lies in the same direction as the rotor unbalance vector $\mathbf{U}$.

In Eq. 3.10, the rigid-body radial unbalance magnitude remains constant for all speeds. Such is not the case when flexible shaft effects are taken into consideration.

Single-Plane Balancing of Rigid-Body Rotor

In Fig. 3.2, let a small balance weight m_b be placed at a radius R on the rim of the wheel 180° out of phase to the eccentricity vector e_u. The resulting centrifugal or inertia loading is given by

$$\mathbf{F}_u = M\mathbf{e}_u\omega^2 - m_b\mathbf{R}\omega^2 \qquad (3.11)$$

The value of m_b may be chosen such that the net centrifugal loading is zero. In this case, the wheel is said to be statically balanced, and the mass center lies along the spin axis of the shaft. In general, we will show that for a rigid body to be in balance, the principal inertia axis must lie along the spin axis.

The vector magnitude of small mass m_b at radius R, out of phase to the mass center eccentricity vector, may be referred to as the *rotor radial balancing* vector

and is given by

$$\mathbf{U}_b = m_b \mathbf{R} \qquad (3.12)$$

The condition for rigid-body balancing the single-plane disk is given by

$$\mathbf{U} + \mathbf{U}_b = 0 \qquad (3.13)$$

It is important to note that both $\mathbf{U}$ and $\mathbf{U}_b$ are vectors, not scalars. This implies that the balancing correction $\mathbf{U}_b$ can be represented by two scalar quantities. The scalar quantities may be either the magnitude and phase (or orientation of the balance weight) or the local cartesian XY components of the balancing correction with respect to an arbitrary reference frame fixed mark in the disk.

In rigid rotor balancing, it is assumed that only small correction weights must be placed on the disk or rotor to balance it.

Example 3.3: Calculation of Balance Magnitude. Compute the balancing magnitude $\mathbf{U}_b$ for Example 3.1 in terms of ounce-inches and gram-inches for a disk with a radius of 3 in.

$$\mathbf{U}_b = -M\mathbf{e}_u = -100 \text{ lb} \times 0.001 \text{ in} = -0.1 \text{ lb} \cdot \text{in}$$

$$= -0.1 \text{ lb} \cdot \text{in} \times 16 \text{ oz/lb} = -1.6 \text{ oz} \cdot \text{in}$$

$$= -0.1 \text{ lb} \cdot \text{in} \times \frac{1000 \text{ g/kg}}{2.2 \text{ lb/kg}} = -45.46 \text{ g} \cdot \text{in}$$

The correction weight that should be placed on the wheel at the 3-in radius is 15 g placed out of phase to the $\mathbf{e}_u$ vector.

Representation of Multiple Unbalances by a Single Unbalance Vector
Figure 3.3 represents a disk of mass M and radius $\mathbf{R}$ with multiple of unbalances m_i, $i = 1$ to n, at a radius of R_i as measured from the center. It is assumed that
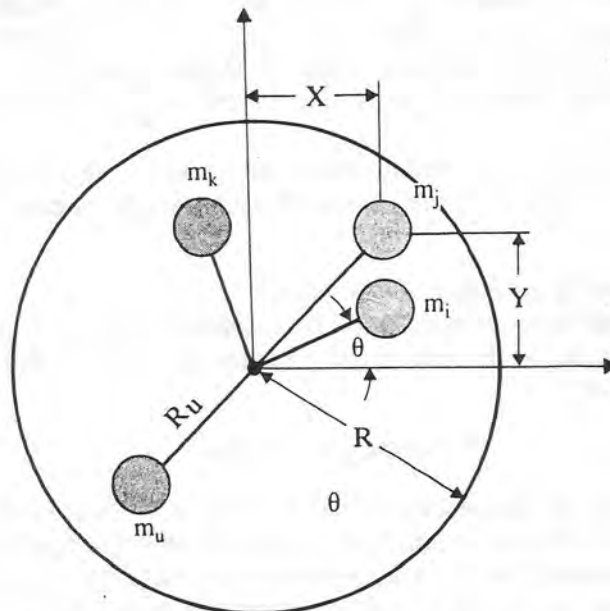
FIGURE 3.3 Single-plane disk with multiple un-balance vectors.

the sum of the unbalance weights is an order of magnitude smaller than the disk weight M. That is,

$$\sum_{i=1}^{n} m_i \ll M \tag{3.14}$$

The number of unbalances n produces a rotating load given by

$$\mathbf{F}_u = \sum_{i=1}^{n} m_i \mathbf{R}_i \omega^2 \tag{3.15}$$

The rotating unbalance load vectors may be replaced by a single mass m_u acting at a vector radius $\mathbf{R}_u$ as follows:

$$\mathbf{F}_u = m_u \mathbf{R}_u \omega^2 \tag{3.16}$$

Equating the two expressions for rotating unbalance force, we have

$$m_u \mathbf{R}_u = \sum m_i R_i = \mathbf{U} \tag{3.17}$$

For the case of a perfectly rigid shaft rotating about the shaft axis, the rotating force generated is

$$\mathbf{F}_u = m_u \mathbf{R} \omega^2 = \mathbf{U} \omega^2 \approx M \mathbf{e}_u \omega^2 \tag{3.18}$$

For a perfectly rigid shaft with the disk located in the center of the bearing span, the bearing reaction $\mathbf{F}_b$ is

$$\mathbf{F}_b = \frac{-M \mathbf{e}_u \omega^2}{2} = \frac{-\mathbf{F}_u}{2} \tag{3.19}$$

Such a statement will not be true for the flexible rotor where the bearing forces transmitted may be more than the rigid-body interia loads (critical and subcritical speed operation) or less than the rigid-body inertia loads (supercritial speed operation). For rigid-body operation with radial unbalance $\mathbf{U}$, the bearing forces increase as the square of the speed.

Note that in a ball-bearing- or roller-element-supported rotor, the bearing life varies approximately inversely to the cube of the bearing loads. Therefore, a doubling of the bearing loads due to unbalance will cause a reduction of the bearing life by a factor of 8, suggesting that ball-bearing-supported rotors must be very carefully balanced.

Equation 3.17 for the total unbalance magnitude is a vector equation and may also be resolved into scalar equations. An arbitrary relative xy axis may be inscribed on the disk with the x axis passing through a reference mark scribed on the disk. The radius vectors and the unbalance components may be expressed in terms of the loacl cartesian reference system fixed in the disk. The placement of the reference (or timing) mark on the disk is arbitrary. Let

$$\mathbf{R}_u = x_u \mathbf{i}' + y_u \mathbf{j}'$$

$$\mathbf{R}_i = x_i \mathbf{i}' + y_i \mathbf{j}'$$

The scalar equations for the cartesian components of unbalance are given by

$$U_x = m_u x_u = \sum m_i x_i = \sum U_{ix} \tag{3.20}$$

$$U_y = m_u y_u = \sum m_i y_i = \sum U_{iy} \tag{3.21}$$

where

$$x_i = R_i \cos \theta_i$$

$$y_i = R_i \sin \theta_i$$

The angle θ from the x axis at which the effective unbalance mass m_u is located is given by

$$\theta = \tan^{-1} \frac{y_u}{x_u}$$

$$= \tan^{-1} \frac{\sum m_i y_i}{\sum m_i x_i} \tag{3.22}$$

The effective unbalance mass m_u is

$$m_u = \frac{[(\sum m_i x_i)^2 + (\sum m_i y_i)^2]^{1/2}}{R_u} \tag{3.23}$$

The total or effective vector unbalance expressed in terms of the local xy cartesian coordinate system fixed in the disk is given by

$$\mathbf{U} = \sum_{i=1}^{n} U_{ix}\mathbf{i}' + \sum_{i=1}^{n} U_{ix}\mathbf{j}' = M\mathbf{e}_u$$

Therefore, a number of unbalance vectors which lie in a plane may be resolved into one single unbalance vector similar to Eq. 3.10.

Example 3.4: Resolution of Multiple Balance Weights into a Single Balance. We are given a 50-lb wheel with 36 holes equally spaced at a 6-in radius, as shown in Fig. 3.4. The holes are labeled in a counterclockwise
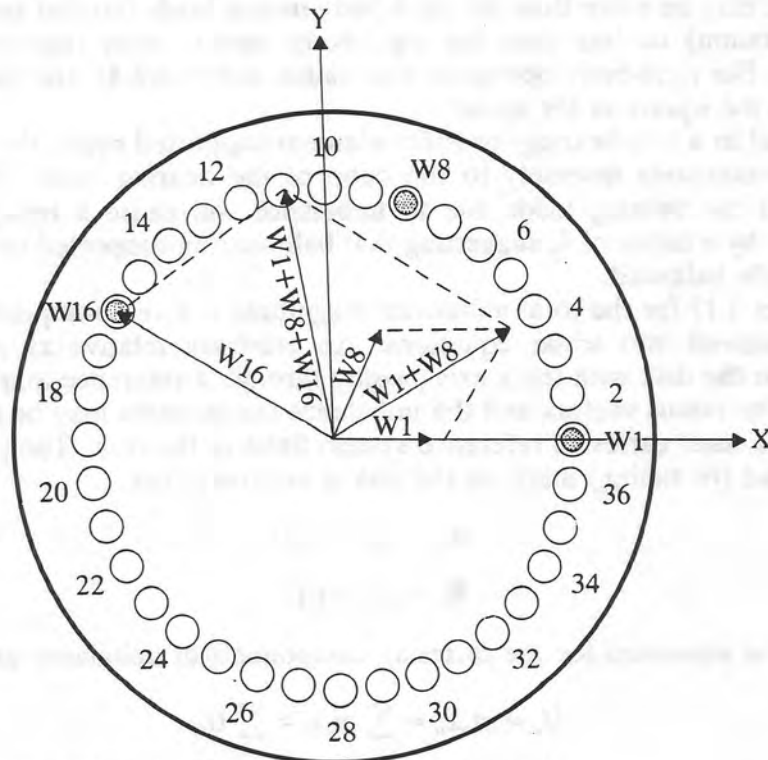

FIGURE. 3.4 Vector addition of balance weights.

direction. There are three weights placed in various holes. Replace the three weights by a single equivalent weight in the nearest hole. The balance weights are

$$w_1 = 1 \text{ oz at hole } 1$$

$$w_8 = 1 \text{ oz at hole } 8$$

$$w_{16} = 2 \text{ oz at hole } 16$$

Solution.   A relative reference axis is drawn on the disk passing through the disk center and hole 1. This line establishes the relative x axis. The holes are spaced at intervals of 10°. The angular location and moments generated by the balance weights are given in Table 3.3. The equivalent balance weight W_b is given

TABLE 3.3   Resolution of Multiple Balance Weights

Number	Weight	Hole	Angle	x_i	y_1	$w_i x_i$	$w_i y_i$
1	1	1	0°	6	0	6	0
2	1	8	70°	2.05	5.64	2.05	5.64
3	2	16	150°	−5.20	3.00	−10.39	6.00
Total	2	11	101°	−1.15	5.89	−2.34	11.64

by

$$w_b = \frac{[(-2.34)^2 + (11.64)^2]^{1/2}}{6 \text{ in}}$$

$$= \frac{11.87 \text{ oz} \cdot \text{in}}{6 \text{ in}} = 1.98 \text{ oz}$$

$$\theta = \tan^{-1}\left(\frac{11.64}{-2.34}\right) = 101.37°$$

An approximate equivalent balance resultant is obtained by placing a 2-oz weight at hole 11. It is seen in the above example that any number of balance weights acting in a single plane may be combined into one single balance vector of weight w_b placed at a radius vector **R**.

The approach used to sum the unbalance magnitudes is called *vector addition*. If U_{bi} are the various individual balance magnitudes acting at a given xy plane, then the effective balance U_b acing at the plane is given by the following vector sum:

$$U_b = U_{b1} + U_{b2} + \cdots + U_{bi} + \cdots + U_{bn} \qquad i = 1 \text{ to } n \qquad (3.24)$$

Example 3.4 may also be solved graphically. Figure 3.4 represents a polar plot of the locations of the balance weights. If plotted on polar paper, then one major division represents 0.5 oz, and full scale is 2.5 oz. As a first step, the three balance

vectors are drawn to scale to represent the weights placed in holes 1, 8, and 16. Next the balancing weights W_1 and W_8 are vectorially added (by using a compass to construct the parallelogram). The resultant vector $W_1 + W_8$ is now added to W_{16} to generate the final resultant balance vector W_b. From the construction, we see that the resultant balance is approximately 2 oz at hole 11.

In a similar fashion, a single balancing weight may be resolved into two or more arbitrary vectors. This process is very important in balancing because it is often encountered in field balancing where the balance hole specified for weight placement already is filled with balance weights. In this case, the equivalent balance may be achieved by placing the proper weights in holes on either side of the specified balancing hole.

So a number of unbalance or balancing weights placed on a disk may always be resolved into a single balancing (or unbalance) weight positioned with respect to a relative *xy* reference frame fixed in the disk.

Single-Plane Balancing by the Influence Coefficient Method

The rotating unbalance in the rigid body rotor creates a force in the bearings that is proportional to the unbalance U. By measuring the forces transmitted through the bearing pedestal via a calibrated strain gauge or force transducer, one may balance the rotor using the influence coefficient method.

In the application of this method, the relative phase angle of the force (or pedestal displacement) with respect to a timing mark on the shaft must be measured along with the magnitude of the force. The force or displacement measured at the pedestal is given by

$$Z = aU \tag{3.25}$$

The measured force is a function of the system influence coefficient a and the unknown rotor unbalance U.

A trial or calibration weight is next placed on the rotor. The new response Z_t is measured after the application of the calibration unbalance:

$$Z_t = a(U + U_t) \tag{3.26}$$

By vector subtraction of the calibration run and the initial run, the system influence coefficient a is

$$a = \frac{Z_t - Z}{U_t} = \frac{\Delta Z}{U_t} \tag{3.27}$$

The influence coefficient a represents the response of this particular rigid-body rotor to a unit unbalance. All rotors of this same class will have the same influence coefficient response. Note that this value represents a vector quantity since it involves both amplitude and phase information.

The inverse of the influence coefficient a is the rotordynamic *stiffness* or *impedance coefficient* d. Once the rotordynamic impedance has been determined, the balancing correction may be computed directly from the value of the dynamic impedance d and the initial vibration Z as follows:

$$U_b = -U = -a^{-1} \times Z = -dZ \tag{3.28}$$

The value of the rotordynamic impedance d will be the same for all rotors of a similar class when operated at the particular speed at which the initial measurements were made. Therefore, a new rotor with an unknown value of unbalance could be directly balanced from the value of the vibration reading by

using the previously determined rotordynamic impedance value **d**. The process of balancing a rotor without the addition of trial weights is referred to as *one-shot balancing*.

The single-plane balancing procedure is well suited to a graphical solution since the vibration values and influence coefficients are two-dimensional vectors. Figure 3.19 is an example of the single-plane balancing graphical procedure. In the graphical solution, the $\Delta \mathbf{Z}$ vector is constructed by vector subtraction of the trial response minus the initial response, and the resultant magnitude and phase angle are measured on polar paper:

$$\Delta \mathbf{Z} = \mathbf{Z}_t - \mathbf{Z} = |\Delta \mathbf{Z}| \angle \Delta \theta°$$

Equation 3.27 may be rewritten for the graphical solution in the form

$$\mathbf{U}_b = -\mathbf{U}_t \frac{\mathbf{Z}}{\Delta \mathbf{Z}} = -U_t \angle \theta_t° \left| \frac{\mathbf{Z}}{\Delta \mathbf{Z}} \right| \angle (\theta° - \Delta \theta°)$$

$$= U_t \left| \frac{\mathbf{Z}}{\Delta \mathbf{Z}} \right| \angle (\theta_t° + \theta° - \Delta \theta° - 180°) = U_b \angle \theta_b° \qquad (3.29)$$

In the graphical solution, the magnitude of the trial unbalance $\mathbf{U}_t$ is multiplied by the scalar value of $|\mathbf{Z}/\Delta \mathbf{Z}|$ to produce the balance magnitude of $\mathbf{U}_b$. The angle at which the balance weight should be placed is rotated from the position of the trial balance by the angle of $\Theta° - \Delta\Theta° - 180°$.

3.2.3 Two-Plane Rigid Rotor Balancing

Figure 3.5 represents a two-mass rotor mounted on rigid shaft in rigid bearings. The disks are assumed to have masses M_1 and M_2, respectively. A small
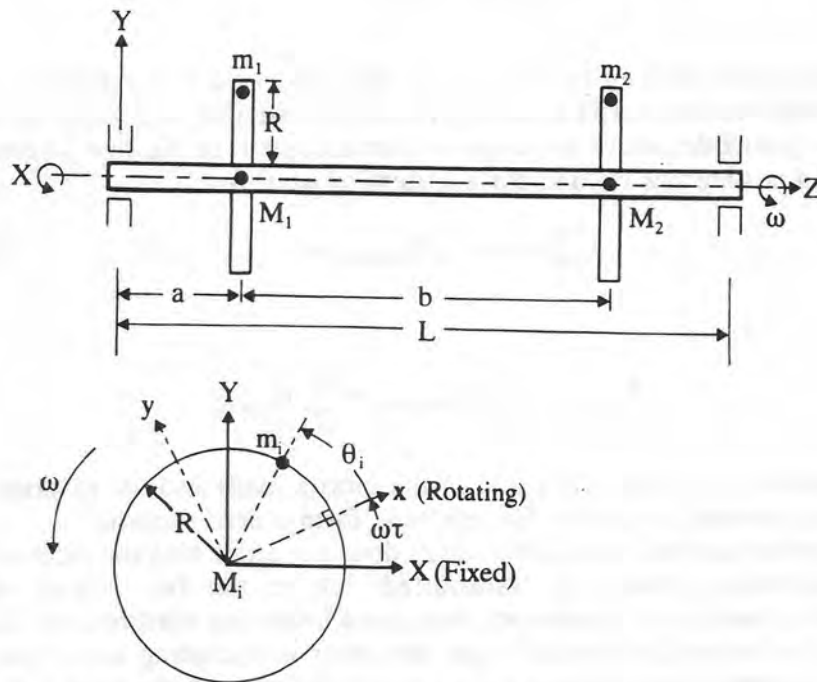

FIGURE 3.5 Two-mass rotor on a rigid shaft.

unbalance weight is attached to each disk, m_1 to M_1 and m_2 to M_2, at angles of θ_1 and θ_2, respectively, as measured from a reference mark on the shaft.

The vector forces generated by the two rotating masses are given by

$$\mathbf{F}_{u1} = m_1 \mathbf{R}_1 \omega^2 = \mathbf{U}_1 \omega^2$$
$$\mathbf{F}_{u2} = m_2 \mathbf{R}_2 \omega^2 = \mathbf{U}_2 \omega^2 \tag{3.30}$$

The unbalances $\mathbf{U}_1$ and $\mathbf{U}_2$ may be resolved in terms of xy components with respect to a local xy coordinate system fixed in the rotor;

$$U_{ix} = m_i R_i \cos \theta_i \qquad U_{iy} = m_i R_i \sin \theta_i \qquad i = 1, 2 \tag{3.31}$$

The vector forces may be resolved into cartesian components in the fixed x and y newtonian reference frame.

$$F_{uX} = \omega^2 \sum_{i=1}^{2} m_i R_i \cos (\omega t + \theta_i) = \omega^2 \sum_{i=1}^{2} U_i \cos (\omega t + \theta_i)$$

$$= \omega^2 \sum_{i=1}^{2} (U_{ix} \cos \omega t - U_{iy} \sin \omega t) = F_{uX_1} + F_{uX_2}$$

$$\tag{3.32}$$

$$F_{uY} = \omega^2 \sum_{i=1}^{2} m_i R_i \sin (\omega t + \theta_i) = \omega^2 \sum_{i=1}^{2} U_i \sin (\omega t + \theta_i)$$

$$= \omega^2 \sum_{i=1}^{2} (U_{ix} \sin \omega t + U_{iy} \cos \omega t) = F_{uY_1} + F_{uY_2}$$

At the instant the reference mark on the shaft corresponds to the horizontal axis, the inertial forces generated in the fixed xy reference frame are given by

$$F_{uX} = \omega^2 \sum U_{ix}$$
$$F_{uY} = \omega^2 \sum U_{iy} \tag{3.33}$$

For a perfectly rigid shaft in rigid bearings, the mass or disk moments of inertia do not contribute to the inertia loading gravitational weight. It is useful to refer to *D'Alembert's principle,* which is simply a rearrangement of Newton's second law of motion and is stated as follows for a system of particles:

$$-\sum M\mathbf{a} + \sum \mathbf{F}_{\text{external}} = 0 \tag{3.34a}$$

where

$$\sum \mathbf{F}_{\text{external}} = \sum_{i=1}^{n} \mathbf{F}_{\text{unbalance}} + \sum_{i=1}^{2} \mathbf{F}_{\text{bearing}} \tag{3.34b}$$

From D'Alembert's principle, the sum of the inertia loads and the external forces (bearing reactions and unbalance forces) must form a zero system.

It is of interest that the mass of the disks does not enter into the expression for the dynamic bearing forces $\mathbf{F}_b$ transmitted due to the two planes of rotor unbalance. In a hard bearing support, low-speed balancing machine, the supports are designed to be sufficiently stiff that the rotor is operating as a rigid rotor. Hence, the bearing forces measured are a direct function of the rotor unbalance,

and the size of the rotor is theoretically not important. Thus, the sensitivity of a hard bearing support balancing machine should be relatively independent of size.

In Fig. 3.5, the unbalance forces acting on the two disks may be resolved into an equivalent force $\mathbf{F}_u$ and the moment or couple $\mathbf{M}_u$ acting at the mass center of the system as follows:

$$\mathbf{F}_u = \omega^2(\mathbf{U}_1 + \mathbf{U}_2) \tag{3.35a}$$

$$\mathbf{M}_u = \omega^2(\mathbf{L}_1 \times \mathbf{U}_1 + \mathbf{L}_2 \times \mathbf{U}_2) \tag{3.35b}$$

In the above formulations, where L_1 and L_2 are the axial distances from the rotor center of gravity to the planes of unbalance, the unbalance magnitudes $\mathbf{U}_1$ and $\mathbf{U}_2$ must be expressed in mass-displacement units.

Vector Resolution of Arbitrary Unbalance into Two Planes
Figure 3.6 represents a rigid-body rotor with an arbitrary unbalance of $\mathbf{U}(m_u\mathbf{R})$ situated at an axial distance of l_u from the rotor mass center. When the x
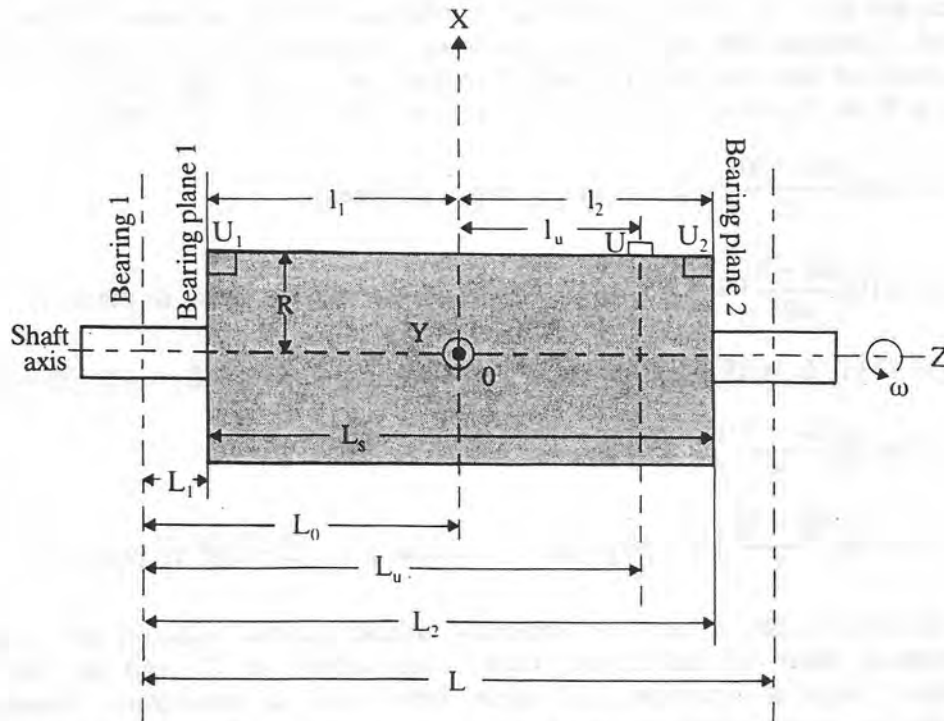

FIGURE 3.6 Rigid-body rotor with arbitrary unbalance.

reference axis fixed in the shaft corresponds with the stationary X axis, the equivalent rotating force and moment acting about the mass center are given by

$$\mathbf{F}_u = \mathbf{F}_{ux} = \omega^2 U\mathbf{i} \tag{3.36a}$$

$$\mathbf{M}_u = \mathbf{M}_{uy} = \omega^2 L_u U\mathbf{j} \tag{3.36b}$$

The arbitrary unbalance $\mathbf{U}$ for a rigid body may be specified in terms of the equivalent unbalance magnitudes of $\mathbf{U}_1$ and $\mathbf{U}_2$ located at two specified planes in the rotor.

The unbalance magnitudes U_1 and U_2 will generate an equivalent force and couple about the rotor mass center as the original arbitrary unbalance U. Assuming that the unbalances U_1 and U_2 lie along relative x axis attached to the rotor,

$$F_{ux} = \omega^2(U_1 + U_2) = \omega^2 U \tag{3.37a}$$

$$M_{uy} = \omega^2(l_2 U_2 - l_1 U_1) = L_u \omega^2 U \tag{3.37b}$$

Solving for U_1 and U_2 gives

$$U_1 = U\frac{l_2 - l_u}{l_1 + l_2} \qquad U_2 = U\frac{l_1 + l_u}{l_1 + l_2} \tag{3.38}$$

And U_1 and U_2 may also be expressed in terms of measurements from the bearing 1 centerline as

$$U_1 = U\frac{L_2 - L_u}{l_s} \qquad U_2 = U\frac{L_u - L_1}{l_s} \tag{3.39}$$

Example 3.5. A 40-in rotor has an unbalance of $10\,g \cdot in$ located 30 in from the end. Calculate the equivalent two-plane unbalance for (a) balance planes at the ends of the rotor and (b) balance planes at $L_1 = 35$ and $L_2 = 40$.
(a) $L_2 = 40$ in, $L_1 = 0$ in, $L_2 = 40$ in, $L_u = 30$ in, and $l_s = L_2 - L_1 = 40$ in.

$$U_1 = 10\left(\frac{40 - 30}{40}\right) = 2.5\,g \cdot in \qquad \text{balance plane 1}$$

$$U_2 = 10\left(\frac{30 - 0}{40}\right) = 7.5\,g \cdot in \qquad \text{balance plane 2 (in phase to plane 1)}$$

(b) $L_2 = 40$ in, $L_1 = 35$ in, $L_s = 5$ in, $L_u = 30$ in, and $l_s = L_2 - L_1 = 40 - 35 = 5$ in.

$$U_1 = 10\left(\frac{40 - 30}{5}\right) = 20\,g \cdot in \qquad \text{balance plane 1}$$

$$U_2 = 10\left(\frac{30 - 35}{5}\right) = -10\,g \cdot in \qquad \text{balance plane 2} - 180° \text{ to plane 1}$$

In Example 3.5b, if the two arbitrary balance planes selected fall outside the original plane of unbalance, then large values of U_1 and U_2 will be generated. Such a situation can occur when one is attempting two-plane balancing on an overhung rotor. A small unbalance weight at the center bull gear can translate into large balance couples on an overhung wheel.

Resolution of Two-Plane Unbalance into Static and Dynamic Components

A single plane or two arbitrary planes of unbalance may always be resolved into equivalent static and dynamic components U_s and U_d, respectively. Figure 3.5, e.g., represents a two-mass system with arbitrary unbalances U_1 and U_2 on the wheels. Figure 3.7 represents the unbalances resolved into static and dynamic components. The vector relationship is given by

$$\mathbf{U_1} = \mathbf{U_s} - \mathbf{U_d} \tag{3.40a}$$

$$\mathbf{U_2} = \mathbf{U_s} + \mathbf{U_d} \tag{3.40b}$$
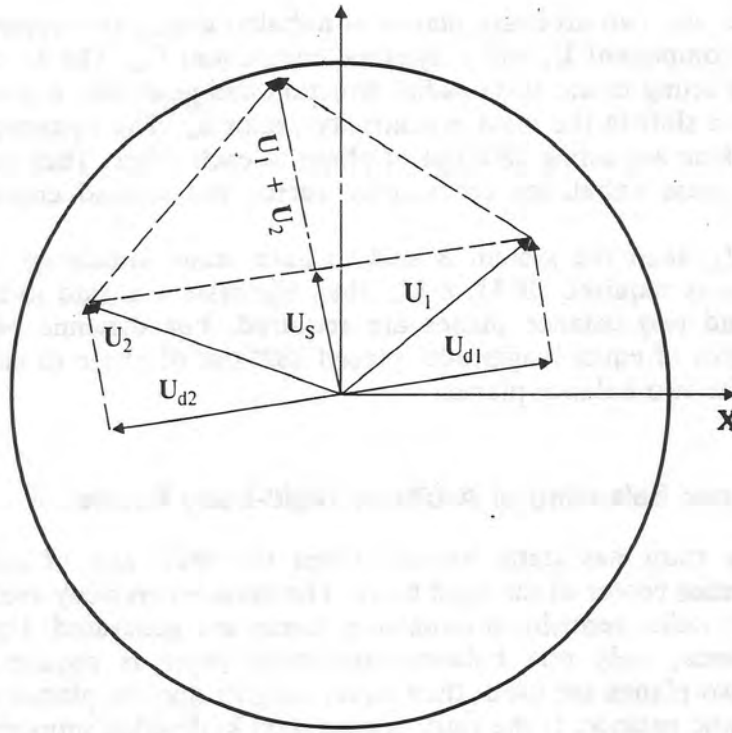
FIGURE 3.7 Resolution of two-plane unbalance into static and dynamic components.

Adding the above two equations, we obtain the effective static unbalance on each wheel as follows:

$$\mathbf{U}_s = \frac{\mathbf{U}_1 + \mathbf{U}_2}{2} \tag{3.41a}$$

The dynamic component or couple is given by

$$\mathbf{U}_d = \frac{\mathbf{U}_2 - \mathbf{U}_1}{2} \tag{3.41b}$$

In two-plane balancing, it is often advantageous to resolve the unbalance or displacements into static and dynamic components. This resolution represents a modal decomposition into static ϕ_s (in-phase) components and dynamic ϕ_d (out-of-phase) components as follows:

$$\phi_s = \begin{Bmatrix} 1 \\ 1 \end{Bmatrix} \qquad \text{static or in-phase mode}$$

$$\phi_d = \begin{Bmatrix} -1 \\ 1 \end{Bmatrix} \qquad \text{dynamic or out-of-phase mode} \tag{3.42}$$

The two-plane unbalance vectors $\mathbf{U}_1$ and $\mathbf{U}_2$ are represented in terms of modal components as follows:

$$\begin{Bmatrix} \mathbf{U}_1 \\ \mathbf{U}_2 \end{Bmatrix} = \{\mathbf{U}\} = \mathbf{U}_s \phi_s + \mathbf{U}_d \phi_d$$

$$\{\mathbf{U}\} = \mathbf{U}_s \begin{Bmatrix} 1 \\ 1 \end{Bmatrix} + \mathbf{U}_d \begin{Bmatrix} -1 \\ 1 \end{Bmatrix} \tag{3.43}$$

Therefore, any two arbitrary planes of unbalance may be vectorially resolved into a static component $\mathbf{U}_s$ and a dynamic component $\mathbf{U}_d$. The $\mathbf{U}_s$ component at each plane is acting in the same radial direction and generates a centrifugal force $\mathbf{F}_u$. It causes a shift in the mass eccentricity vector $\mathbf{e}_u$. The dynamic components $\mathbf{U}_d$ at each plane are acting 180° out of phase to each other. They do not cause a shift of the mass unbalance eccentricity vector but instead create a dynamic moment $\mathbf{M}_u$.

If $\mathbf{U}_s \gg \mathbf{U}_d$, then the system is said to have static unbalance and only one balance plane is required. If $\mathbf{U}_d \gg \mathbf{U}_s$, then the system is said to have dynamic unbalance and two balance planes are required. For dynamic balancing, two balance weights of equal magnitude, placed 180° out of phase to each other, are required at the two balance planes.

3.2.4 Dynamic Balancing of Arbitrary Rigid-Body Rotors

A rigid-body rotor has static balance when the shaft axis of rotation passes through the mass center of the rigid body. The mass eccentricity vector $\mathbf{e}_u$ is zero, hence no net radial centrifugal unbalance forces are generated. For the case of static unbalance, only one balance correction plane is required to achieve balance. If two planes are used, then equal weights may be placed at each plane to achieve static balance. If the rotor is placed on knife-edge supports or a bubble balance (e.g., a tire-balancing machine), then no apparent unbalance appears to exist in the rotor.

The most general case of rotor unbalance is any arbitrary unbalance distribution. This arbitrary unbalance distribution can be resolved into static and dynamic components. Upon spinning a rotor that has been statically balanced, however, large bearing forces may be encountered. This is caused by the existence of dynamic unbalance in the rotor, creating a dynamic moment about the rotor mass center.

Dynamic unbalance exists whenever the spin axis of the shaft does not correspond to the rotor principal inertia axis. The rotor may be in static balance because the spin axis passes through the rotor center of gravity, but may be dynamically unbalanced if the spin axis or axis of shaft rotation does not correspond to the principal inertia axis. Dynamic unbalance normally cannot be corrected by a single-plane balancing correction. In general, two balancing planes are required for dynamic rigid-body rotor unbalance.

Rigid-Body Constrained Motion about Z Axis
Assume that the rotor of Fig. 3.6 is constrained to rotate about the Z axis. This condition is similar to the situation of a hard bearing balancing machine.

The dynamic moments created about the x, y, z axes fixed in the rotor are given by

$$M_x = \alpha I_{zz} - \omega^2 I_{yz}$$
$$M_y = \alpha I_{yz} + \omega^2 I_{xz} \qquad (3.44)$$
$$M_z = \alpha I_{zz}$$

For constant angular speed of rotation ω ($\alpha = 0$), the constrained Euler equations reduce to

$$M_x = -\omega^2 I_{yz}$$
$$M_y = +\omega^2 I_{xz} \qquad (3.45)$$

The product-of-inertia terms for a rigid body are defined by

$$I_{xz} = -\int_v \rho xz \, dv \qquad I_{yz} = -\int_v \rho yz \, dv$$

For a rigid-body rotor to be dynamically balanced, the product-of-inertia terms I_{yz} and I_{xz} must be zero.

Example 3.6: Dynamic Moment Caused by Unbalance. Calculate the product of inertia caused by a 2-g weight on mass 2 and the dynamic moment generated at 3600 rpm in Fig. 3.6. Assume $R = 5$ in and $L_2 = 10$ in. Then

$$I_{yz} = -\sum m_i y_i z_i = 0$$

$$I_{xz} = -\sum m_i x_i z_i = \frac{-10 \, g \times 2.2 \, lb/kg \times 5 \, in \times 10 \, in}{1000 \, g/kg \times 386 \, in/s^2}$$

$$I_{xz} = -2.85 \times 10^{-3} \, lb \cdot in \cdot s^2$$

At 3600 rpm, the dynamic moment about the rotating **y** axis generated by the unbalance weight is given by

$$M_y = \omega^2 I_{xz} = \left(\frac{3600}{60} \times 2\pi\right)^2 I_{xz} = 405 \, in \cdot lb$$

Euler's Equations for Principal Axes

A set of coordinate axes may always be determined in which the product-of-inertia terms I_{xz} and I_{yz} vanish. A rigid body spinning freely will tend to rotate about either the maximum or the minimum principal inertia axis. This is the basic principle of a soft bearing balancing machine. The soft bearing spring rate allows the rotor to spin about a principal inertia axis.

Figure 3.8 represents a disk of mass M, radius R, and thickness T which is attached to a rigid shaft at an inclined angle of τ degrees from the XY plane fixed
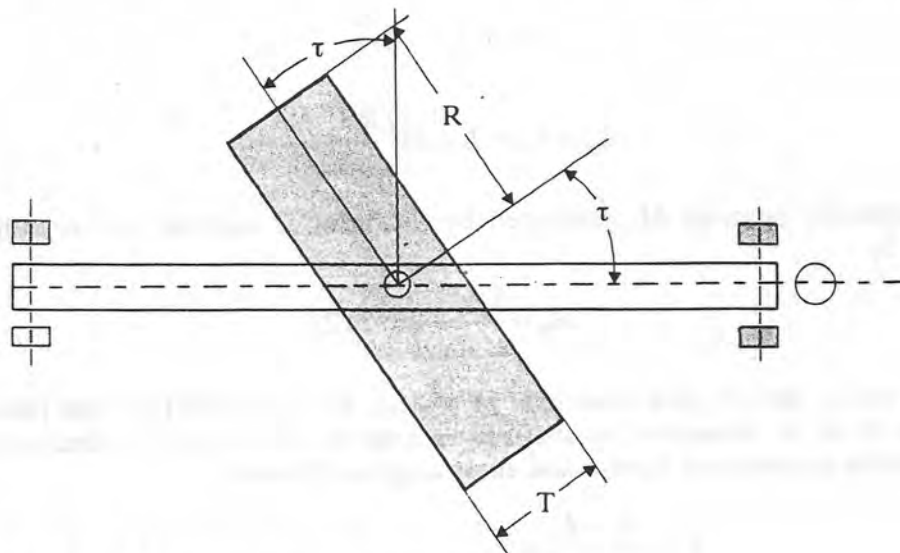
FIGURE 3.8 Skewed circular disk on massless shaft.

in the shaft. The x, y, z axes are a set of principal axes fixed in the disk. The shaft is assumed to rotate about the Z axis (directed along the bearing centerline) with an angular velocity of ω.

The principal axes of the disk are the x, y, and z coordinates fixed in the disk. If the bearing constraints were removed, then the disk would tend to rotate about the local **z** axis, which is normal to the disk. By constraining the skewed disk to rotate about the fixed Z axis, a dynamic moment or couple is created. This dynamic moment may be expressed either in terms of products of inertia by using the X, Y, Z axes set fixed in the shaft or in terms of principal moments of inertia and skew angle by using the **x**, **y**, **z** principal axes fixed in the disk.

Euler's equations for principal axes reduce to

$$M_x = \dot{\omega}_x I_{xx} + \omega_y \omega_z (I_{zz} - I_{yy})$$
$$M_y = \dot{\omega}_y I_{yy} + \omega_x \omega_z (I_{xx} - I_{zz}) \tag{3.46}$$
$$M_z = \dot{\omega}_z I_{zz} + \omega_x \omega_y (I_{yy} - I_{xx})$$

The angular velocity vector **ω** is given in terms of the **x**, **y**, **z** axes fixed in the disk by

$$\boldsymbol{\omega} = \omega \mathbf{K} = \omega_x \mathbf{i} + \omega_y \mathbf{j} + \omega_z \mathbf{k} \tag{3.47}$$

$$\boldsymbol{\omega} = -\omega \sin \tau \mathbf{i} + \omega \cos \tau \mathbf{k}$$
$$\omega_x = -\omega \sin \tau \qquad \omega_z = \omega \cos \tau \tag{3.48}$$

For constant angular velocity ω, the moment expressions are given by

$$M_x = 0$$
$$M_y = -(\omega^2 \sin \tau \cos \tau)(I_{xx} - I_{zz}) \tag{3.49}$$
$$M_z = 0$$

For a uniform disk or a cylinder of radius R and length L, the principal moment of inertia I_{zz} is referred to as the *polar moment of inertia I_p*, and the principal moments of inertia I_{yy} and I_{zz} are called the *transverse moments of inertia I_t*. These values are given by

$$I_{zz} = I_p = M \frac{R^2}{2} \tag{3.50}$$

$$I_{xx} = I_{yy} = I_t = M \left(\frac{R^2}{4} + \frac{L^2}{12} \right) \tag{3.51}$$

The dynamic moment M_y generated by the rotating skewed disk or cylinder is given by

$$M_y = \frac{\mathbf{I}_p - \mathbf{I}_t}{2} \omega^2 \sin 2\tau \tag{3.52}$$

Since the y and Y axes coincide, $M_y = M_Y$, we conclude that the product-of-inertia term as measured in shaft fixed axes is related to the disk polar and transverse moments of inertia and skew angle as follows:
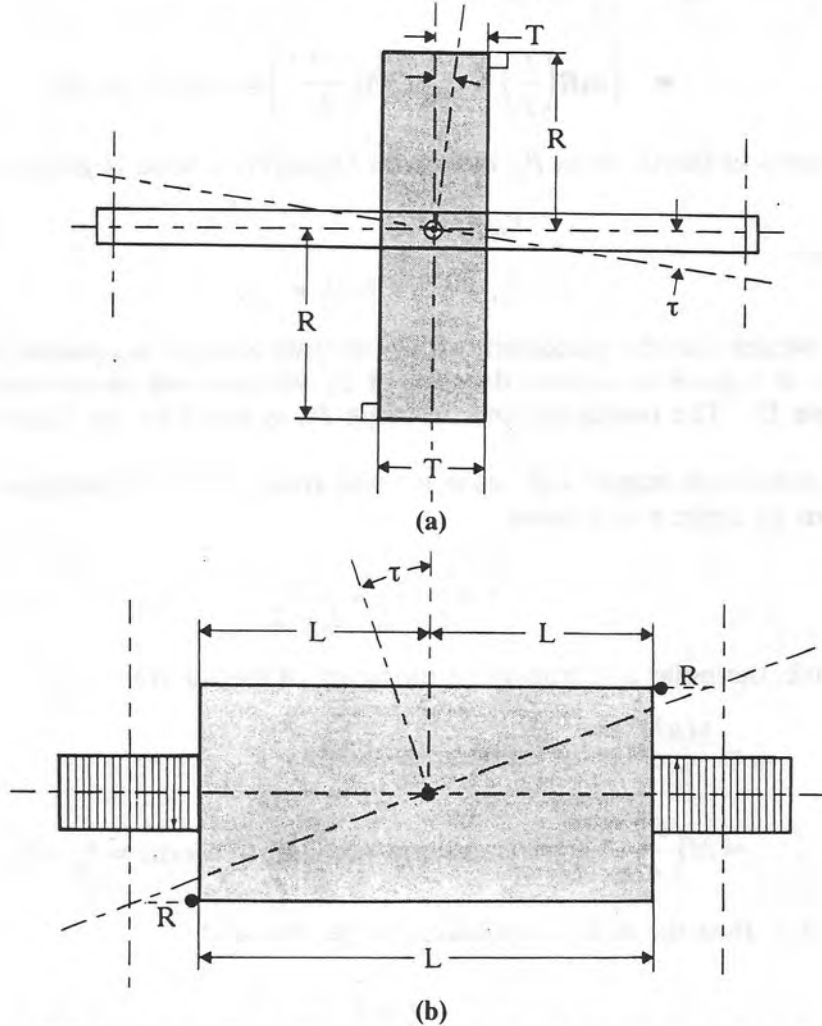
$$I_{xz} = \frac{I_p - I_t}{2} \sin 2\tau \tag{3.53}$$

$$\approx \tau(I_p - I_t) \qquad \text{for small skew angles} \tag{3.54}$$

Hence in a soft bearing balancing machine, the runout angle τ is given by

$$\tau = \frac{I_{xy}}{I_p - I_t} \tag{3.55}$$

Figure 3.9a represents a balanced disk of radius R and thickness $L = T$. Two unbalance weights of mass m are placed at a radius of R on either side of the

(a)

(b)

FIGURE 3.9 (a) Disk with two-plane couple unbalance; (b) cylinder with two-plane couple unbalance.

faces of the disk 180° out of phase to each other. If the disk is rotated about the Z axis with an angular velocity of ω rad/s, a dynamic couple or moment acting along the relative or rotating y axis is

$$\mathbf{M}_y = \mathbf{R}_1 \times \mathbf{F}_1 + \mathbf{R}_2 \times \mathbf{F}_2$$

$$= \frac{T}{2}\mathbf{k} \times \omega^2 R m_1 \mathbf{i} + \left(-\frac{T}{2}\mathbf{k}\right) \times (-\omega^2 R m_2 \mathbf{i})$$

$$= \omega^2 m R T \mathbf{j} = \omega^2 U T \mathbf{j}$$

$$= \omega^2 U_c \mathbf{j} \tag{3.56}$$

where

$$U_c = \text{unbalance couple} = UT$$

Since the unbalance weights lie in the xz plane attached in the disk, the product-of-inertia term I_{xz} corresponding to the x, z axes is given by

$$I_{xz} = -\sum_{i=1}^{2} m_i x_i z_i$$

$$= -\left[mR\left(\frac{T}{2}\right) + m(-R)\left(\frac{-T}{2}\right)\right] = -mRT = -U_c \qquad (3.57)$$

The product-of-inertia term P_{xz} in various engineering texts is given as

$$P_{xz} = -I_{xz}$$

therefore $\qquad\qquad\qquad\qquad\qquad\qquad\qquad\qquad\qquad\qquad\qquad (3.58)$

$$P_{xz} = mRT = U_c = -I_{xz}$$

Hence, we see that the placement of two weights of equal magnitude but 180° out of phase at a plane separation distance of T, will generate an unbalance moment or couple $\mathbf{U}_c$. The product-of-inertia value P_{xz} is equal to the unbalance couple $\mathbf{U}_c$.

The unbalance couple will cause a small rotation of the principal axes about the **y** axis by angle τ as follows:

$$\tau = \frac{I_{xz}}{I_p - I_t} = \frac{-\mathbf{U}_c}{I_p - I_t} \qquad (3.59)$$

For a disk, the polar and transverse moments of inertia are

$$I_p = \frac{MR^2}{2} = \text{polar moment of inertia} = I_{zz}$$

$$= M\left(\frac{R^2}{4} + \frac{T^2}{12}\right) = \text{transverse moment of inertia} = I_{xx} = I_{yy}$$

If $T/R \ll 1$, then the disk is considered to be thin and

$$I_t = \frac{I_p}{2}$$

For a thin disk, the skew angle τ is given by

$$\tau_{\text{disk}} = \frac{-U_c}{I_p/2} = \frac{-mRT}{MR^2/4} = -\frac{8T}{D}\frac{m}{M} \qquad \text{rad} \qquad \frac{m}{M} \ll 1$$

(The unbalance mass m is assumed to be small in comparison to the disk mass.) The dynamic or inertia moment generated about the rotating **y** axis is given by

$$M_{y,\text{inertia}} = -M_y = -\omega^2 I_{xz} = \omega^2 P_{xz} = \omega^2 U_c$$

If bearings of very low spring rate were placed at the bearing locations, the disk would rotate about the **z** principal inertia axis as shown in Fig. 3.9a.

Figure 3.9b is similar to Fig. 3.9a except that the unbalance weights have been placed on the ends of a cylinder of length L. A cylinder is differentiated from a disk in that the transverse moment of inertia I_t is greater than the polar moment of inertia:

$$I_t > I_p \quad \text{for a cylinder}$$

For a uniform circular cylinder

$$I_t = M\left(\frac{R^2}{4} + \frac{L^2}{12}\right) \quad I_p = \frac{MR^2}{2}$$

Hence, an object may be considered to be a cylinder if

$$\frac{L}{R} > 0.866 \tag{3.60}$$

The angle τ for the principal inertia axes for a cylinder is given by

$$\tau_{\text{cylinder}} = \frac{-U_c}{MR^2/4 - ML^2/12} = +\frac{R}{L}\frac{m}{M}\frac{12}{(1 - 3(R/L)^2)} \tag{3.61}$$

Thus the inclusion of a dynamic unbalance couple on a rigid body will cause a shift in the principal inertia axes by a small amount τ. The rotational angle τ is negative for a disk and positive for a cylinder.

3.2.5 Two-Plane Rigid-Body Balancing by the Influence Coefficient Method

In general, two planes are required to balance a rigid-body rotor with arbitrary unbalance. Although the selection of the two balance planes is arbitrary, there are numerous practical considerations for proper selection. On long cylindrical rotors, the balance planes may be at the ends of the rotor. On a turbocharger shaft assembly, the planes may be the opposite disk faces rather than the extreme ends of the rotor.

The method of two-plane balancing was first presented by Thearle in 1934. Before the advent of the hand calculator and computer-generated solutions of the complex influence coefficients, the two-plane balancing method as originally presented by Thearle was a semigraphical procedure. The concepts presented by Thearle form the basis for the current influence coefficient method of balancing.

In balancing by the influence coefficient method, the values of the rotor mass or bearing properties do not have to be known. Measurements must be taken at two planes of motion with sufficient separation to yield two distinct sets of readings. The balancing planes do not have to correspond to the measurement planes.

The measurements may be of the bearing forces or supports (as in a hard bearing balancing machine), or of displacements of the rotor, or even velocity or acceleration of the casing or foundation. A third transducer, called the *key phasor,* is required to establish a timing reference mark on the shaft. The timing reference mark is compared to the peak amplitude (or zero crossing) of the vibration transducer to produce a phase reference angle of the vibration with respect to the timing mark.

The basic assumption of the influence coefficient method is that the vibration measured at a particular location at a fixed speed is the product of a linear combination of unbalances U_i and rotor influence coefficients a_{ij}. The influence coefficients, therefore, are not a function of unbalance or loading, but vary only with speed. This condition is identical to the assumption that the rotordynamic equations of motion are linear. For the normal situation in which the rotor unbalance weights are very small in comparison to the total rotor weight, this condition is closely approximated. For the case of a rotating gyroscope with large unbalance, the equations of motion are highly nonlinear, and an iterative balancing procedure must be used.

In employing the influence coefficient method of balancing, the rotor is spun to a fixed rotational speed. The synchronous amplitude and phase at the two vibration planes are recorded. These vibrations must remain constant in amplitude and phase with time, or else other factors such as thermal warping, bowing, or loose parts must be investigated.

The initial vibration readings at the two planes for the fixed speed ω are given by

$$\mathbf{Z}_1(\omega) = Z_1 \angle \phi_1 \qquad \mathbf{Z}_2(\omega) = Z_2 \angle \phi_2$$

where Z_i = amplitude of ith transducer and ϕ_i = relative phase angle in degrees.

The vibrations $\mathbf{Z}_1$ and $\mathbf{Z}_2$ are assumed to be linear combinations of the unknown unbalances $\mathbf{U}_1$ and $\mathbf{U}_2$ as follows:

$$\begin{aligned} \mathbf{Z}_1 &= \mathbf{a}_{11}(\omega)\mathbf{U}_1 + \mathbf{a}_{12}(\omega)\mathbf{U}_2 \\ \mathbf{Z}_2 &= \mathbf{a}_{21}(\omega)\mathbf{U}_1 + \mathbf{a}_{22}(\omega)\mathbf{U}_2 \end{aligned} \qquad (3.62)$$

To determine the speed-dependent influence coefficients, a trial weight $\mathbf{U}_t$ is placed at each balance plane, and the new vibrations are recorded.

After the placement of the trial balance weight $\mathbf{U}_{t1}$ at plane 1, these vibrations are recorded:

$$\begin{aligned} \mathbf{Z}_{11} &= \mathbf{a}_{11}(\mathbf{U}_1 + \mathbf{U}_{t1}) + \mathbf{a}_{12}\mathbf{U}_2 \\ \mathbf{Z}_{21} &= \mathbf{a}_{21}(\mathbf{U}_1 + \mathbf{U}_{t1}) + \mathbf{a}_{22}\mathbf{U}_2 \end{aligned} \qquad (3.63)$$

where $\mathbf{Z}_{11}$ and $\mathbf{Z}_{21}$ are the new vibrations recorded at planes 1 and 2 due to the trial weight placed in plane 1.

The influence coefficients $\mathbf{a}_{11}$ and $\mathbf{a}_{21}$ may now be computed as follows:

$$\mathbf{a}_{11} = \frac{\mathbf{Z}_{11} - \mathbf{Z}_1}{\mathbf{U}_{t1}} \qquad \mathbf{a}_{21} = \frac{\mathbf{Z}_{21} - \mathbf{Z}_2}{\mathbf{U}_{t1}} \qquad (3.64a)$$

In the normal influence coefficient method, the first trial weight is removed and a second trial weight $\mathbf{U}_{t2}$ is placed in the second plane (it is not necessary that the trial weights be identical). The resulting vibrations are

$$\mathbf{Z}_{12} = \mathbf{a}_{11}\mathbf{U}_1 + \mathbf{a}_{12}(\mathbf{U}_1 + \mathbf{U}_{t2}) \qquad (3.64b)$$

$$\mathbf{Z}_{22} = \mathbf{a}_{21}\mathbf{U}_1 + \mathbf{a}_{22}(\mathbf{U}_2 + \mathbf{U}_{t2}) \qquad (3.64c)$$

The influence coefficients $\mathbf{a}_{12}$ and $\mathbf{a}_{22}$ are given by

$$\mathbf{a}_{12} = \frac{\mathbf{Z}_{12} - \mathbf{Z}_1}{\mathbf{U}_{t2}} \qquad \mathbf{a}_{22} = \frac{\mathbf{Z}_{22} - \mathbf{Z}_2}{\mathbf{U}_{t2}} \qquad (3.64d)$$

In matrix form,

$$\begin{Bmatrix} \mathbf{Z}_1 \\ \mathbf{Z}_2 \end{Bmatrix} = \begin{bmatrix} \mathbf{a}_{11} & \mathbf{a}_{12} \\ \mathbf{a}_{21} & \mathbf{a}_{22} \end{bmatrix} \begin{Bmatrix} \mathbf{U}_1 \\ \mathbf{U}_2 \end{Bmatrix} \qquad (3.64e)$$

The balance correction weights are

$$\begin{Bmatrix} \mathbf{U}_{b1} \\ \mathbf{U}_{b2} \end{Bmatrix} = - \begin{Bmatrix} \mathbf{U}_1 \\ \mathbf{U}_2 \end{Bmatrix} = - \begin{bmatrix} \mathbf{a}_{11} & \mathbf{a}_{12} \\ \mathbf{a}_{21} & \mathbf{a}_{22} \end{bmatrix}^{-1} \begin{Bmatrix} \mathbf{Z}_1 \\ \mathbf{Z}_2 \end{Bmatrix} \qquad (3.65)$$

The balance correction $\mathbf{U}_{b1}$ for plane 1 is given by

$$\mathbf{U}_{b1} = - \frac{\begin{vmatrix} \mathbf{Z}_1 & \mathbf{a}_{12} \\ \mathbf{Z}_2 & \mathbf{a}_{22} \end{vmatrix}}{\begin{vmatrix} \mathbf{a}_{11} & \mathbf{a}_{12} \\ \mathbf{a}_{21} & \mathbf{a}_{22} \end{vmatrix}}$$

$$= - \frac{\mathbf{Z}_1 \mathbf{a}_{22} - \mathbf{Z}_2 \mathbf{a}_{12}}{\mathbf{a}_{11} \mathbf{a}_{22} - \mathbf{a}_{12} \mathbf{a}_{21}} \qquad (3.66)$$

The balance correction $\mathbf{U}_{b2}$ for plane 2 is given by

$$\mathbf{U}_{b2} = - \frac{\begin{vmatrix} \mathbf{a}_{11} & \mathbf{Z}_1 \\ \mathbf{a}_{21} & \mathbf{Z}_2 \end{vmatrix}}{\begin{vmatrix} \mathbf{a}_{11} & \mathbf{a}_{12} \\ \mathbf{a}_{21} & \mathbf{a}_{22} \end{vmatrix}}$$

$$= - \frac{\mathbf{Z}_2 \mathbf{a}_{11} - \mathbf{Z}_1 \mathbf{a}_{21}}{\mathbf{a}_{11} \mathbf{a}_{22} - \mathbf{a}_{12} \mathbf{a}_{21}} \qquad (3.67)$$

Example 3.7: Two-Plane Rigid Rotor Balancing by the Influence Coefficient Method.   The initial vibration readings on a rigid-body rotor are

$$\mathbf{Z}_1 = 8.6 \text{ mils } \angle 63° \qquad \mathbf{Z}_2 = 6.5 \text{ mils } \angle 206°$$

A trial balance weight of $U_{t1} = 10 \text{ g}$ is placed at a relative phase angle of 270°:

$$\mathbf{U}_{t1} = 10 \text{ g } \angle 270°$$

The resulting vibrations at planes 1 and 2 due to the placement of the trial weight at plane 1 are

$$\mathbf{Z}_{11} = 5.9 \text{ mils } \angle 123° \qquad \mathbf{Z}_{21} = 4.5 \text{ mils } \angle 228°$$

The influence coefficients $\mathbf{a}_{11}$ and $\mathbf{a}_{21}$ may be calculated as follows:

$$\mathbf{a}_{11} = \frac{\mathbf{Z}_{11} - \mathbf{Z}_1}{\mathbf{U}_{t1}} = \frac{5.9 \angle 123° - 8.6 \angle 63°}{10 \angle 270°} = \frac{7.61 \angle 200.9°}{10 \angle 270°}$$

$$= 0.7612 \angle -69.13° = 0.7612 \angle 290.9°$$

$$\mathbf{a}_{21} = \frac{\mathbf{Z}_{21} - \mathbf{Z}_2}{\mathbf{U}_{t1}} = \frac{4.5 \angle 228° - 6.5 \angle 206°}{10 \angle 270°} = 0.287 \angle 80°$$

The first balance trial weight is removed, and a trial weight of $U_{t2} = 12$ g at $180°$ is placed at plane 2. The resulting vibration readings are

$$Z_{12} = 6.2 \text{ mils} \angle 36° \qquad Z_{22} = 10.4 \text{ mils} \angle 162°$$

The influence coefficients at planes 1 and 2 caused by the trial weight placed at plane 2 are given by

$$a_{12} = \frac{Z_{12} - Z_1}{U_{t2}} = \frac{6.2\angle 36° - 8.6\angle 63°}{12\angle 180°} = 0.347\angle 105°$$

$$a_{22} = \frac{Z_{22} - Z_2}{U_{t2}} = \frac{10.4\angle 162° - 6.5\angle 206°}{12\angle 180°} = 0.6076\angle 303°$$

Let

$$\Delta = a_{11}a_{22} - a_{12}a_{21}$$
$$= (0.762\angle 291°)(0.608\angle 303°) - (0.347\angle 105°)(0.287\angle 80°)$$
$$= 0.398\angle 245°$$

Balance correction U_{b1} is given by

$$U_{b1} = -\frac{(8.6\angle 63°)(0.60\angle 303°) - (6.5\angle 206°)(0.384\angle 105.5°)}{0.398\angle 245°}$$

$$= -10.75 \text{ g} \angle 149° = +10.75 \text{ g} \angle 329°$$

and

$$U_{b2} = -\frac{a_{11}Z_2 - a_{21}Z_1}{\Delta} = -\frac{4.95\angle 136.8 - 2.47\angle 143°}{0.398\angle 295°}$$

$$= -6.27 \text{ g} \angle 245° = +6.27 \text{ g} \angle 65°$$

Figure 3.10 represents the relative positions on balance planes 1 and 2 of the trial balance weights and the final balance corrections. On each balance plane, 16 balance holes have been assumed. The balance holes have been labeled against rotation. In Fig. 3.10a, the first trial weight U_{t1} is shown placed at $270°$, which corresponds to balance hole 13. The final balance correction U_{b1} is a total of 10.76 g, and this should be placed between holes 15 and 16. A vector split of the 10.76-g balance weight is given as 5.31 g at hole 15 and 5.66 g at hole 16.

The balance weights satisfy the vector equation

$$U_{b1} = U_{15} + U_{16} \tag{3.68}$$

Figure 3.10b represents the placement of the trial balance weights and final balance correction for the second balance plane. The trial weight of 12 g at $180°$ corresponds to a weight placement at balance hole 9. The final balance correction U_{b2} is shown as 6.2 g to be placed in balance hole 4. If one chooses not to remove the initial trial weight from hole 9 for balance plane 2, then a trim balance correction of 15.63 g may be placed in balance hole 2. In cases where a trial weight is welded on, it may be desirable to add an additional trim weight rather than to remove the original trial weight.

The trim, trial, and balance weights in plane 2 satisfy the vector relationship

$$U_{b2} = U_{t2} + U_{\text{trim 2}} \tag{3.69}$$

Balance Plane 1

$$U_{b1} = 10.8 \text{ g} < 329^{\circ}$$

Balance Plane 2

$$U_{b2} = 6.2 \text{ g} < 65^{\circ}$$
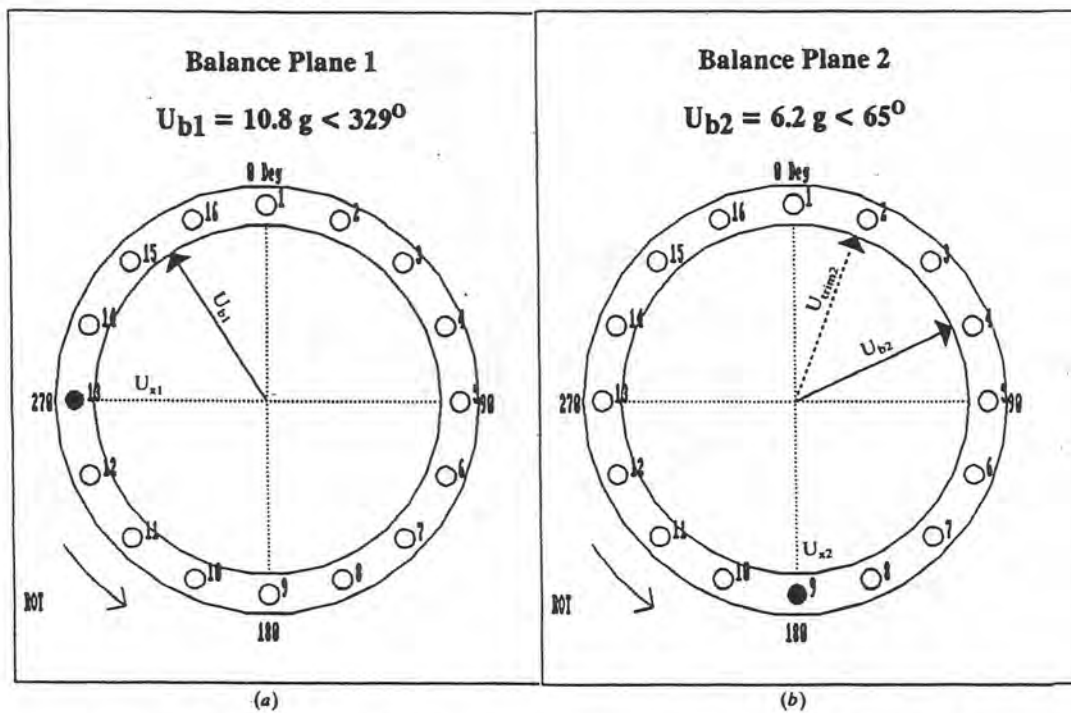
FIGURE 3.10 Radial and couple unbalance caused by an offset mass on a rigid body.

In cases where the balance correction is greater than 120° from the trial balance weight, it is preferable to remove the original trial weight. In this case, with the trial weight of 12 g left in hole 9, it would require a large trim weight of almost 16 g.

3.3 THEORY OF FLEXIBLE ROTOR BALANCING

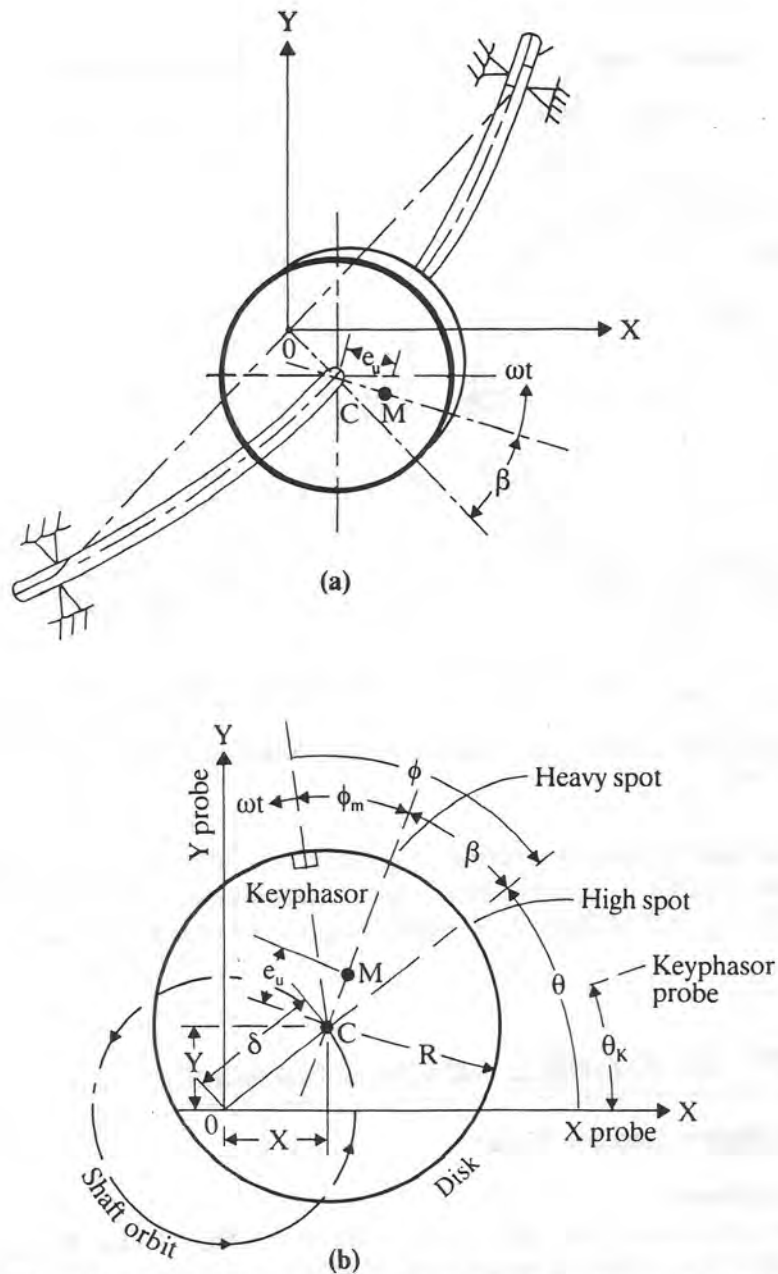### 3.3.1 Single-Mass Jeffcott Rotor

Description of Rotor

The idealized single-mass flexible rotor is shown in Fig. 3.11a. It represents a single-mass disk situated on a massless elastic shaft of stiffness K. The mass center of the disk is displaced from the center of the elastic shaft by distance e_u.

The analysis of the idealized single-mass rotor was first performed by H. H. Jeffcott (1919), to examine the effect of unbalance on the whirl amplitude and forces transmitted to the bearings.

Figure 3.11b represents a cross section of the Jeffcott rotor illustrating the mass-displacement relationships for the single-mass rotor. In the Jeffcott rotor, the mass is assumed to be located at the disk, and the shaft is assumed to be massless. The disk is assumed to be rotating with constant speed ω.

The mass center M is displaced from the shaft elastic centerline C by the distance e_u. The distance e_u is referred to as the *disk unbalance eccentricity*. The total rotor effective unbalance U is eual to the product of the mass of the disk or rotor and the unbalance eccentricity e_u.

The displacement of the disk mass M from the shaft elastic axis C causes a centrifugal unbalance to be exerted on the shaft at point C. This rotating

(a)

(b)

FIGURE 3.11 (*a*) Schematic view of deflected single-mass Jeffcott rotor; (*b*) cross section of Jeffcott rotor illustrating the mass displacement–phase relationship.

unbalance force causes the shaft centerline to precess or orbit about the idealized bearing centerline, point O, with a radius of δ at an angular velocity of ω rad/s. This motion is referred to as *synchronous circular precession*.

A reference mark called the *key phasor* is prescribed on the disk. It is used to determine a relative phase between the timing reference mark and the displacement vector $\boldsymbol{\delta}$. The angular location ϕ_m of the mass center or eccentricity vector $\mathbf{e}_u$ is measured from the keyphasor to the line of CM extended in a direction opposite to the direction of rotation.

The total inertial loading on the bearings is a function of the vector sum of the displacement $\boldsymbol{\delta}$ and the mass unbalance eccentricity vector $\mathbf{e}_u$. At low speeds

(below the rotor critical speed or natural resonance frequency), the unbalance eccentricity vector e_u and the shaft displacement vector δ are in phase.

The line of OC extended to the disk radius R marks a point on the shaft referred to as the *high spot of motion*. (For example, if one were to touch the orbiting shaft with chalk or a marking pen, the resulting mark would indicate the high spot of motion.)

The line of CM extended represents the line of action of the rotating unbalance load. The intersection of this line with the disk radius R is referred to as the disk *heavy spot*. At any given speed ω, the relative angular position of the triad of points O, C, and M is fixed with respect to each other. Points C and M orbit about the origin O with respect to a relative phase angle β, which is speed-dependent.

Flexible Rotor Equations of Motion

The forces acting on the flexible disk are the shaft elastic restoring force, rotor damping, rotor unbalance, and inertia force due to the mass of the disk. These forces may be combined by D'Alembert's principle to yield the rotor equation of motion

$$\mathbf{F}_{elastic} = -K\delta \tag{3.70}$$

where $K =$ shaft elastic stiffness coefficient and $\delta =$ vector deflection of the shaft centerline C from the bearing line of centers O. The angular speed ω rad/s of the rotor is assumed to be constant and is represented by the time derivative of the angle formed by the line CM fixed in the disk with respect to the fixed reference axis OX. The rotation of the disk causes a rotating unbalance force with magnitude

$$\mathbf{F}_u = Me_u\omega^2 = \mathbf{U}\omega^2 \tag{3.71}$$

The damping force opposing the motion is assumed to be proportional to the velocity and is given by

$$\mathbf{F}_d = -C\mathbf{V} = -C[\dot{X}\mathbf{i} + \dot{Y}\mathbf{j}] \tag{3.72}$$

The equations of motion for the single mass with radial unbalance is given in fixed cartesian coordinates by

$$\begin{aligned} M\ddot{X} + C\dot{X} + KX &= Me_u\omega^2 \cos(\omega t - \phi_m) \\ M\ddot{Y} + C\dot{Y} + kY &= Me_u\omega^2 \sin(\omega t - \phi_m) \end{aligned} \tag{3.73}$$

The equations of motion for the single-mass Jeffcott rotor may be combined into one complex vector equation by means of the complex variable transformation $\mathbf{Z} = X + iY$ as follows:

$$M\ddot{\mathbf{Z}} + C\dot{\mathbf{Z}} + K\mathbf{Z} = Me_u\omega^2 e^{i(\omega t - \phi_m)} \tag{3.74}$$

The complex variable $\mathbf{Z}$ represents the motion of the shaft centerline C.

Synchronous Unbalance Response of the Jeffcott Rotor

The vibration of the rotor as governed by Eq. 3.74 consists of an initial transient motion and a steady-state whirling or synchronous response caused by the rotating unbalance force:

$$\mathbf{Z} = \mathbf{Z}(t)_{transient} + \mathbf{Z}(\omega)_{steady\ state}$$

The steady-state complex rotor motion due to unbalance is given by

$$\mathbf{Z}_{\text{steady state}} = \frac{Me_u\omega^2}{K - M\omega^2 + iC\omega} e^{i(\omega t - \phi_m)} \qquad (3.75)$$

The complex rotor motion may also be expressed in terms of amplitude of the whirl orbit radius δ and the phase lag angle ϕ by

$$\mathbf{Z}(\omega) = \delta(\omega)e^{i(\omega t - \phi)} \qquad (3.76)$$

where δ = whirl orbit radius
$$= Me_u\omega^2[(K - M\omega^2)^2 + C\omega^2]^{-\frac{1}{2}}$$
ϕ = phase lag = $\phi_m + \beta$ $\qquad\qquad\qquad\qquad\qquad (3.77)$
ϕ_m = angular location of mass center with respect to keyphasor
$$\beta = \text{relative phase lag angle} = \tan^{-1}\frac{C\omega}{K - M\omega^2} \qquad (3.78)$$

The amplitude and phase may be further expressed in dimensionless form by using the following variables:

$$\omega_{\text{cr}} = \sqrt{\frac{K}{M}} = \text{natural frequency of shaft on rigid supports, rad/s}$$

$$C_c = 2M\omega_c = \text{critical damping, lb} \cdot \text{s/in}$$

$$\frac{C}{C_c} = \xi = \text{damping ratio}$$

$$\frac{\omega}{\omega_{\text{cr}}} = f = \text{frequency ratio}$$

$$\frac{C\omega}{K} = 2\xi f$$

$$A = \frac{\delta}{e_u} = \text{amplification factor}$$

The dimensionless shaft amplitude is given by

$$A = \frac{f^2}{\sqrt{(1 - f^2)^2 + (2\xi f)^2}} \qquad (3.79)$$

The relative phase-angle lag of the deflection vector from the rotating unbalance load is given by

$$\beta = \tan^{-1}\frac{2\xi f}{1 - f^2} \qquad (3.80)$$

There are three speed ranges of operation of the Jeffcott rotor that are of interest. These speed ranges are defined in terms of the frequency ratio f of the rotor angular velocity ω to the system critical speed ω_{cr}. The rotor amplitude and phase relationships vary considerably between the three speed regions.

From the standpoint of balancing, it is important to know in what speed range

the rotor is operating, in order to properly place correction weights on the rotor for the determination of influence coefficients for balancing.

The three speed ranges of interest are as follows:

1. Subcritical speed operation: $f < 1$, $\beta < 90°$

$$A \approx f^2$$

(Unbalance eccentricity vector $\mathbf{e}_u$ and deflection vector $\boldsymbol{\delta}$ are in phase.)

2. Critical speed operation: $f = 1$, $\beta = 90°$

$$A = \frac{1}{2\xi} = A_{cr} \qquad \text{critical speed amplification factor}$$

(Unbalance eccentricity vector $\mathbf{e}_u$ is leading the deflection vector by $\approx 90°$.)

**3.** Supercritical speed operation: $f \gg 1$, $\beta > 90°$

$$A = 1$$

Unbalance eccentricity vector $\mathbf{e}_u$ is out of phase to the deflection vector $\boldsymbol{\delta}$.

Figure 3.12 represents the dimensionless rotor synchronous response versus the speed ratio f for various values of the damping parameter $D = 2\xi$. Below $f = 1$ and for the curve $D = 0$ (no rotor damping), the rotor unbalance response increases as the square of the speed. Figure 3.13a represents the relative phase-angle change β, between the unbalance inertia load and the shaft centerline displacement vector $\boldsymbol{\delta}$, as given by Eq. 3.80.

For low values of D and for speeds below the critical speed ($f < 1$), the
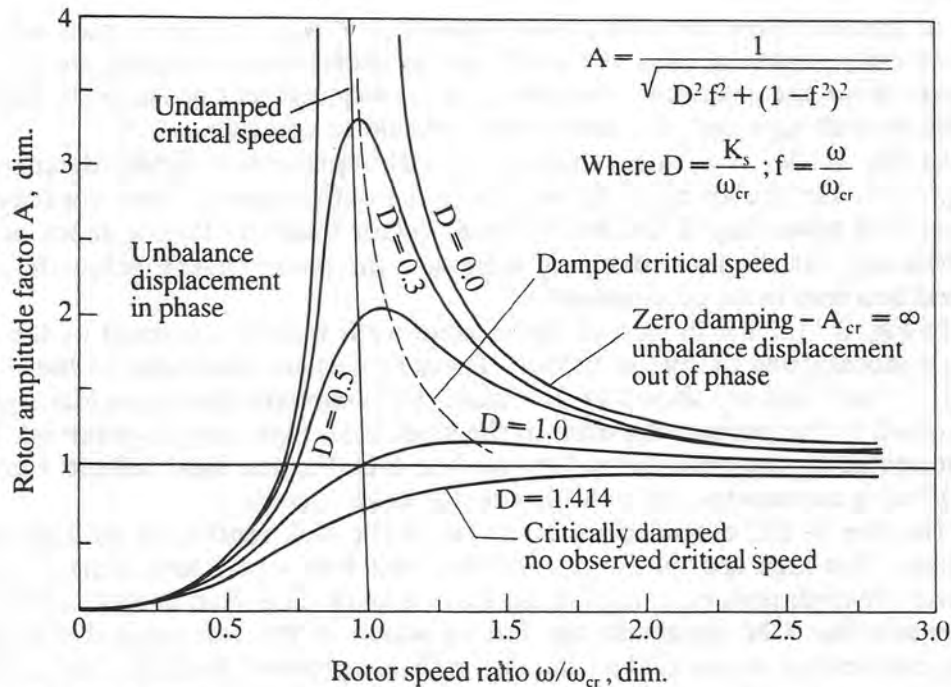
FIGURE 3.12 Dimensionless synchronous rotor unbalance versus speed ratio f for various values of damping parameter $D = 2\xi$ (Gunter, 1966).
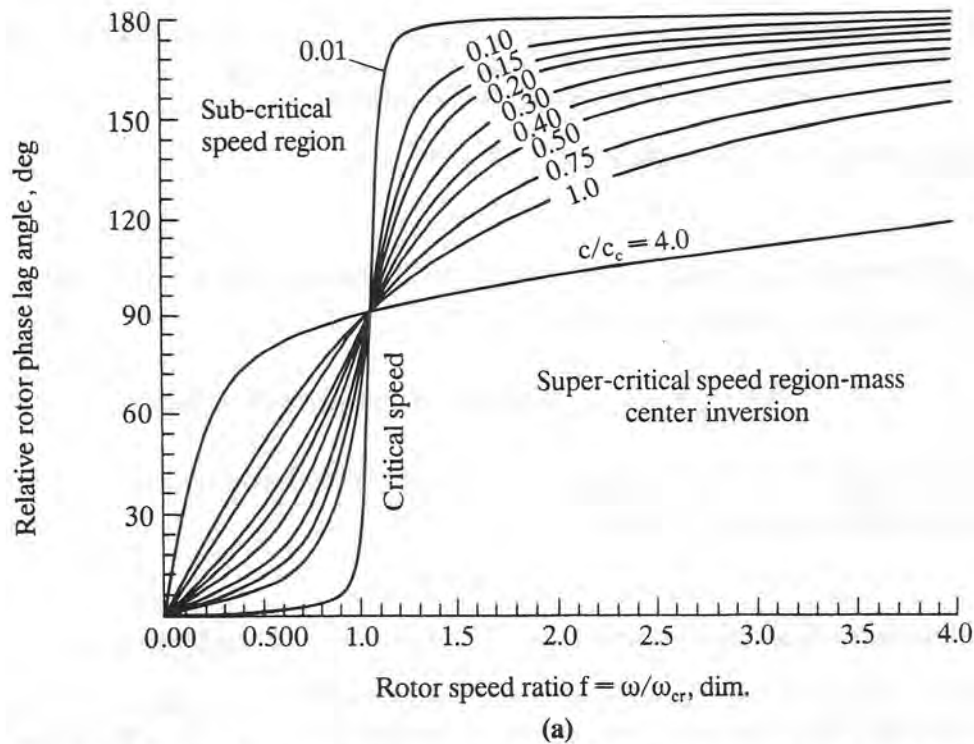
FIGURE 3.13 (*a*) Rotor relative unbalance force-displacement phase lag angle for various values of dimensionless damping ξ; (*b*) rotor displacement-mass phase relationship below, at, and above the critical speed; (*c*) definition of high spot with noncontacting proximity probe (Bently-Nevada Company, 1984a, b).

deflection vector δ lies along the same line of action as the rotating unbalance force.

At speeds below the rotor critical speed ($N < N_{cr}$), the rotor mass unbalance eccentricity vector e_u and the shaft elastic displacement vectors are in phase. Under these circumstances, the relative mass-displacement phase angle β is small, and the shaft high spot and heavy spot are said to coincide.

In Fig. 3.13*a*, e.g., the value of $\xi = 0.01$ represents a lightly damped rotor ($A_{cr} = 50$). For speeds up to 80 percent of the critical speed, there are only a few degrees of phase lag of the displacement vector from the forcing function (rotor unbalance). As the rotor damping increases, the phase change below the critical speed becomes more pronounced.

In Fig. 3.11*b*, the motion of the flexible rotor may be observed by the use of two noncontacting proximity probes. These probes are illustrated as the X probe and Y probe and are shown in the figure. By combining the sinusoidal signals as observed by the probes, the orbit of the shaft centerline may be observed. This is represented by the orbit formed by the line OC. For the ideal Jeffcott rotor with no bearing asymmetry, the orbit is circular at all speeds.

The line of OC extended to the radius of the disk represents the high spot of motion. The high spot is the part of the shaft that would first contact a closely fitting labyrinth seal, e.g., and would leave a mark on a shaft at this location. The extension line CM represents the line of action of the rotating unbalance load. The intersection of line CM on the disk radius represents the heavy spot, point U. The extension of line CM to point B represents the location on the disk wheel where the balance correction weight should be applied to counteract the unbalance eccentricity of the shaft.
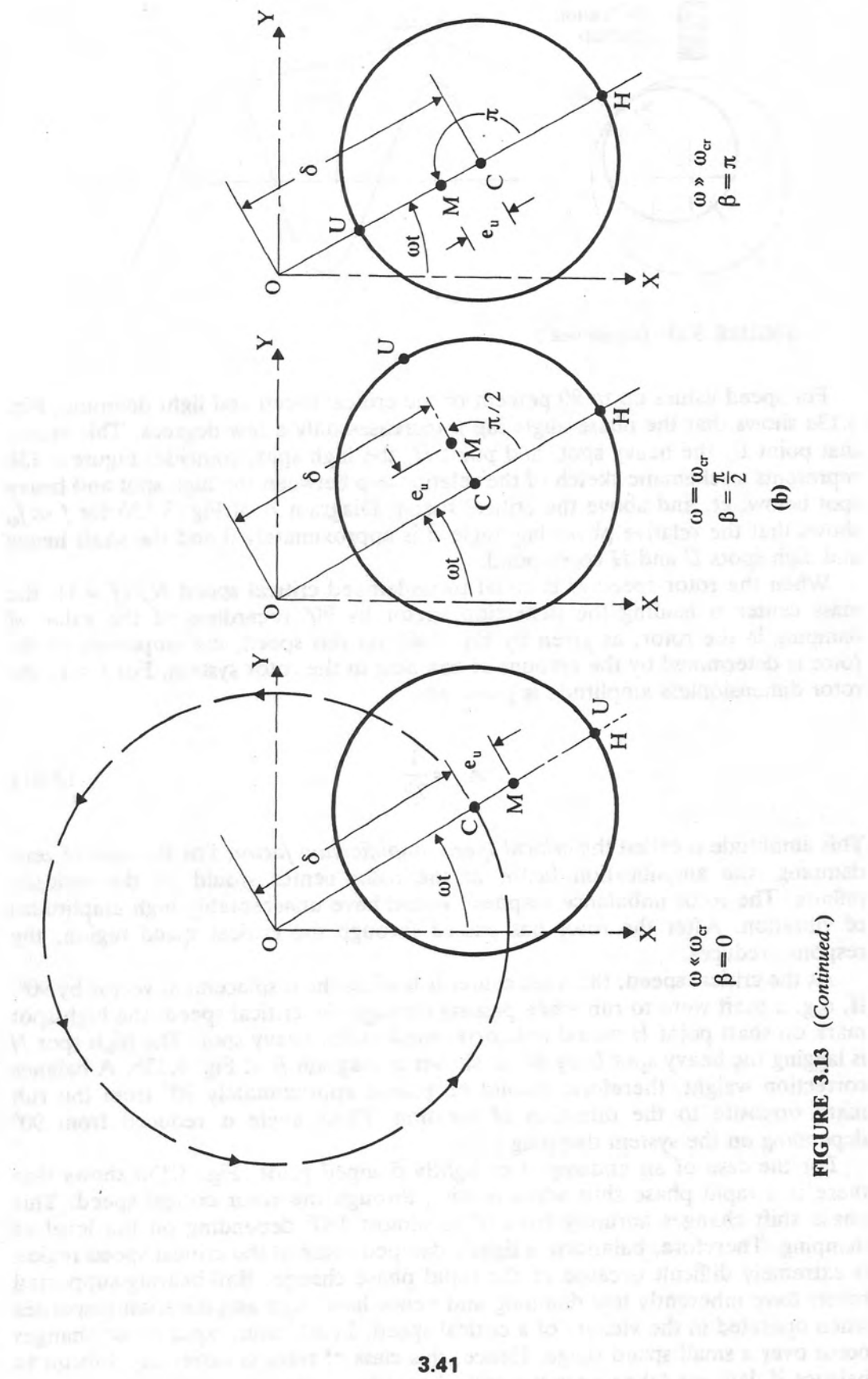
Y

X

O

δ

U

H

M

C

ω t

e_u

$\omega \ll \omega_{cr}$
$\beta = 0$

Y

X

O

δ

U

H

M

C

ω t

e_u

π/2

$\omega = \omega_{cr}$
$\beta = \dfrac{\pi}{2}$

(b)

Y

X

O

δ

U

H

M

C

ω t

e_u

π

$\omega \gg \omega_{cr}$
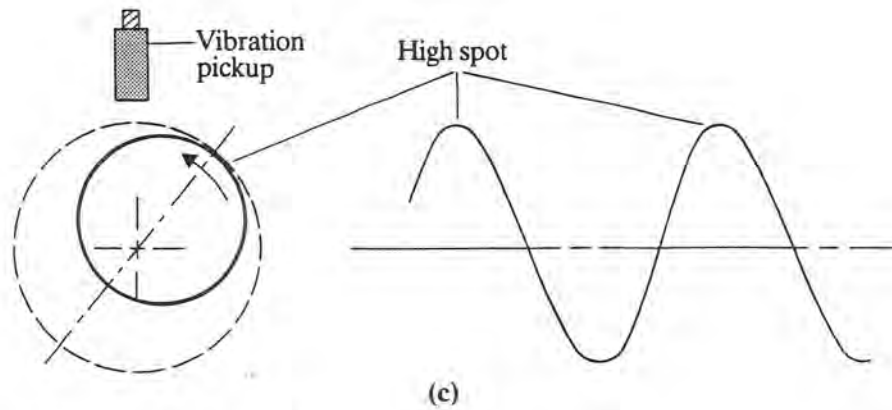$\beta = \pi$

FIGURE 3.13 (Continued.)

(c)

FIGURE 3.13 (*Continued.*)

For speed values up to 80 percent of the critical speed and light damping, Fig. 3.13a shows that the phase-angle lag β increases only a few degrees. This means that point U, the heavy spot, and point H, the high spot, coincide. Figure 3.13b represents a schematic sketch of the relationship between the high spot and heavy spot below, at, and above the critical speed. Diagram A of Fig. 3.13b for $f \ll f_{cr}$ shows that the relative phase lag angle β is approximately 0 and the shaft heavy and high spots U and H correspond.

When the rotor speed N is equal to undamped critical speed N_{cr} ($f = 1$), the mass center is leading the deflection vector by 90° regardless of the value of damping in the rotor, as given by Eq. 3.80. At this speed, the amplitude of the rotor is determined by the amount of damping in the rotor system. For $f = 1$, the rotor dimensionless amplitude is given by

$$A_{ct} = \frac{1}{2\xi} \tag{3.81}$$

This amplitude is called the *critical speed amplification factor*. For the case of zero damping, the amplification factor at the rotor center would be theoretically infinite. The rotor unbalance response would have unacceptably high amplitudes of vibration. After the rotor has passed through the critical speed region, the response reduces.

At the critical speed, the mass center is leading the displacement vector by 90°. If, e.g. a shaft were to rub while passing through the critical speed, the high-spot mark on shaft point H would not correspond to the heavy spot. The high spot H is lagging the heavy spot U by 90° as shown in diagram B of Fig. 3.13b. A balance correction weight, therefore, should be placed approximately 90° from the rub mark opposite to the direction of rotation. (This angle is reduced from 90° depending on the system damping.)

For the case of an undamped or lightly damped rotor, Fig. 3.13a shows that there is a rapid phase shift while passing through the rotor critical speed. This phase shift changes abruptly from 0° to almost 180° depending on the level of damping. Therefore, balancing a lightly damped rotor in the critical speed region is extremely difficult because of the rapid phase change. Ball-bearing-supported rotors have inherently low damping and hence have high amplification responses when operated in the vicinity of a critical speed. In addition, rapid phase changes occur over a small speed range. Hence, this class of rotor is extremely difficult to balance if data are taken near the critical speed region.

After the rotor passes through the critical speed ($f > 1$), the relative phase angle β increases beyond 90° and approaches 180° for speeds well above the critical speed ($f \gg 1$). This speed of operation is referred to as the supercritical speed range.

When the rotor is operating in the supercritical speed range, the eccentricity mass vector $\mathbf{e}_u$ and the deflection vector $\boldsymbol{\delta}$ are out of phase. The mass center M approaches point O, the spin axis center, in the limit as the rotor speed becomes very high.

Under these conditions, the rotor is said to be *self-balanced*. The heavy spot U approaches point O and is 180° out of phase to the rotor high spot, point H, as shown in diagram C of Fig. 3.13b.

Figure 3.12 shows that the rotor dimensionless amplitude A approaches unity at speeds well above the critical speed. This implies that the rotor whirl radius δ approaches the unbalance eccentricity $\mathbf{e}_u$ in magnitude, but 180° out of phase. If a chalk mark were placed on the rotor to indicate the high spot during supercritical speed operation, it would be 180° out of phase to the mass eccentricity vector. Therefore, an initial trial balancing weight should be placed at the location of the chalk mark or indicated high spot.

The high spot of shaft motion may be observed experimentally by means of a noncontact displacement probe mounted near the shaft. Figure 3.13c represents a shaft moving in a circular synchronous orbit. The vibration pickup records the sinusoidal motion as observed in that plane.

The harmonic waveform may be displayed on an oscilloscope. The high spot is represented by the peak amplitude on the waveform. As the shaft passes under the vibration pickup, the gap between the pickup and shaft reduces until the maximum amplitude of motion occurs when the shaft is directly under the probe.
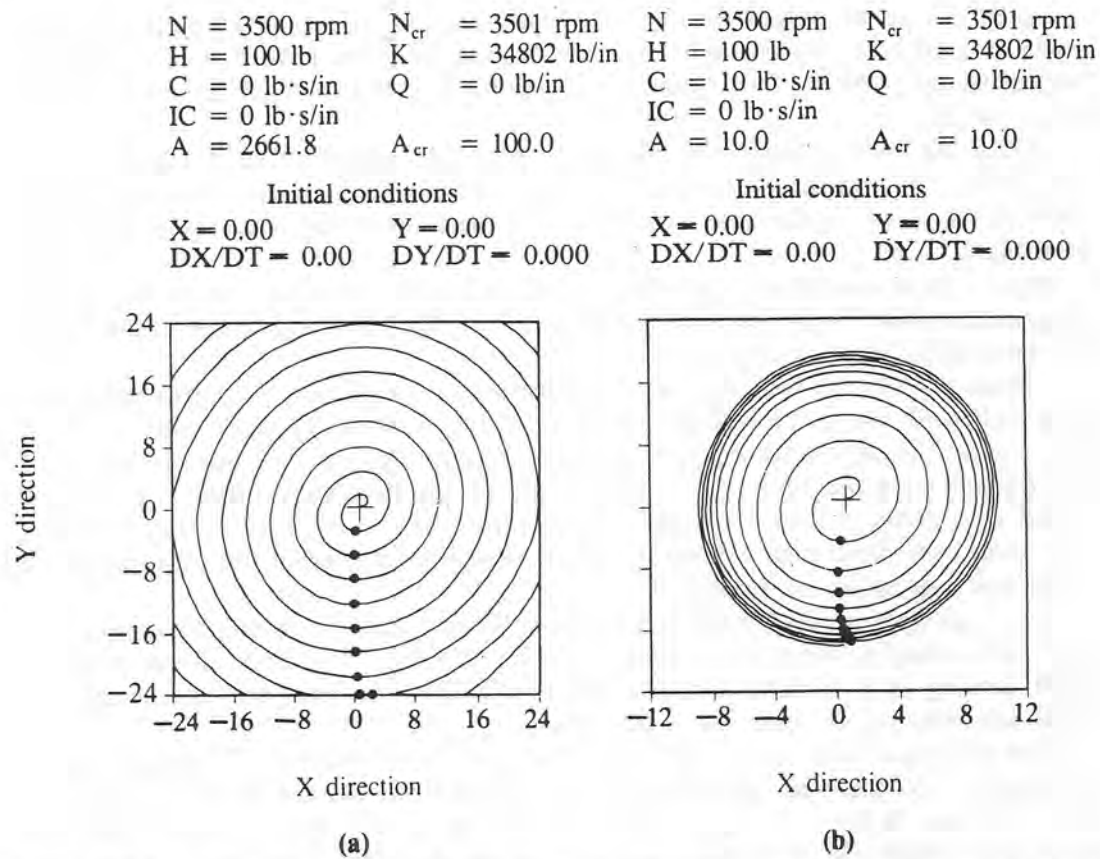
To find the high spot on the shaft, a timing mark must be provided on the shaft as a reference point to measure the phase between the moment when the timing mark passes under the probe and the maximum amplitude.

Figure 3.14 represents the transient motion of a rotor with a suddenly applied unbalance while operating at the critical speed. The situation simulates the loss of a turbine blade on an engine. Figure 3.14a represents the motion of the rotor at the critical speed with no damping in the system. The motion shown in this figure is similar to the motion that would occur with a ball bearing rotor attempting to operate in the critical speed region. This figure shows that the rotor amplitude increases with time in a linear fashion. The unbalance orbit will become unbounded unless the action of nonlinear shaft forces creates a limit cycle orbit.

If the rotor, however, is accelerated and the speed is increased above the critical speed, then the undamped rotor amplitude will decrease. Therefore, with sufficient acceleration, an undamped or lightly damped rotor may be forced to traverse the critical speed region without encountering unbounded amplitudes of response.

If the undamped rotor is slowly decelerated, when it reaches the critical speed region, the amplitude of motion will again start to increase linearly with time, unless there is a sufficiently rapid deceleration rate to remove it from the critical speed region.

On these orbits, timing marks for each cycle of motion have been placed to represent the effect of a keyphasor probe. These timing marks represent a 90° phase shift opposite to the direction of rotation from the location of the timing marks at speeds well below the critical speed. The observation of the location of the timing mark on the orbit is useful in determining the location of initial trial weights for balancing.

N = 3500 rpm	N_{cr} = 3501 rpm	N = 3500 rpm	N_{cr} = 3501 rpm
H = 100 lb	K = 34802 lb/in	H = 100 lb	K = 34802 lb/in
C = 0 lb·s/in	Q = 0 lb/in	C = 10 lb·s/in	Q = 0 lb/in
IC = 0 lb·s/in		IC = 0 lb·s/in	
A = 2661.8	A_{cr} = 100.0	A = 10.0	A_{cr} = 10.0

Initial conditions

X = 0.00	Y = 0.00
DX/DT = 0.00	DY/DT = 0.000

Initial conditions

X = 0.00	Y = 0.00
DX/DT = 0.00	DY/DT = 0.000

(a)   (b)

FIGURE 3.14 Transient motion at critical speed with suddenly applied blade loss (Kirk and Gunter, 1973): (a) no rotor damping, (b) $A_c = 10$.

The keyphasor probe fires when the shaft notch passes under the keyphasor probe. This signal may be inserted into the Z axis of an oscilloscope to form a timing mark on the orbit. For the case of Fig. 3.14b it is known that the shaft orbit corresponds to the rotor critical speed. In this case, the mass center is leading the displacement vector by 90°.

In Fig. 3.14b, the rotor has finite damping and an amplification factor of 10. This implies that the maximum response at the critical speed will be 10 times the unbalance eccentricity vector. Hence, the lower the amplification factor, the lower the response will be at the critical speed. Figure 3.14b shows that the orbit initially spirals outward in a fashion similar to the case of the undamped rotor. However, due to the action of the damping, the initial transient motion is suppressed, and a limit cycle synchronous whirl orbit of 10 times the unbalance eccentricity is achieved.

Polar Representation of Rotor Synchronous Amplitude and Phase Response
The synchronous Jeffcott rotor response and phase-angle change with speed as given by Eqs. 3.77 and 3.78 may be combined in a polar form, as shown in Fig. 3.15. In Fig. 3.15, the individual amplitude and phase plots, commonly referred to as *Bode plots,* are shown on the right-hand side (Bently-Nevada, 1984a, b). The amplitude and phase may be combined into a polar or Nyquist plot similar to the theory of transfer functions as employed in electric circuits. In this figure, the
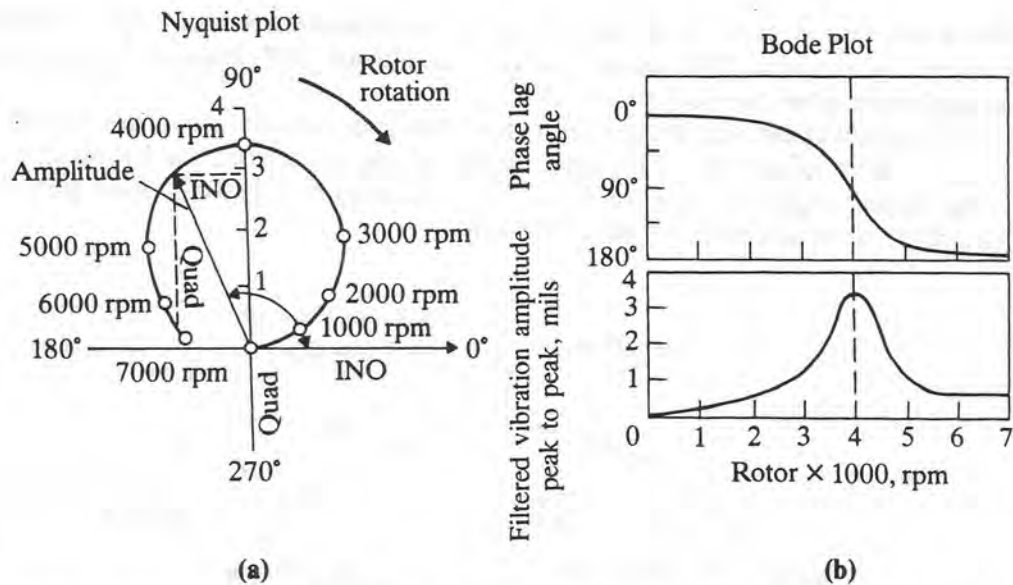
FIGURE 3.15 Typical Nyquist (polar) and Bode plots (Bently-Nevada Company, 1984a, b).

mass center is assumed to be located along the line of the timing mark or the keyphasor.

The rotor phase angle lag is measured from the X axis which is the $0°$ reference mark. As the rotor speed increases, the amplitude and phase increase, forming a polar plot. The phase-angle increase for the Jeffcott rotor is plotted in a direction opposite to that of shaft rotation.

The component of amplitude measured along the **X** axis is often referred to as the *co-component,* and the amplitude of motion measured along the **Y** axis is referred to as the *quad component.* For the Jeffcott rotor, the dimensionless co-component and quad component are given as

$$Co = \frac{f^2(1-f^2)}{(1-f)^2+(2\xi f)^2} \tag{3.82a}$$

$$Quad = \frac{-2\xi f^3}{(1-f^2)^2+(2\xi f)^2} \tag{3.82b}$$

The zero crossing of the in-phase or co-component indicates the location of the critical speed. The maximum value of the quad component, which occurs at the zero crossing of the in-phase curve, is equal to the rotor amplification factor. For example, in the Nyquist plot of Fig. 3.15 at a rotor speed of 4000 rpm, the rotor phase angle has shifted by $90°$. The $90°$ phase shift occurs at the rotor undamped critical speed.

As the rotor speed increases, the rotor amplitude reduces and the phase angle becomes greater than $90°$. At speeds above approximately twice the rotor speed, and the quad or out-of-phase component of the amplitude diminishes until a $180°$ phase shift is obtained. For the sample rotor plotted in Fig. 3.15, the phase inversion occurs approximately at speeds above 7000 rpm. Under these circumstances, the rotor displacement is $180°$ out of phase with the rotor mass center. The distance from the origin to the 7000 rpm speed point on the polar plot represents twice the rotor unbalance eccentricity value, assuming that the plot of

rotor amplitude is peak to peak. The rotor amplification factor may be quickly estimated by measuring the maximum quad amplitude (90° phase shift) divided by the amplitude after the 180° phase shift.

In an actual rotor, the mass center does not generally lie along the line of the timing mark or keyphasor. The mass center is displaced from the keyphasor axis by the phase angle ϕ_m. Figure 3.16, e.g., represents a typical polar plot of a single-mass rotor (Bently-Nevada, 1984a, b).

FIGURE 3.16 Polar plot for vertical probe (Bently-Nevada Company, 1984a, b).

In the displacement phase convention adopted by Bently-Nevada, the 0° reference mark is placed at the location of the monitoring probe. In this particular case, the probe is located at the vertical axis. Probe orientation is not restricted to either the horizontal or the vertical axis, but may, in general, be in any arbitrary orientation.

In the polar plot shown in Fig. 3.16, the direction of rotation is clockwise. The phase-angle change for the Jeffcott Rotor (in the absence of shaft bow or rub effects) is always against rotation. In this example, the phase lag angle is plotted in the clockwise direction.

The rotor has an amplification factor of 5. The resonance frequency occurs at 3000 rpm. At 9000 rpm which is 3 times the critical speed, the phase increases to 180°. This represents the inversion speed. A tangent drawn from this point to the origin represents the line of action of the mass unbalance.

For the rotor system illustrated, the mass unbalance lies along the 300° mark with respect to the vertical probe. Balancing weights, therefore, should be

applied at the 120° location. Figure 3.16 represents the dimensionless polar (Nyquist) plot for Q or the amplification factor for $A = 5$ (or $Q = 5$) for various values of the speed ratio f (Bently-Nevada, 1984a, b). In this idealized polar plot of the dimensionless rotor amplitude, the angular location of the rotor mass center ϕ_m from the timing mark is 300° against rotation. The peak amplitude is shown to occur at 3000 rpm with a corresponding phase lag angle of 30°. This represents a 90° phase shift from the low-speed value of 300°.

Phase Lag Angle at Maximum Rotor Unbalance Response Speed

It is important to understand that the maximum rotor response does not occur at the critical speed corresponding to the 90° phase shift. The maximum rotor response occurs at slightly higher speed and is given by

$$\omega_u = \text{unbalance response speed} = \frac{\omega_{cr}}{(1 - 2\xi^2)^{1/2}} \tag{3.83}$$

For $A = 5$ or $\xi = 0.10$, the speed ratio of maximum response is $f_{max} = 1.0102$. At this speed ratio the relative phase lag angle of the deflection vector to the rotor eccentricity vector $\mathbf{e}_u$ is 95.8°.

The speed at which maximum unbalance response is achieved, the *resonance response speed*, is higher than the rotor undamped critical speed depending on the system damping value, given by Eq. 3.83. For low to moderate values of ξ, the difference between the undamped critical speed and the maximum response speed is only a few percent.

There are three resonance frequencies or eigenvalues associated with the Jeffcott rotor. These frequencies are the system damped natural frequency ω_d, the system undamped natural frequency or critical speed ω_{cr}, and the speed at which maximum unbalance response amplitude is obtained ω_u. The relationship between these frequencies is

$$\omega_u > \omega_{cr} > \omega_d \tag{3.84}$$

where ω_d = damped natural frequency = $\omega_{cr}(1 - \xi^2)^{1/2}$

ω_u = maximum unbalance response frequency = $\omega_{cr}/(1 - 2\xi^2)^{1/2}$

The damped natural frequency (or damped system eigenvalue) is the frequency observed by striking or impacting the rotor. This frequency is always lower than the undamped rotor critical speed for the Jeffcott rotor. When the rotor speed reaches the value of the theoretical system natural frequency or critical speed, the mass center is leading the deflection vector by 90°. However, the theoretical critical speed (based on the undamped system eigenvalue) does not precisely represent the speed at which the maximum unbalance response will be obtained.

The speed of maximum unbalance response ω_u will always be slightly higher than the theoretical critical-speed value. Hence, the phase-angle relationship between the rotor mass center and the rotor deflection vector at maximum rotor response will be larger than 90°. The amount of phase increase beyond 90° is dependent upon the system damping.

Table 3.4 presents the relative phase angle β between the mass center and rotor deflection at the maximum unbalance response speed for various values of dimensionless damping ξ. For rotors with amplification factors above 10, the mass center is leading the deflection vector at the maximum response speed by approximately 90°. As the damping in the rotor system increases, the relative phase lag between the mass center and the displacement vector increases. For the

TABLE 3.4 Phase Angle and Frequency Ratio at Maximum Unbalance Response for Various Values of Damping ξ or Rotor Amplification Factor A_{cr}

ξ	A_{cr}	A_{max}	f_{max}	β_{max}	$\phi_{balance}$
0.05	10	10.0125	1.0025	92.9	87.1
0.10	5	5.025	1.0102	95.8	84.2
0.125	4	4.03	1.0160	97.2	82.8
0.15	3.33	3.371	1.0233	98.7	81.3
0.1667	3.0	3.042	1.0290	99.7	80.3
0.20	2.5	2.552	1.0426	101.8	78.2
0.25	2.0	2.06	1.0690	105.0	75.0
0.30	1.667	1.747	1.1043	108.3	71.7
0.40	1.250	1.364	1.2127	115.9	64.1
0.50	1.00	1.15	1.4142	125.0	55.0

relatively large amplification factor of 10, there is approximately a 3° increase in the phase angle beyond 90° at the maximum response speed.

As the system damping increases and the rotor amplification reduces, the speed at which the maximum unbalance response occurs increases. For example, for an amplification vector of 5, there is only a 1 percent increase in the forced response frequency above the natural frequency. However, the relative mass-displacement phase angle β is 96° at peak amplitude.

For highly damped rotors, the phase shift angle β at the maximum unbalance response speed may be substantial. For example, with a well-damped rotor with an amplification factor of only 2, the phase angle between unbalance and displacement at the forced response resonance frequency is 105°.

The value of $\xi = 0.5$ may be taken as the value of critical damping required for the Jeffcott rotor. For $\xi = 0.5$, the rotor critical speed amplification factor A_{cr} is 1.0. However, the maximum unbalance response occurs at 41 percent of the rotor critical speed. The maximum amplification factor at this speed is 1.15. The phase-angle shift observed at this speed is 125°. This represents a 35° shift beyond the theoretical value at the undamped critical speed.

3.3.2 Balancing the Single-Mass Jeffcott Rotor

There are various methods of balancing the flexible single-mass Jeffcott rotor. The first is sometimes referred to as factory balancing and consists of simply balancing the rotor and assembly as a rigid body on either a hard bearing or soft bearing balancing machine.

The other methods are often referred to as field balancing and involve operating the rotor through various speeds below, at, or above the critical speed and recording the appropriate amplitude and phase of motion. These various methods of field balancing are referred to as the influence coefficient method, the one-shot balance method, the modal method of balancing without trial weights, and the three-trial-run procedure without phase measurements. Each of these procedures has its distinct advantages and disadvantages.

Balancing by the Influence Coefficient Method—Ideal Single-Plane Balancing Analytical Procedure with Noncontact Probes

The influence coefficient method of balancing is one of the standard and widely used procedures today for field balancing of rotating equipment. The advantage of the influence coefficient method is that it requires very little knowledge of the rotating system (although this fact can also be a serious disadvantage). The procedure involves measuring the rotor synchronous amplitude and phase at one or more speeds. The rotor is then stopped, and a known trial or calibration weight is placed on the rotor at a specific radius and angular location as measured from a reference mark on the disk. Although the placement of the trial or calibration weight is arbitrary, it is preferable to place it so as to reduce the rotor response. Proper placement of the calibration weight may often be quickly determined by viewing the polar plot of the rotor response, if available.

For example, to place a calibration weight on the sample rotor as shown in Fig. 3.16, the timing mark on the disk would be lined up with the vertical probe. A calibration weight would be placed at 120° from the timing mark opposite the direction of rotation. This would place a component of correction unbalance at approximately 180° out of phase to the mass unbalance in the shaft. The magnitude of the calibration weight may be predicted or computed from the polar plot or computed by using the basic guideline that the calibration weight should create a rotating unbalance load of approximately 10 percent of the rotor static weight. This will ensure that an excessive amount of trial weight is not placed on the rotor, which could result in permanent shaft bowing or distortion, particularly with a built-up rotor configuration.

Equation 3.75 represents the complex vector response of the system with an unbalance. The rotor response Z may best be represented by a complex influence coefficient a, multiplied by the system unbalance U_u. When the influence coefficient method is used, it is assumed that the influence coefficient a is a function of rotor speed only. This implies that if a small correction weight is placed on the rotor, the influence coefficient at a particular speed will not change.

In an actual situation, the influence coefficient, for a given speed, does change with respect to the level of unbalance. This is due to various nonlinear effects in the system. Therefore, if a flexible rotor is badly out of balance, several balancing runs may be required to obtain a low vibration level due to the change in the influence coefficients with unbalance loading.

The rotor synchronous amplitude response Z may be expressed in terms of a complex influence coefficient a and the vector unbalance U_u as follows:

$$Z = a(\omega)U_u \qquad (3.85)$$

where

$$a(\omega) = \frac{f^2}{M(1 - f^2 + i2\xi f)}$$

and

$$U_u = Me_u e^{-i\phi_m} = Ue^{-i\phi_m}$$

The idealized influence coefficient is linear and is dependent on the speed. Therefore, it is not a function of the magnitude of the balance weight. In actual practice, the influence coefficient is affected by large balance weights due to various nonlinear effects in the system such as fluid-film bearings, seals, and nonlinear shaft effects under large deformation.

The vector unbalance U_u is expressed in terms of the product of the rotor mass M and unbalance eccentricity $e_u(U)$ and the phase lag angle ϕ_m. This angle represents the location where the unbalance U_u is located from the timing reference mark on the shaft, as measured in a direction opposite to rotation.

When the idealized single-mass Jeffcott rotor is balanced by using the influence coefficient method, it is assumed that the influence coefficients are repeatable at any given speed (no thermal bowing) and that the shaft is straight with no appreciable amount of runout. The object of the single-plane balancing by the influence coefficient method is to be able to determine the amount and angular location of the balance correction weight to be placed on the shaft. Thus, in single plane balancing, two unknown quantities must be solved for.

To employ the influence coefficient method of balancing, a trial or calibration weight is placed on the shaft at a given radius R and at a known angular location from the shaft timing or reference mark. The location of the trial weight should be such that the overall amplitude of motion is reduced upon application of the weight. The rotor response is then measured at the same speed as the initial vibration reading. The new amplitude of vibration may be expressed in terms of the influence coefficient a and trial unbalance U_t as

$$Z_t = a \times (U_u + U_t) \tag{3.86}$$

By subtracting the initial amplitude, the rotor complex influence coefficient may be obtained as follows:

$$a = \frac{Z_t - Z}{U_t} \tag{3.87}$$

The amount of unbalance in the system is given by

$$U_u = \frac{Z}{a} = Z \times \frac{U_t}{Z_t - Z} \tag{3.88a}$$

The balance correction weight U_b is considered to be equal and opposite to the rotor unbalance vector U. Hence the final balancing correction weight is

$$U_b = -U_u = Z \times \frac{U_t}{Z - Z_t} \tag{3.88b}$$

Example 3.8: Single-Plane Balancing Via a Mathematical Solution—Noncontact Probe. A rotor weighing 1000 lb has a recorded amplitude of 3.0 mils (peak to peak) at a phase lag angle of 270° using a standard noncontact displacement probe. A trial weight of 0.174 oz is placed at a radius of 9 in at a position of 30° from the timing mark against rotation. The equivalent trial unbalance is 1.57 oz · in. The rotating force caused by this magnitude of unbalance at 6000 rpm is

$$F_u = \frac{1.57 \text{ oz} \cdot \text{in}}{16 \text{ oz/lb} \times 386} \left(\frac{6000}{60} \times 2\pi \right)^2$$

$$= 100 \text{ lb}$$

The trial balance U_t thus exerts a force of 10 percent of the rotor static weight. This represents a reasonable magnitude of balance weight to apply to the rotor. One must be careful not to apply an excessive amount of trial weight that would

cause unbalance forces equal to the magnitude of the rotor weight, as this would lead to nonlinear effects.

After the trial weight is applied, a new rotor response is recorded with a magnitude of 2 mils at 170°. The influence coefficient is given by

$$
\begin{aligned}
\mathbf{a} &= \frac{\mathbf{Z}_t - \mathbf{Z}}{\mathbf{U}_t} \\
&= \frac{2e^{-i170} - 3e^{-i270}}{1.57e^{-i30}} \\
&= \frac{2[\cos(-170) + i\sin(-170)] - 3[\cos(-270) + i\sin(-270)]}{U_t} \\
&= -2.469e^{i89.5} - 2.469e^{-i90.5}
\end{aligned}
$$

The balance correction is given by

$$
\begin{aligned}
\mathbf{U}_b &= -\frac{\mathbf{Z}}{\mathbf{a}} = \frac{-3.0e^{-270}}{2.469e^{-i90.5}} \\
&= -1.21e^{-i179.5} \\
&= 1.21e^{-i359.5}
\end{aligned}
$$

Therefore, a correction balance of 1.21 oz · in (0.134 oz at 9-in radius) should be placed at the 0° reference mark.

Trim Balance Weight Correction

If the balance weight is left in the rotor, since the overall rotor amplitude is reduced, the resulting balance correction weight is referred to as a *trim balance correction*. The trim balance correction is based on Eq. 3.86, the rotor response after the initial trial weight has been added to the shaft. For the case where a weight is welded onto the rotor, it may not be convenient to remove the initial trial weight. If, however, the rotor response is much larger than the original rotor amplitude, not only should the trial weight be removed, but also the trial run $\mathbf{Z}_t$ should be repeated with either a reduced trial weight or a change in the angular location of the weight. The trim balance correction vector is given by

$$
\begin{aligned}
\mathbf{U}_{\text{trim}} &= -(\mathbf{U}_u + \mathbf{U}_t) = -\frac{\mathbf{Z}_t}{\mathbf{a}} \\
&= \frac{2.0e^{-i170}}{2.469e^{-90.5}} = -0.810e^{-i79.5} \quad (\text{since } -1 = e^{-i180}) \\
&= 0.810e^{-i259.5}
\end{aligned}
\tag{3.89}
$$

Therefore, the trim magnitude is 0.810 oz · in placed at an angle of 295.5° against rotation.

Figure 3.17 represents the balance plane in which the trial weight is added. In this example the balance plane is shown with 12 balance holes spaced evenly around the disk. In this case, the first hole is placed at the location of the keyphasor or timing reference mark on the shaft. The holes are labeled in the opposite direction to rotation. This is the preferred direction in which to label the balance holes. The holes will then appear in increasing sequence when the shaft is rotated or rolled over.

Single plane balancing of rotor with noncontact displacement probe rotor
speed = 6000 rpm, rotor weight = 1000 lb, U_t = 1.57 oz·in phase angle
convention: phase angles against rotation; trial U_t and U_b against rotation

Balance plane 1: near plane

Trial weight (solid circle):
U_{trial} = 1.57 oz·in
Phase = 30.00°
Total balance (solid line):
U_{total} = 1.21 oz·in
Phase = 359.53°
Trim balance (dashed line):
U_{trim} = 0.81 oz·in
Phase = 259.53°

Hole split: trim
0.294 oz·in @ hole 9
0.540 oz·in @ hole 10

FIGURE 3.17 Single-plane balancing with noncontacting vertical displacement probe.

For an impeller or fan, the fan blades should also be labeled opposite to the direction of rotation.

In this example, the placement of the trial balance component of $U_t = 1.57e^{-i30}$ oz·in implies the placement of 0.174 oz (5 g) at balance hole 2, which is at a radius of 9 in. The trial balance phase angle of −30° implies placing a weight in an angular position 30° against rotation, from the timing shaft reference mark.

The dark dot on Fig. 3.17 represents the placement of the trial balance weight in the second balance hole. If the trial weight is totally removed, then the calculated balance weight is 1.21 oz·in/9 in = 0.134 oz (or 3.831 g) to be placed in hole 1. Thus, the correct balance weight is 77 percent of the original trial unbalance, and the corrected angle is 30° clockwise from the placement of the original trial weight. If the correction angle is more than 90° from the location of the original trial weight, then an additional trim balance run may be needed for further improvement.

It is possible to leave the original trial weight in place and add a trim weight. Figure 3.17 shows that the trim weight should be 0.81 oz·in/9 in = 0.09 oz or 2.55 g between balance holes 9 and 10. Since the trim weight does not lie on top of a balancing hole, the trim vector may be split into two components for holes 9 and 10 to produce an equivalent effect. The hole split for holes 9 and 10, respectively, is 0.294 and 0.540 oz·in or 0.926 and 1.7 g to be placed in holes 9 and 10.

Thus the final balance correction for the wheel could consist of removing the original trial weight at hole 2 and placing 3.81 g in hole 1, or leaving in the original trial weight and placing approximately 1 g in hole 9 and $1\frac{3}{4}$ g in hole 10. Note that the hole-splitting computations could easily be performed with holes 8 and 11 if holes 9 and 10 already contain balance weights.

In the calculations shown, a right-handed coordinate system of units has been

adapted to correspond to Fig. 3.11*b* with the rotation vector in the +**Z** direction (counterclockwise) and positive angles measured from the *X* axis in the counterclockwise direction. Hence, in this convention, positive angles in an orthogonal right-handed coordinate system are measured in the direction ·of rotation (lead), and lag angles ·are measured against rotation. Since the same phase conventions for the balance weights and rotor response have been chosen (lag), identical results may be obtained by reversing the signs of the phase angles in the calculations.

Table 3.5 presents a summary of the balance calculations for the simple-plane correction using a noncontact displacement probe. The table shows the value of the initial amplitude and phase and the amplitude and phase after the trial or calibration weight has been placed on the shaft. The resulting influence coefficient · and total balance and trim balance connections are shown.

The standard phase-angle convention used with displacement probes is a lag phase-angle convention. This phase convention was initiated by Bently (1982) and is illustrated in Fig. 3.18 for shaft rotation in clockwise and counterclockwise directions.

The upper figure illustrates the phase convention for shaft clockwise rotation. When the timing reference pickup (or keyphasor probe) lines up with the timing mark on the shaft, a timing signal is generated. The timing reference signal is shown as a dot on the waveform, as illustrated on the right side of the shaft configuration.

The rotation or orbiting of the shaft generates a sinusoidal waveform, as shown in Fig. 3.18. In many cases, a pure harmonic waveform is not obtained. Under these circumstances, the output of the vibration sensor to a synchronous tracking filter will produce the required harmonic waveform. The phase angle is measured from the timing mark on the waveform to the peak amplitude. Figure 3.18*a* depicts a phase lag angle of 135° and clockwise rotation. From the measured phase angle, the high spot on the shaft may be determined. The shaft high spot is obtained by first lining up the keyphasor pickup to the timing mark on the shaft. The high spot on the shaft is determined by measuring from the probe (not the keyphasor!) in a direction opposite to rotation.

Figure 3.18*b* represents the phase convention with counterclockwise rotation. Note that, regardless of shaft rotation, the phase lag angle is measured on the waveform, in the direction of increasing time, to the first high spot on the waveform.

When synchronous tracking filters are used to obtain amplitude and phase, it is important to determine what phase convention the device is following. For example, one could measure from the timing mark to the zero crossover point, or one could measure from the peak amplitude to the timing mark. If this procedure is adopted, then one has a lead phase-angle convention.

In Table 3.5, to be consistent with the phase lag convention, the balance weight angle locations are measured from the timing mark against rotation. Therefore, it is critical in balancing to record the phase convention adopted for the balancing calculation and the type of instruments used in obtaining the experimental values of the amplitude and phase.

In Fig. 3.17, hole 1 has been assigned as the 0° reference position. The 0° position is usually placed at the location of the shaft reference mark. The angular coordinate system is labeled against rotation.

In summary, the phase angle measured with a noncontact probe is taken as the phase angle recorded from the point where the timing mark is triggered to the point where the peak amplitude of response ·is encountered. This procedure is

TABLE 3.5 Single-Plane Balancing with Noncontacting Displacement Probe—Lag Phase Convention

Rotor balancing computed results

Single-plane balancing of rotor with noncontact displacement probe: rotor speed, 6000 rpm; rotor weight, 1000 lb; $U_t = 1.57$ oz·in. Phase-angle convention: phase angles against rotation; trial U_t and U_b against rotation

System influence coefficients: units of mils or oz·in. All probe readings are in the lag convention.

Balance shot									Influence coefficient		
No.	Amp	Phase	Speed rpm	Prb no.	Amp 1, mils	Phase 1, deg	Amp 2, mils	Phase 2, ded	(Mag.)	Deg	Relative lag*
1	1.57	30	6	1	3.000	270	2.000	170	2.474	90	300

Initial and current response and predicted residual response

Speed no.	Probe no.	Initial		Current		Predicted		Change in amp	
		Amp mils	Phase, deg	Amp mils	Phase deg	Amp mils	Phase deg	Predicted initial	Predicted current
6	1	3.000	270	2.000	170	0.000	204	−3.000	−2.000

Balance correction weights

No.	Balance plane location	Total balance		X	Y	Trim balance	
		Mag., oz·in	Phase (lag)			Mag., oz·in	Phase (lag)
1	Near plane	1.21	360	1.2	−0.0	0.81	260

* Relative lag = amount the influence coefficient lags the trial weight.
† Note: Trim balance = (total balance) − (trial weight left in rotor).

3.54
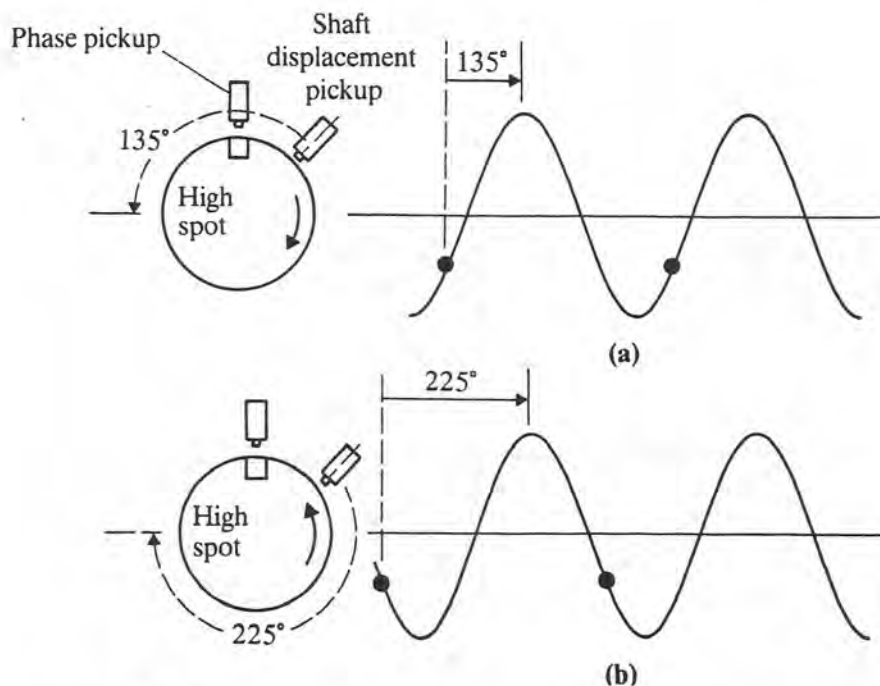
FIGURE 3.18 Phase lag measurements with shaft noncontacting probe for (a) clockwise and (b) counterclockwise rotation (Bently, 1982).

independent of the direction of shaft rotation. The high point on the shaft is obtained by measuring the required angle backward (against rotation) from the probe, after the timing mark has been lined up with the keyphasor probe. The identical result is also obtained by rolling the shaft forward (in the direction of rotation) by the required angle. The indicated high spot will lie under the probe. It is also preferable to use a consistent coordinate system for the placement of the balance weight. The balance weight locations are also measured from the keyphasor opposite to the direction of shaft rotation.

A lead phase convention could also be adopted for the balancing procedure when noncontact probes are used. There are currently on the market several designs of synchronous tracking filters that either give the phase angle as a lead angle or may be manually switched from a lag to lead phase convention. The lead phase convention is simply the complement of the lag angle; it is the angle measured from the peak response to the timing mark. If one adopts a lead phase convention, then it is desirable to measure the balance weight angles also in a lead convention. The lead convention for the angular placement of weights is taken as positive for angles measured in the direction of rotation.

Graphical Solution of Balancing with Noncontacting Probes

The balancing equation given by Eq. 3.89 may be represented by a graphical solution. It is only in the last decade that computer solutions to balancing have become standard with the introduction of small inexpensive handheld calculators.

Before the advent of the scientific handheld calculators (particularly with the ability to perform complex arithmetic), the standard procedure for single-plane balancing was to use a graphical solution. Graphical solutions are still highly desirable as checks on computer calculations.

Figure 3.19 represents the graphical balancing solution for the single-plane
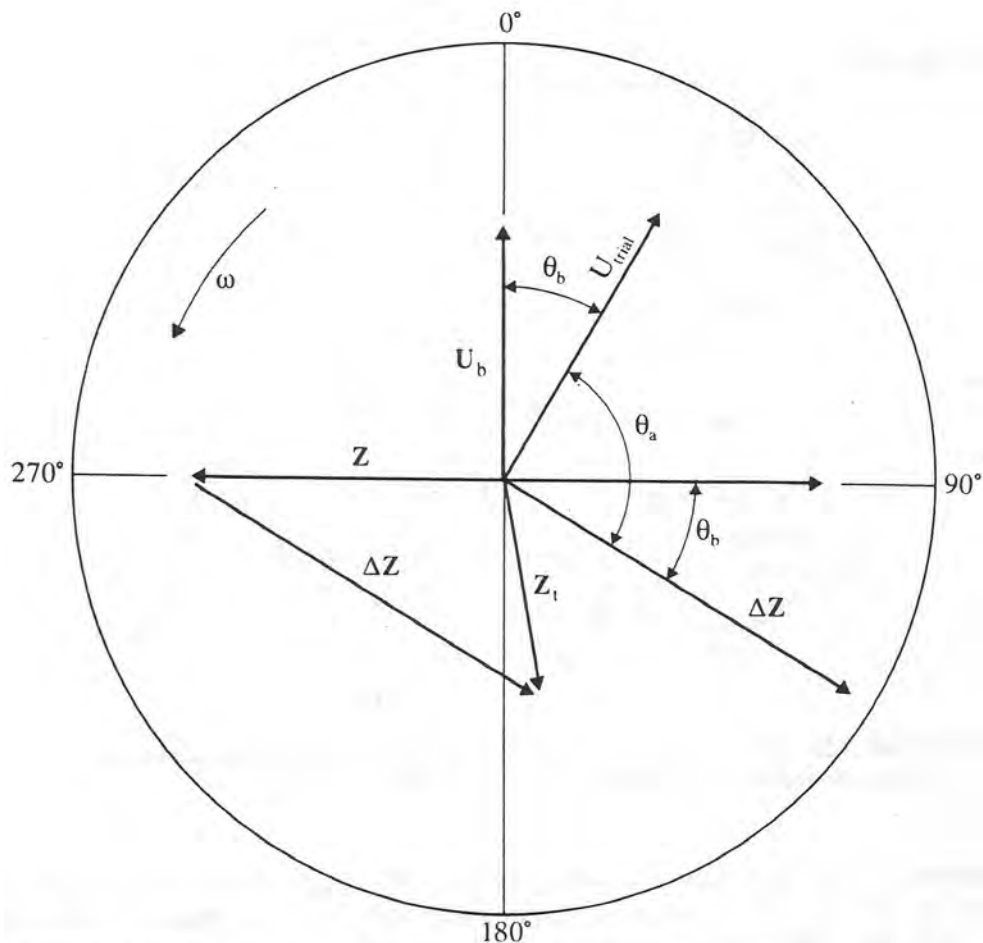
FIGURE 3.19 Single-plane balancing graphical solution with noncontacting displacement probes.

rotor using noncontact displacement probes. In the figure, the direction of rotation is shown as counterclockwise. The angles for phase and balancing are labeled in the clockwise direction, opposite to rotation.

The initial vector $Z = 3.0\angle 270°$ is drawn on the figure. The vector response $Z_t = 2.0\angle 170°$, obtained after the placement of the trial weight, is drawn next. The difference vector ΔZ is now constructed by drawing a vector from Z to the end of vector Z_t. The value of ΔZ is given by

$$\Delta Z = Z_t - Z = 2.0\angle 170° - 3.0\angle 270° = 3.88\angle 120.5°$$

A parallelogram is now constructed by using vectors Z and ΔZ. Thus, $\Delta Z = 3.88$ at 120° is graphically constructed.

Next the mirror image of Z is constructed. The angle between ΔZ drawn through the origin and the mirror of Z is measured. This angle is approximately 30°. It is desired that the placement of the new weight create a ΔZ vector which is equal to the original Z vector but acts in the opposite direction or along the mirror of Z. To have ΔZ act along the inverse Z direction, the balance weight must be shifted by 30° in the clockwise direction, as shown in Fig. 3.19.

The original trial balance had a magnitude of 1.57 oz · in. This trial balance caused a net rotor response of 3.88 mils. The magnitude of the influence

coefficient is

$$|\mathbf{a}| = \frac{|\Delta \mathbf{Z}|}{|\mathbf{U}_t|} = \frac{3.88}{1.57} = 2.47 \text{ mils/(oz} \cdot \text{in)}$$

Since the magnitude of the original vector $\mathbf{Z}$ is only 3 mils, the final correction weight is smaller than the trial weight and is given by

$$\mathbf{U}_b = \frac{|\mathbf{Z}|}{|\mathbf{a}|} = \frac{3.0}{2.47} = 1.215 \text{ oz} \cdot \text{in}$$

Thus the final balance is achieved by removing the trial weight and attaching a new balance magnitude of $1.21\,\text{oz} \cdot \text{in}$ from the original trial correction by approximately 30° in the counterclockwise direction.

The complete influence coefficient for this case may now be determined from the vector diagram. The trial vector is acting at 30° while the vector response is acting at approximately 120°. Thus the trial unbalance vector is leading the response vector by 90° in the direction of rotation. For the Jeffcott rotor, the 90° phase angle for the influence coefficient implies that the balancing calculation is being performed on top of the critical speed. One must be extremely careful when performing balancing calculations by the influence coefficient method at the critical speed since small changes in speed cause considerable changes in the influence coefficient. (We will show that the three-run method may be used to produce accurate balancing by recording the rotor amplitude at the critical speed.)

If the influence coefficient phase angle θ_a is greater than 90° but less than 180°, then the rotor is operating in the supercritical speed region and the mass center has inverted and is approaching the axis of rotation. It is preferable to take balancing readings in either the subcritical or supercritical speed region.

If, however, the influence coefficient phase angle θ_a, is greater than 180°, then the system is not a true single-mass Jeffcott rotor. The fact that the value of the influence coefficient phase angle is greater than 180° implies the influence of shaft bow, disk skew, or the approach of a second critical speed. Therefore, additional balance planes may have to be considered to achieve a low level of vibration response.

Single-Plane Balancing with Velocity Pickup and Strobe Light

For the case of flexible elastic rotor with little casing motion, it is preferable to balance by using noncontacting probes to monitor the shaft motion. For fairly stiff rotors mounted in rolling-element bearings, such as various types of motors, pumps, and fans, the relative shaft-bearing displacement may be small. There are a wide class of machines in which substantial vibration may be imparted to the bearing housing. Under these circumstances, the vibration may be monitored with a velocity pickup.

Another method to measure phase uses a strobe light which is triggered to flash based on the signal received from the vibration analyzer. The strobe light is made to flash on the shaft, freezing it in place. The strobe light flashes as the signal goes from negative to positive or positive to negative depending on the analyzer design (see Jackson, 1979).

The phase angle between the sensor's position and the distance that the high spot has traveled at the time the strobe light freezes the reference mark, placed on the rotor shaft end or a balancing ring, is very important in balancing. With a

tunable analyzer, the phase can vary with the filter adjustment and hence is correct only at the center band of the filter. There is also a phase shift with decreasing speed due to the frequency response of the velocity pickup, if it is a seismic sensor.

When a stobe light is used for a phase reference indication in balancing, the determination of the rotor high spot is not as simple or straightforward as when a noncontact probe and a keyphasor reference mark are used. Figure 3.20
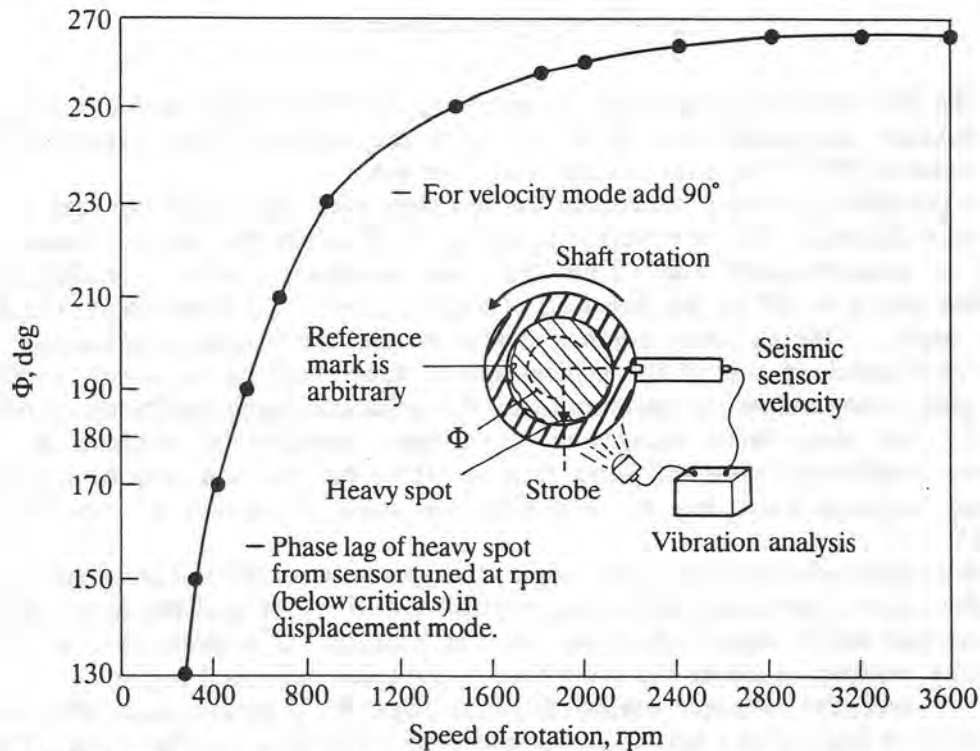

FIGURE 3.20 Phase lag from seismic velocity sensor to the rotor heavy spot.

represents the phase angle for a typical seismic vibration analyzer in the displacement mode. The seismic pickup measures the velocity of the bearing housing or foundation. Integrating the velocity signal to produce the displacement causes a 90° shift. In addition to the 90° phase shift, when one is integrating to obtain displacement, there is an inherent electronic phase shift of the instrument as well as a speed-dependent rolloff phase shift due to the inertia effects of the velocity sensor at low frequencies.

Figure 3.20 was developed by Jackson (1979) to help find the rotor heavy spot for guidance in placement of the initial trial weight for influence coefficient balancing. For example, if balancing of a subcritical speed rotor is to be accomplished at 1200 rpm, Fig. 3.20 shows that the phase angle of the high spot is located 244° from the sensor in the direction of rotation.

The rotor then is positioned where the reference mark is shown at 1200 rpm. (If an analyzer with a tuned filter is used, the analyzer must be carefully tuned to 1200 cycles/min, or a significant error will result.) If the rotor is assumed to be subcritical, then the high spot will coincide. A trial weight should then be placed 180° out of phase to the high spot for the first trial run to find the system influence coefficient.

Figure 3.21a represents the phase angle obtained with a perfectly balanced rotor after a 2-g trial weight has been placed on the rotor (Mechanalysis). The
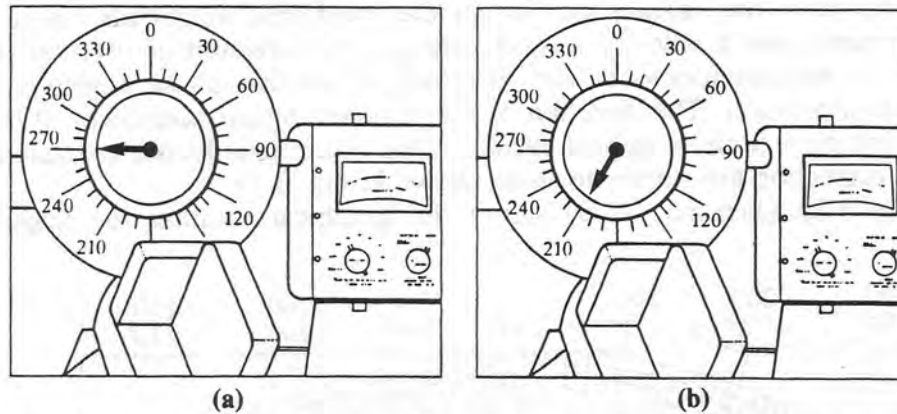
FIGURE 3.21 Phase reading with 2-g unbalance on balanced rotor: (*a*) placed on balanced rotor; (*b*) shifted 60° clockwise. (Mechanalysis).

phase angle here is shown drawn in a clockwise direction. In Fig. 3.21*b*, the weight is moved clockwise by 60°. The new phase angle recorded here is 210°. Hence, when a strobe is used to measure phase angles, movement of the rotor weight in the clockwise direction causes the phase angle to move in the counterclockwise direction. This effect is the same regardless of the direction of rotation.

When one is seeking a vector balancing solution with a strobe light reference system, the balancing procedure is modified. If the addition of the rotor trial weight has shifted the new vector Z_t in the clockwise direction, then the balance correction weight is moved from the relative angular location of the trial weight by the angle θ_a in the counterclockwise direction. Thus, the relative weight move is always opposite to the direction of shift of the trial vector Z_t, regardless of the direction of rotation.

Figure 3.22 represents the phase convention for the vibration signals and the
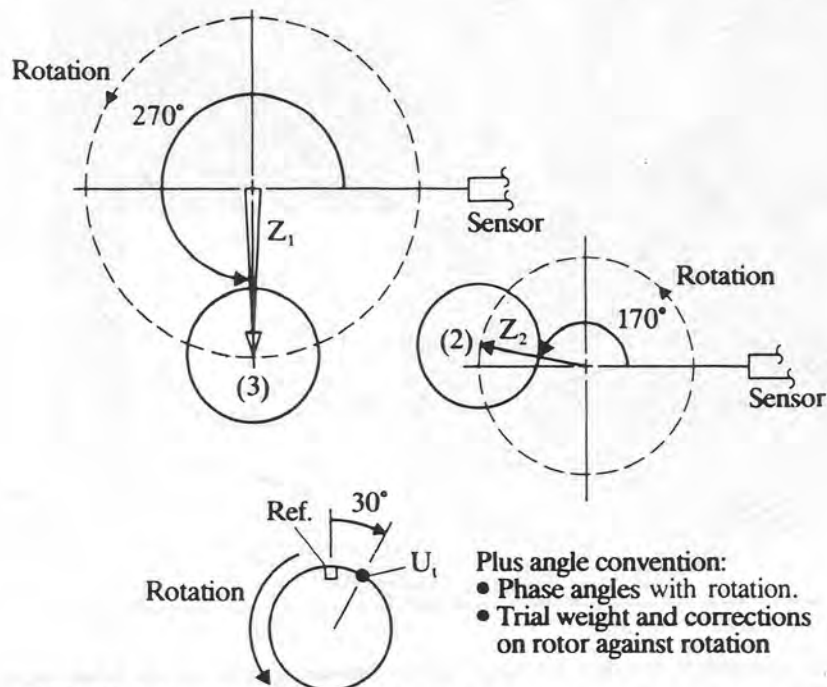
FIGURE 3.22 Single-plane balancing solution with strobe phase measurements.

measurement of the angular location of the rotor trial weight for strobe phase measurements and a velocity seismic pickup. The direction of rotation for this example is counterclockwise. The direction of positive phase angles is in the direction of rotation. The direction of the positive angular placement of the trial weight and corrections is against rotation. The resulting influence coefficients and angular correction are similar to those shown in Fig. 3.17.

Figure 3.23 (Jackson, 1979) shows the graphical solution for single-plane

FIGURE 3.23 Graphical solution for single-plane balancing with strobe phase measurements (Jackson, 1979).

balancing with a strobe phase reference using the IRD convention of weight movement. In this figure the initial vector **O** is drawn from the seismic sensor in the direction of shaft rotation (counterclockwise) by 270°. Afte a trial weight is placed on the shaft, the vector **O** + **T** results. This vector is 170° counterclockwise from the sensor. It has moved in the clockwise direction in relationship to **O**. The trial vector **T** forms an angle of 30° with respect to the negative initial vector (−**O**). Using the balance phase convention for strobe phase measurements, the final balance weight is moved 30° counterclockwise from the position of the initial trial weight since the vector **O** + **T** (or **Z**$_t$) moved clockwise.

3.3.3 Jeffcott Rotor with Shaft Bow

The dynamic unbalance response and balancing of the Jeffcott rotor with shaft bow were extensively investigated by Nicholas et al. (1976). Figure 3.24 represents the end and side views of the Jeffcott rotor with shaft bow. The amount of shaft bow is given by δ_r which represents the radial displacement or warp of the shaft from the theoretical axis of rotation. If the shaft were placed on knife-edges and slowly rotated, the disk centerline would describe an orbit of radius δ_r.
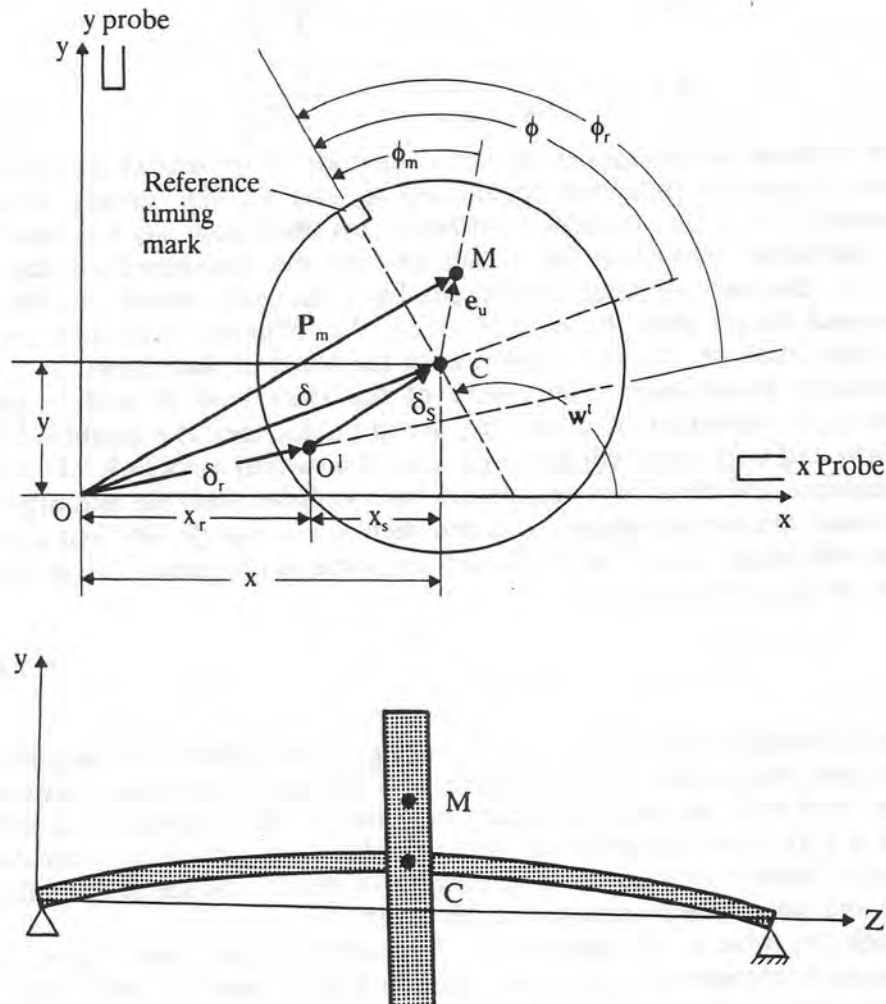
FIGURE 3.24 Single-mass flexible rotor with bowed shaft, end and side views.

The shaft bow is a vector and requires two quantities to describe it. The shaft bow is specified in terms of radial bow displacement δ_r and the phase lag angle ϕ_r from the shaft timing reference mark to the line of action of the bow. The shaft bowing produces an equivalent unbalance of magnitude $U_r = M\delta_r$. Therefore, only a few mils of shaft bow may result in a large equivalent unbalance.

In fact, this effective unbalance may be so large that it may be physically impossible to place enough correction weight on the shaft to compensate for the bow. Under these circumstances, the shaft bow must be reduced. This has often been accomplished in the field by peening the shaft on the high side to draw it.

In Fig. 3.24, the shaft X and Y probes observe the motion of the shaft centerline, point C. The complex vector equation of motion to describe the rotor response of the shaft centerline C is given by

$$M\ddot{Z} + C\dot{Z} + KZ = Me_u\omega^2 e^{i(\omega t - \phi_m)} + K\delta_r e^{i(\omega t - \phi_r)} \tag{3.90}$$

The steady-state synchronous response is given by

$$Z(\omega) = a_u e_u + a_r \delta_r \tag{3.91}$$

where

$$a_u = \frac{M\omega^2}{K - M\omega^2 + ic\omega} = \frac{f^2}{1 - f^2 + i2\xi f}$$

$$a_r = \frac{K}{K - M\omega^2 + ic\omega} = \frac{f^1}{1 - f^2 + i2\xi f}$$

The rotor response is determined by the magnitude of unbalance and shaft bow times their respective influence coefficients a_u and a_r. For speeds below the critical speed ($f < 1$), the influence coefficient for shaft bow has a greater effect than the influence coefficient for unbalance. At the undamped critical speed where $f = 1$, the two influence coefficients have identical values. As the speed becomes much larger than the critical speed, the influence coefficient for shaft bow becomes much smaller in comparison to the effect of shaft bow.

The relative phase-angle relationship of the shaft bow ϕ_r with respect to unbalance ϕ_m is important. If ϕ_r and ϕ_m are in phase, then the combined effects of shaft bow and unbalance will act to increase the overall amplitude of vibration. If the unbalance and shaft bow vectors are out of phase, then the two effects will help to reduce the overall vibration. If the vectors are exactly 180° out of phase, then there will exist a speed at which zero response is obtained. The dimensionless speed at which this occurs is

$$f = \left(\frac{\delta_r}{e_u}\right)^{1/2} \tag{3.92}$$

This speed is referred to as the self-balancing speed. The rotor amplitude of motion is zero only at this speed. Figure 3.25 represents the rotor response in which the shaft bow vector is one-half the value of the unbalance eccentricity vector ($\delta_r = 0.5$). The dimensionless rotor amplitude is plotted as a function of the frequency ratio f. At a speed of 70 percent of the critical speed, the effects of shaft bow and unbalance compensate each other.

Although the rotor is well balanced at 70 percent of the critical speed, clearly its unbalance characteristics are not satisfactory at other speeds. This is typical of the balance that would be achieved by the conventional single-plane method of balancing if performed at this speed. Conventional single-plane balancing would
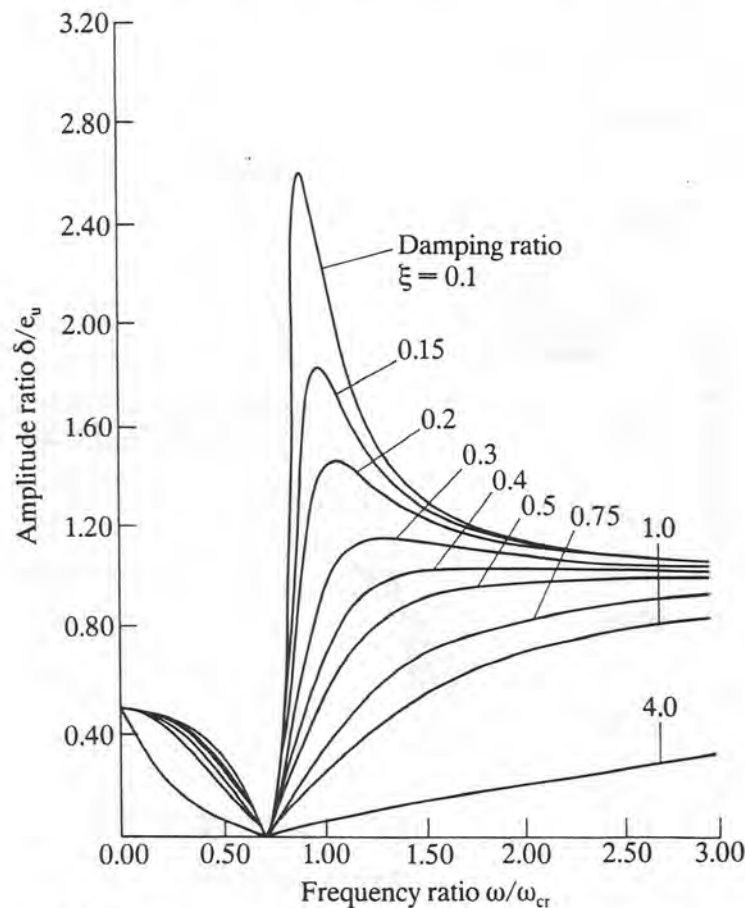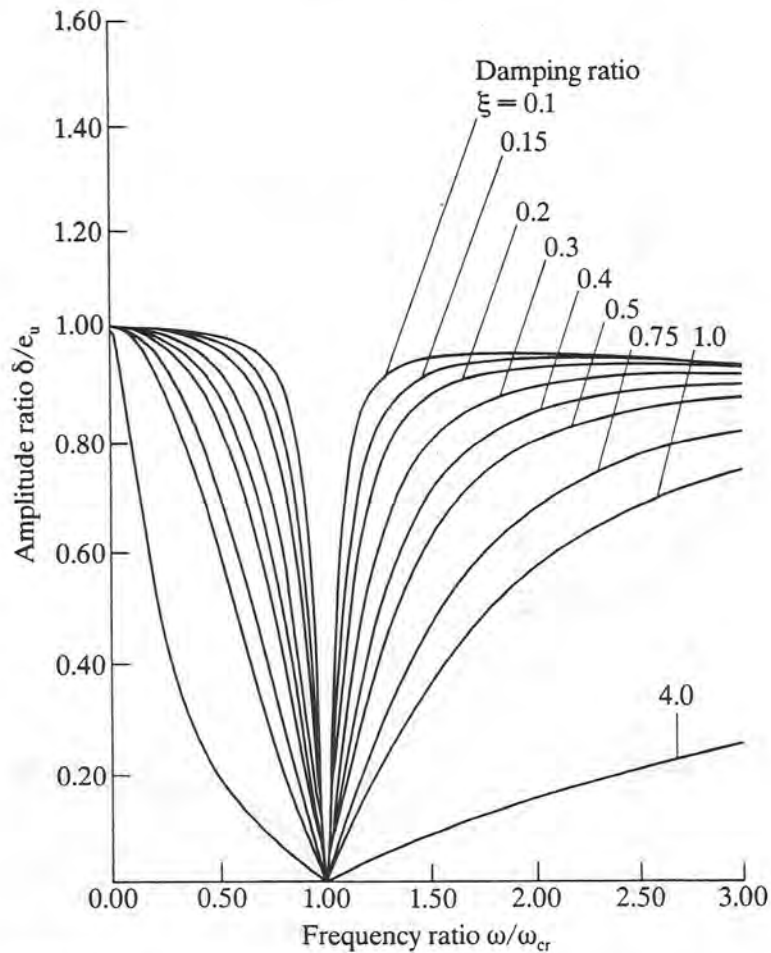
FIGURE 3.25 Response of a warped shaft with small shaft bow, out of phase to unbalance ($\delta_r = 0.5$, $\phi_r = 180°$) (Nicholas et al., 1976).

reduce the rotor response to zero, but the rotor would still be badly out of balance at the critical speed.

If the rotor amplitude starts to diminish before the critical speed, this then may be an indication that shaft bow is present in the shaft and out of phase with the unbalance. The relative magnitude of the shaft bow with respect to the rotor unbalance eccentricity may be obtained by observing the low-speed amplitude (the bow vector δ_r) in comparison to the high-speed response above the critical speed (the e_u vector).

In Fig. 3.25, the low-speed or slow-roll amplitude is only one-half the magnitude of the response above $f = 2$. This, then, is an indication that the effective rotor unbalance is twice the shaft bow. In this case, balancing will result in adding additional weight to the rotor in phase with the current bow vector, to reduce the overall response.

Figure 3.26 represents the rotor phase change for the shaft bow vector that is one-half the magnitude of the unbalance eccentricity vector and out of phase to it. The low-speed phase angle starts at 180° (since the bow vector is dominant). The phase angle increases until 70 percent of the critical speed is achieved. At this speed the rotor approaches zero amplitude. There is a 180° abrupt phase change after passing through this region. If the shaft bow vector is not exactly 180° out of phase, then a phase reversal will occur.

If the shaft bow is larger than and out of phase with the unbalance eccentricity,
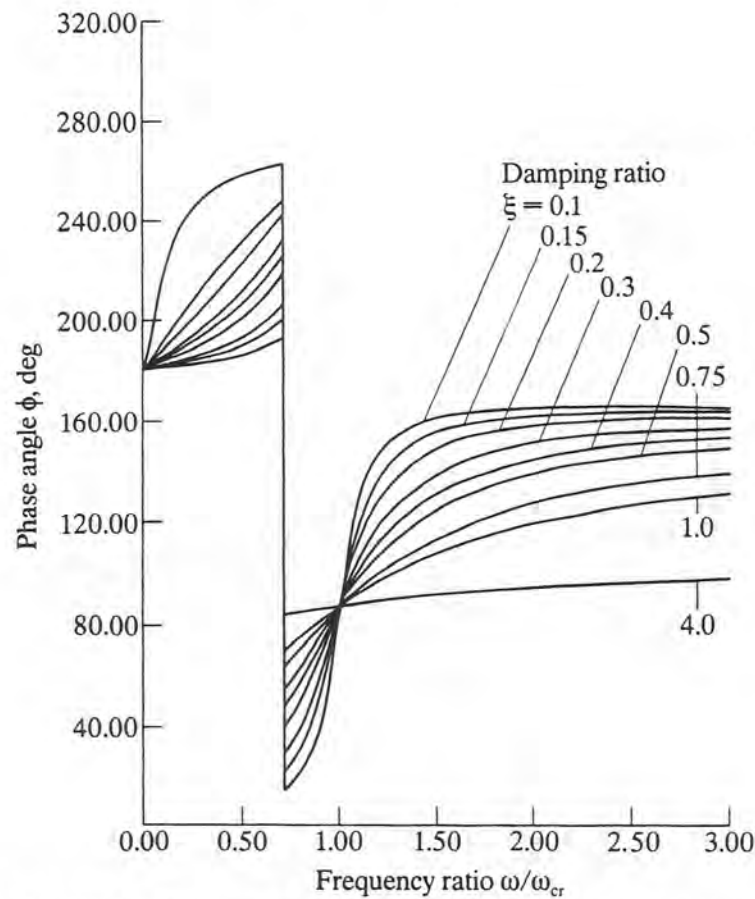
FIGURE 3.26 Phase angle of warped shaft ($\delta_r = 0.5$, $\phi_r = 180°$). Phase-angle curves with $\delta_r = 0.5$, $\phi_r = 180°$ for various damping ratios.

then the speed at which zero rotor response is observed will be above the critical speed. Figure 3.27 represents the rotor response in which the shaft bow vector is twice the unbalance eccentricity vector. In this case, the shaft self-balancing speed is 1.41 times the rotor critical speed.

If the shaft bow is identically equal to, but out of phase with, the rotor unbalance eccentricity vector, then the rotor will be self-balanced at the critical speed. Figure 3.28 shows the case where the shaft bow and unbalance eccentricity are equal but out of phase. At low speed the shaft runout is observed. As the rotor approaches the critical speed, the effects of shaft bow and unbalance cancel and the rotor motion reduces to zero. Upon a further increase in speed, this rotor amplitude increases and approaches e_u in the limit. To have the unbalance be exactly equal to and out of phase with the shaft bow is quite unusual in practice. However, such a situation has been observed by Jackson (1979) on acceptance tests for a large steam turbine.

The shaft bow vector is usually at an angle with respect to the rotor unbalance. Figure 3.29 represents the unbalance response of a bowed rotor in which the shaft bow is one-half the rotor unbalance eccentricity and lagging by 90°. By comparing the low-speed rotor amplitude to the response of the rotor above the rotor critical speed, one can determine the relative magnitude of shaft bow in comparison to
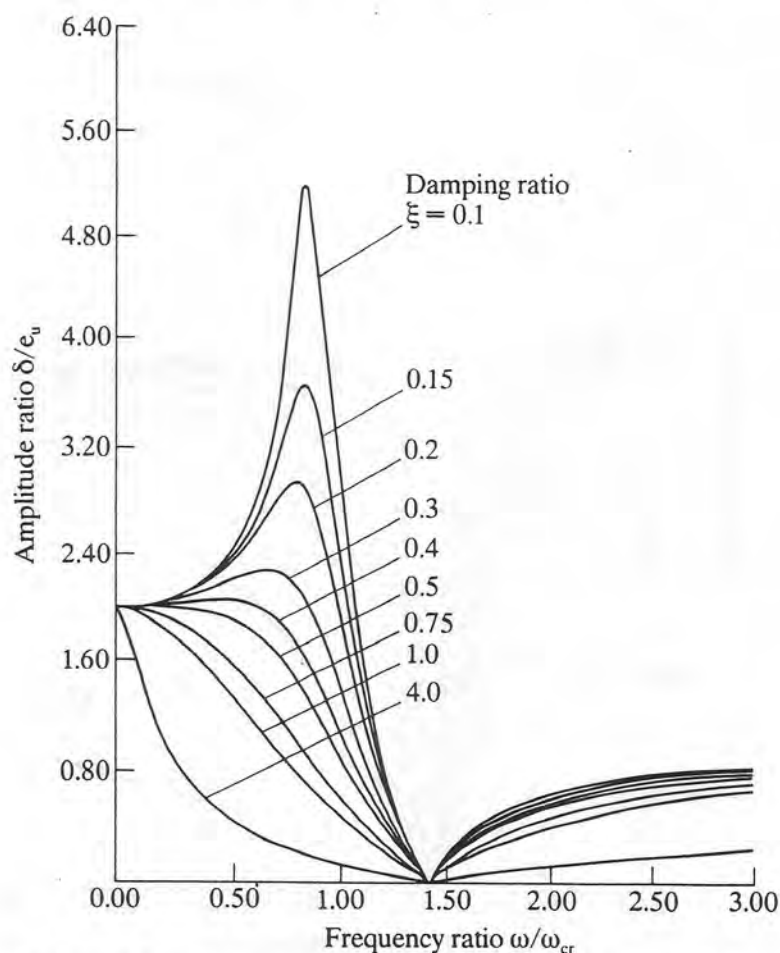
FIGURE 3.27 Response of a warped shaft with large shaft bow, out of phase to unbalance ($\delta_r = 2.0$, $\phi_r = 180°$).

rotor unbalance. In this case, the rotor response at high speeds is twice the low-speed or slow-roll runout vector.

Figure 3.30 represents the phase-angle change for various amounts of damping when the shaft bow vector lags the unbalance by 90°. The phase at low speed is at 90°. The bow vector, then, is lagging the timing mark by 90°. If one were to attempt to straighten out the shaft mechanically, one would first line up the shaft timing mark with the keyphasor probe. Then one would roll the shaft in the direction of rotation by 90°. The corresponding point on the shaft under the displacement probe represents the position of the shaft bow. This bow could be reduced by either mechanical loading or shaft peening.

One must be careful not to confuse a constant-runout vector with true shaft bow. If one is, e.g., monitoring the motion of a rotor at the impeller hub, rather than the shaft, one usually obtains a large runout vector. This runout vector is a constant and is superimposed on the actual shaft motion. The constant vector is due to the fact that it is impossible to machine a perfectly round and concentric hub at a large diameter. One always picks up a considerable runout vector. With a shaft bow, the vector response is not constant but varies with speed in magnitude and phase according to Eq. 3.91.

In Fig. 3.30, the initial phase is at 90°. As the speed is increased, the phase

FIGURE 3.28 Response of a warped shaft with shaft bow equal to unbalance, out of phase ($\delta_r = 1.0$, $\phi_r = 180°$).

angle reduces as the unbalance eccentricity vector begins to dominate. The minimum phase is observed at 70 percent of the critical speed. After this speed is reached, the total phase angle begins to increase. Since the phase reversal occurs at 70 percent of the critical speed, the shaft bow is less than the unbalance eccentricity. The ratio of shaft bow to unbalance is given as the square root of the speed at which phase reversal occurs. Hence δ_r is one-half of the unbalance eccentricity.

The rotor phase angle begins to increase until it reaches its maximum value at 180°. From this value, it is apparent that the unbalance eccentricity lies at the 0° position.

The total phase change of the rotor with shaft bow is only 180°. If the total phase change is over 180°, then other effects are occurring such as a second mode, disk skew, or foundation effects.

One can often identify the presence of shaft bow in a rotor by observing the timing mark on the rotor orbit. (This is similar to recording the phase.) Figure 3.31 is a schematic showing the movement of the timing mark on an oscilloscope screen for various values of shaft bow δ_r and angular location ϕ_r for an underdamped rotor.

In Fig. 3.31a we see the location of the shaft bow in relationship to the
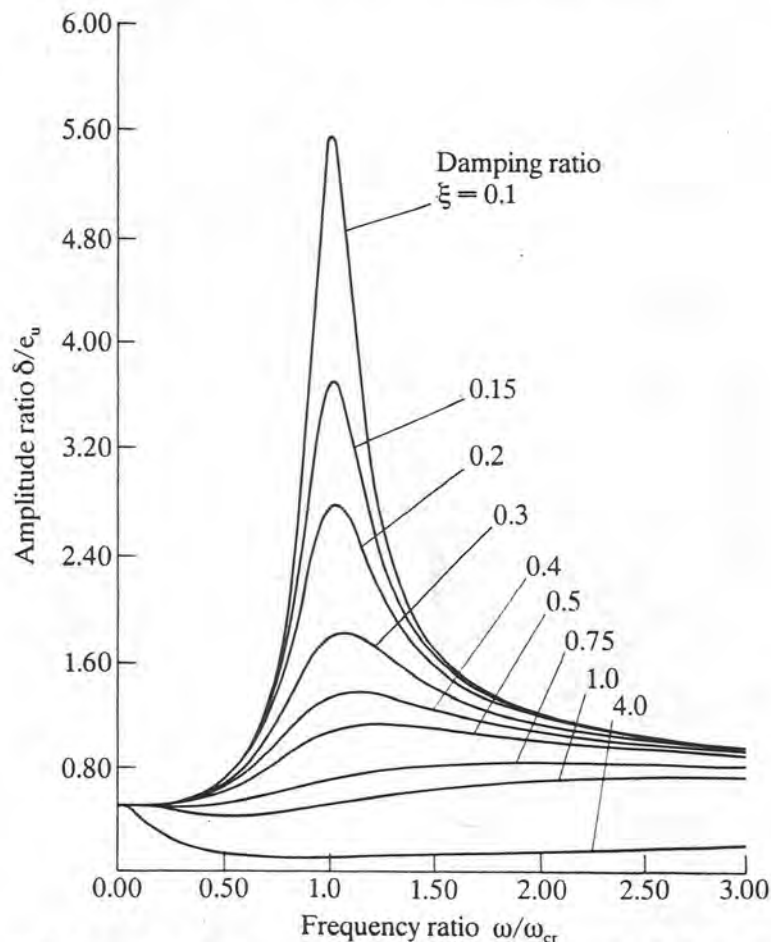
FIGURE 3.29 Response of a warped rotor with small shaft warp, 90° phase lag to unbalance ($\delta_r = 0.5$, $\phi_r = 90°$).

unbalance eccentricity vector, which is situated at the zero reference mark. Figure 3.31b shows the path of the timing mark for the case of no shaft bow. At low speed, $f = 0$, the timing reference mark is at 0°. As speed increases, the timing mark moves opposite to the direction of rotation until it is 180° out of phase at high speed ($f \gg 1$).

Figure 3.31c represents a rotor with a relative shaft bow of $\delta_r = 0.5$ at 90° lag from the unbalance. At low speed the initial phase is recorded at 90° (which is the influence of the bow vector only). As the speed increases to 60 percent of the critical speed, the phase angle reduces to 60°. Upon a further increase in speed, the phase angle increases, and at the critical speed the angle is 120° rather than 90°, as for pure shaft unbalance. Upon a further increase in speed, the phase angle approaches 180° in the limit as the rotor speed greatly exceeds the critical speed. In all cases shown, the timing mark will eventually reach 180° since at high speeds the mass unbalance eccentricity vector predominates and the shaft bow straightens out.

In Fig. 3.31d, the shaft dimensionless bow, δ_r, is twice the unbalance eccentricity vector e_u and is at 135°. Since the shaft bow is larger than the unbalance eccentricity, the shaft bow motion predominates until after the rotor has passed through the critical speed. At 110 percent of the critical speed, the maximum phase angle of 245° is observed. As the speed further increases, the phase angle reverses and approaches 180° in the limit.
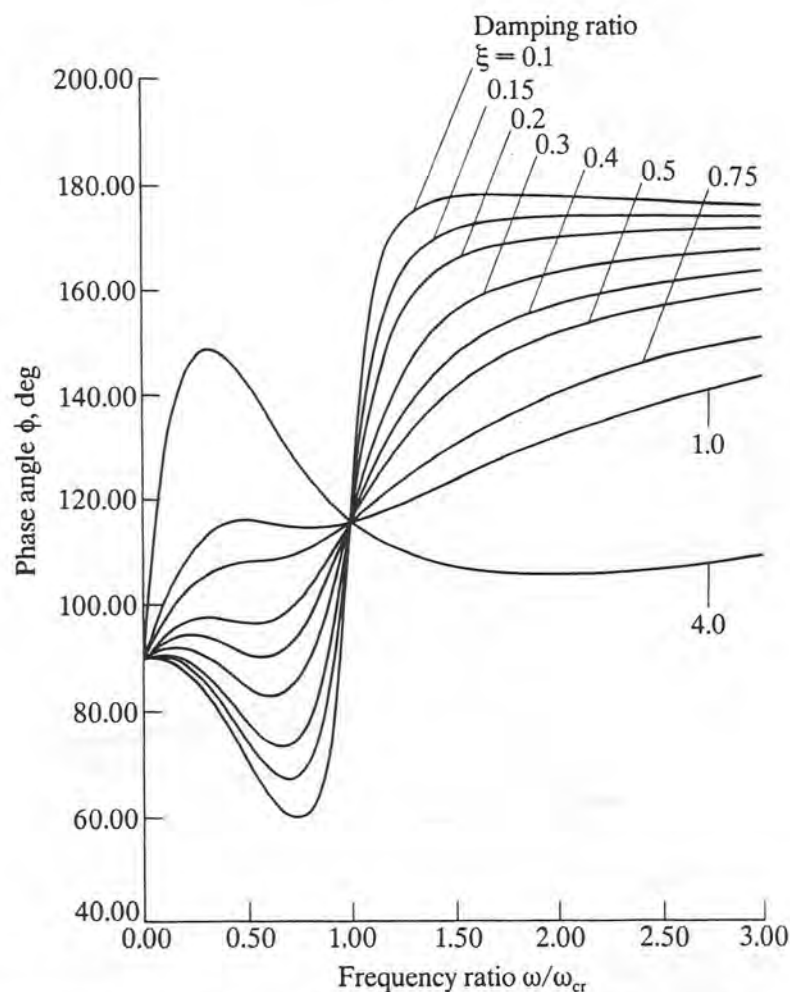
FIGURE 3.30 Phase angle with small shaft warp, 90° phase lag to unbalance ($\delta_r = 0.5$, $\phi_r = 90°$).

Hence, we see from these diagrams that the position of the inital timing mark on the orbit shows the orientation of the shaft bow. If phase reversal occurs below the critical speed, then the shaft bow is smaller than the unbalance eccentricity vector. If, however, the phase reversal occurs above the critical speed, then the shaft bow is larger than the unbalance eccentricity. It may not be desirable to attempt to balance a rotor with a large shaft bow since the required weights may be excessive and the bow vector may change with time.

Balancing the Single-Mass Jeffcott Rotor with Shaft Bow

There are several methods to balance a rotor with shaft bow. These methods may be best illustrated by the following example.

Example 3.9: Balancing a Bowed Rotor. We are given a rotor of 3.8 lb (1.73 kg) with a stiffness $K = 467$ lb/in (317.8 N/cm) and a damping $C = 0.22$ lb $\cdot$ s/in (0.385 N $\cdot$ s/cm). The unbalance eccentricity $e_u = 0.001$ in (1 mil) and is at a phase location of $\phi_m = 0°$.

The unbalance is in line with the timing mark. The shaft bow vector δ_r is 0.001 in and lags the unbalance vector by 90°. A schematic diagram of the unbalance and shaft bow is shown in Fig. 3.32 (Nicholas et al., 1976). The

(a) Sample scope setup   **(b)** Zero warp

(c) $\delta_r = 0.5$ $\phi_r = 90°$ **(d)** $\delta_r = 2.0$ $\phi_r = 135°$
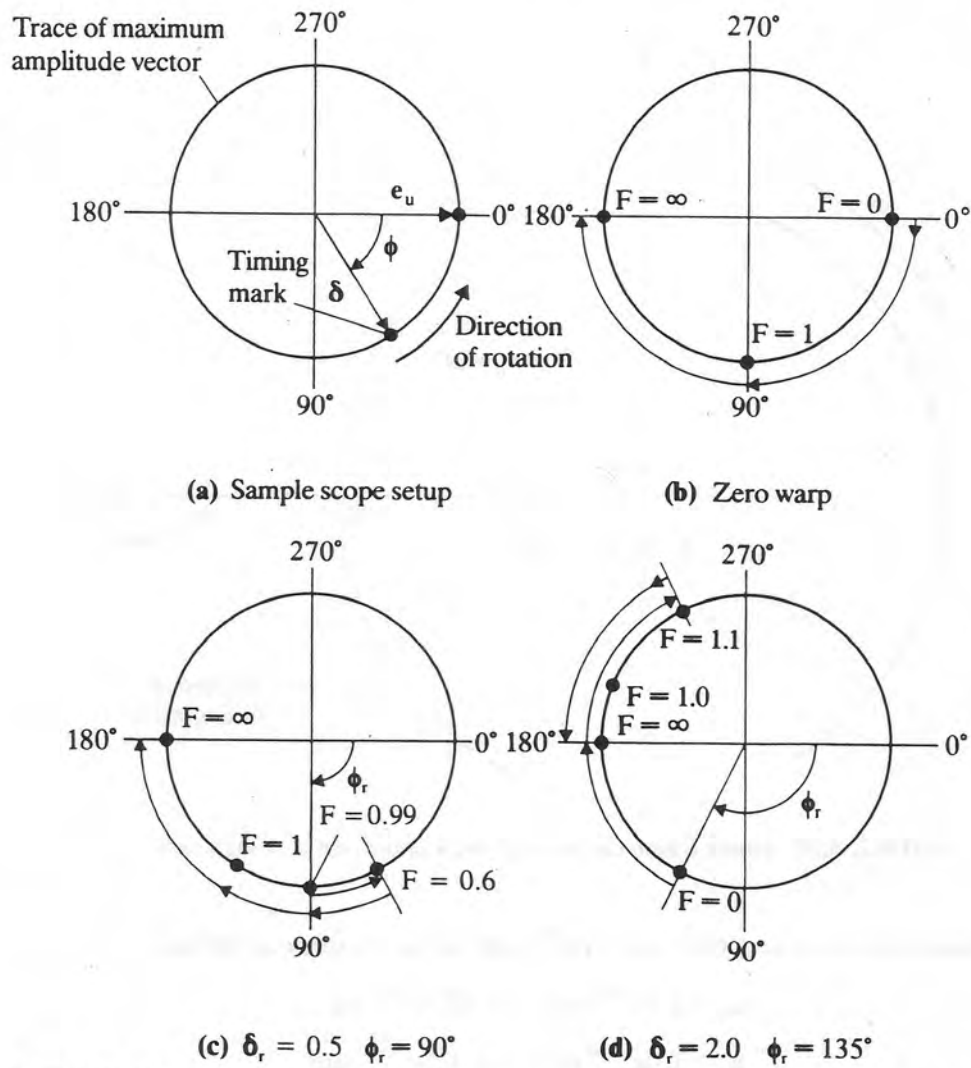
FIGURE 3.31 Schematic showing the movement of the timing mark on an oscilloscope screen as speed increases for various δ_r and ϕ_r values (Nicholas et al., 1976).

equivalent mechanical unbalance in the rotor is

$$U_u = 3.8 \text{ lb} \times 0.001 \text{ in} = 0.0038 \text{ lb} \cdot \text{in} = 1.72 \text{ g} \cdot \text{in}$$

$$\omega_{cr} = \sqrt{\frac{k}{m}} = \sqrt{\frac{467 \times 386}{3.8}} = 217.8 \text{ rad/s}$$

$$N_{cr} = 2080 \text{ rpm} = \text{critical speed}$$

$$C_c = 2M\omega_{cr} = 2 \times 3.8 \times \frac{217.8}{386} = 4.23 \text{ lb} \cdot \text{s/in}$$

$$\xi = \frac{C}{C_c} = \frac{0.22}{4.28} = 0.0514$$

$$A_{cr} = \frac{1}{2\xi} = 9.73$$

Note that the influence coefficient phase lag angle for the effect of shaft bow is identical to that for the unbalance response. Also note that since the balancing is performed below the critical speed, the influence coefficient due to shaft bow is larger than the influence coefficient for unbalance by the relationship

$$\frac{\mathbf{a}_u}{\mathbf{a}_r} = \frac{1}{f^2} \tag{3.95}$$

The total initial response at the balancing speed is given by

$$\mathbf{Z}_1 = \mathbf{a}_u \mathbf{e}_u + \mathbf{a}_r \mathbf{\delta}_r$$

$$= 2.79\angle -19.4° + 3.77\angle -109°$$

$$= 4.69\angle -72.9° \text{ mils } (11.9 \times 10^{-3} \angle -72.9° \text{ cm})$$

If a trial weight is placed on the shaft, the resulting amplitude $\mathbf{Z}_t$ is given by

$$\mathbf{Z}_t = \mathbf{a}_u(\mathbf{e}_u + \mathbf{e}_t) + \mathbf{a}_r \mathbf{\delta}_r \tag{3.96}$$

The influence coefficient for the effect of rotor mechanical unbalance is obtained by subtracting the initial response and dividing by the trial unbalance eccentricity $\mathbf{e}_t$:

$$\mathbf{a}_u = \frac{\mathbf{Z}_t - \mathbf{Z}_1}{\mathbf{e}_t} = 2.79\angle -72.9° \tag{3.97}$$

(Note that the units of $\mathbf{a}_u$ may vary depending on how one wishes to express the trial calibration component; mils eccentricity, gram-inches, etc.)

In the standard influence coefficient method of balancing it is assumed that the rotor response is dependent on only the mechanical unbalance. The balance eccentricity is given by

$$\mathbf{Z}_{\text{balance}} = \mathbf{a}_u(\mathbf{e}_u + \mathbf{e}_b) = \mathbf{Z}_1 + \mathbf{a}_u\mathbf{e}_b = 0$$

$$\mathbf{e}_b = -\frac{\mathbf{Z}_1}{\mathbf{a}_u} = \frac{-4.69\angle -72.9°}{2.79\angle -19.4°} \tag{3.98}$$

$$= 1.681\angle -233.5 \text{ mils } (0.0427 \text{ mm})$$

Assuming a balance radius of 1.5 in, the balance correction weight in grams is

$$\mathbf{U}_b = w\mathbf{e}_b = w_b\mathbf{R} = 3.8 \text{ lb} \times 0.00168 \text{ in}$$

$$= 0.00639 \text{ lb} \cdot \text{in} = 2.90 \text{ g} \cdot \text{in}$$

$$w_b = \frac{2.90 \text{ g} \cdot \text{in}}{1.5 \text{ in}} = 1.93 \text{ g}$$

The balance weight to produce zero amplitude is 1.93 g, and it should be placed at an angular location of 233.5° from the timing mark opposite to the direction of rotation.

Although the rotor is apparently perfectly balanced at 1800 rpm, the rotor will have a substantial response at the critical speed.

The influence coefficient for both unbalance and shaft bow at the critical speed is given by

$$\mathbf{a}_u = \mathbf{a}_r = A_{cr}\angle -90° = 9.74\angle -90°$$

The amplitude at the critical speed is given by

$$\mathbf{Z}_{cr} = (\mathbf{e}_u + \boldsymbol{\delta}_r) \times \mathbf{A}_{cr}$$

$$= (1.0\angle 0° + 1.0\angle -90°) \times 9.74\angle -90° = 13.774\angle -135° \qquad (3.99a)$$

The rotor response at the critical speed is given by

$$\mathbf{Z}_{cr,b} = \mathbf{a}_u(\mathbf{e}_u + \mathbf{e}_b) + \mathbf{a}_r\boldsymbol{\delta}_r$$

$$= 3.41 \text{ mils } \angle 0° \ (0.0866 \text{ mm}) \qquad (3.99b)$$

Figures 3.33 and 3.34 show the rotor amplitude and phase before and after balancing by method I (the conventional influence coefficient method). The rotor
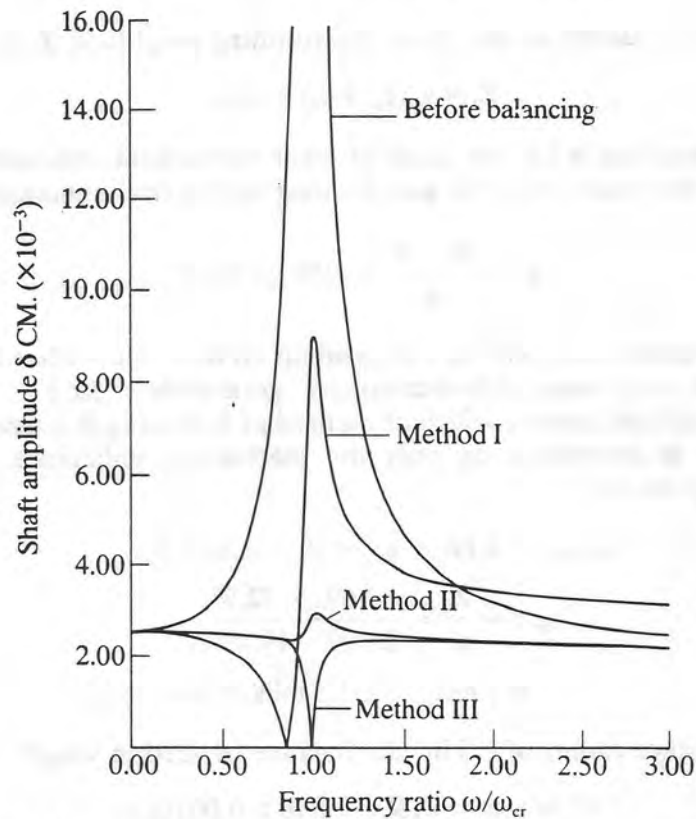
FIGURE 3.33 Bowed rotor response curves before and after balancing by methods I, II, and III.

amplitude, after balancing at 1800 rpm results in zero response at this speed. As the speed is increased, the shaft amplitude increases and reaches 3.41 mils, or 8.66×10^{-3} cm. The total unbalance in the rotor is $\mathbf{e}_u + \mathbf{e}_b = 1.35\angle -270°$, which is out of phase to the bow vector.

The ratio of the total unbalance in the rotor to the bow vector is

$$\frac{e_{\text{total}}}{\delta_r} = \frac{1}{f_b^2} = 1.35 \qquad (3.100)$$

The rotor is balanced to zero amplitude at 1800 rpm by method I. This causes a
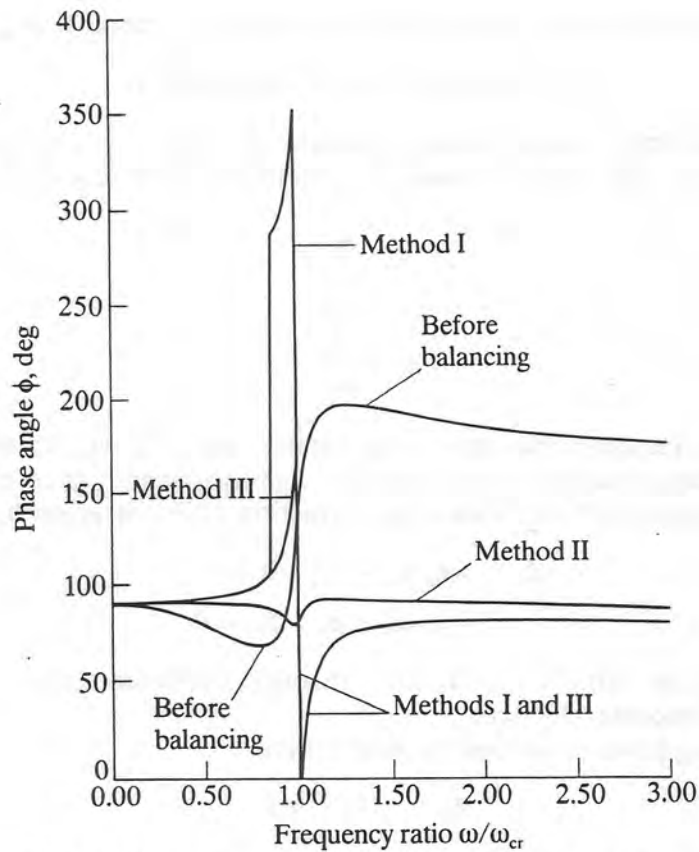
FIGURE 3.34 Phase-angle curves before and after balancing a bowed shaft by methods I, II, and III.

180° phase reversal above 1800 rpm and a large amplitude response is encountered at the critical speed. Balancing by method I is clearly unsatisfactory.

Balance Method II: Runout Subtractions. The procedure of placing a trial weight on the shaft will determine only the influence coefficient due to mechanical unbalance. The bow influence coefficient cannot be directly measured, e.g., by applying a trial bow vector.

The rotor response is assumed to be represented by the approximate equation

$$\mathbf{Z} = \mathbf{a}_u \mathbf{e}_u + \mathbf{a}_r \boldsymbol{\delta}_r \approx \mathbf{a}_u \mathbf{e}_u + \boldsymbol{\delta}_r \qquad (3.101)$$

Solving for the balancing eccentricity vector gives

$$\mathbf{e}_b = -\mathbf{e} = -\frac{\mathbf{Z} - \boldsymbol{\delta}_r}{\mathbf{a}_u}$$

$$= 1.31 \text{ mils } \angle -228.8° \qquad (3.102)$$

This procedure is equivalent to minimizing the elastic shaft deflection at the balance speed.

The balance correction by method II is

$$\mathbf{U}_b = w\mathbf{e}_b = 2.267 \text{ g} \cdot \text{in } \angle -228.8°$$

$$w_b = \frac{2.267 \text{ g} \cdot \text{in}}{1.5} = 1.5 \text{ g}$$

The amplitude at the critical speed after balancing by method II is

$$\mathbf{Z}_{cr} = 1.18 \text{ mils } \angle -84.2° \ (0.0299 \text{ mm})$$

Method III: Bow Vector Compensation. In this method, the influence coefficient for the bow vector is computed indirectly from Eq. 3.95:

$$\mathbf{a}_r = \frac{\mathbf{a}_u}{f_b^2} \tag{3.103}$$

where

$$f_b = \frac{N_b}{N_{cr}}$$

This procedure requires that the rotor critical speed be accurately known. If the balancing procedure is carried out at the critical speed, then the amplitude at the critical speed with the balancing correction added is given by

$$\mathbf{Z}_{cr,b} = \mathbf{a}_u(\mathbf{e}_u + \mathbf{e}_b) + \mathbf{a}_r \boldsymbol{\delta}_r$$

$$= \mathbf{a}_{cr}(\mathbf{e}_u + \mathbf{e}_b + \boldsymbol{\delta}_r) = 0 \tag{3.104}$$

Since $f_b = 1$ at the critical speed, the influence coefficients due to shaft bow and unbalance become identical.

The balancing criterion in this method is that

$$\mathbf{e}_b = -(\mathbf{e}_u + \boldsymbol{\delta}_r) \tag{3.105}$$

This is identical to the condition that the mechanical unbalance eccentricity vector be equal but out of phase to the shaft bow vector.

If the balancing speed does not correspond to the critical speed, then Eq. 3.104 is given by

$$\mathbf{Z}_b = \mathbf{a}_u\left(\mathbf{e}_b + \mathbf{e}_u + \frac{\boldsymbol{\delta}_r}{f_b^2}\right) \neq 0 \tag{3.106}$$

The balance eccentricity vector $\mathbf{e}_b$ is given by

$$\mathbf{e}_b = \frac{\mathbf{Z}_1}{\mathbf{a}_u} + \boldsymbol{\delta}_r\left(1 - \frac{1}{f_b^2}\right) \tag{3.107}$$

With the value of shaft bow δ_r measured at low speed and the ratio f_b of the balance speed to the critical speed, the value of the balancing eccentricity is computed

$$\mathbf{e}_b = 1.41 \text{ mils } \angle -225° \ (0.0359 \text{ mm})$$

The corresponding balance correction weight for a radius of 1.5 in is 1.62 g. Figure 3.33 shows that the rotor amplitude at the critical speed will reduce to zero by balancing method III. Similar experimental and theoretical response curves for balancing a uniform flexible shaft with shaft bow are shown by Bishop and Parkinson (1965a, b; 1972).

Table 3.6 shows that balancing a bowed rotor by the standard influence coefficient method usually will result in overbalancing the rotor by 20 to 30 percent. From a practical standpoint, it is impossible to distinguish between shaft bow and conventional unbalance. In general, the vibration observed on the shaft

TABLE 3.6 Balance Corrections and Angular Location for a Bowed Rotor by Various Methods

Method	Balance corrections, g	Balance location, deg lag
I. Standard influence coefficient	1.93	233.5
II. Influence coefficient assuming constant runout vector	1.50	228.8
III. Bow vector compensation	1.62	225.0

may be a function of mechanical unbalance, shaft bow, and a constant runout vector δ_0 as follows:

$$\mathbf{Z} = \mathbf{a}_u \mathbf{e}_u + \mathbf{a}_r \delta_r = \delta_0 \tag{3.108}$$

At low speeds, where the effect of the unbalance is minimal (that is, $\mathbf{a}_u \ll 1$), the low-speed or residual runout vector $\mathbf{Z}_0$ is given by

$$\mathbf{Z}_0 = \delta_r + \delta_0 \tag{3.109}$$

It is not, in general, possible to distinguish between a shaft constant runout vector δ_0 and true mechanical shaft bow δ_r.

In comparing methods II and III, we see that method II generates an extremely good value of balance for the bowed rotor by treating the bow as a constant vector. A modified influence coefficient method of balancing is used in which the slow-roll vector $\mathbf{Z}_0$ is recorded.

The modified balancing procedure is similar to the standard single-plane balancing in Eq. 3.90 except that the procedure is modified to subtract the slow-roll runout vector $\mathbf{Z}_0$ as follows:

$$\mathbf{U}_b = (\mathbf{Z} - \mathbf{Z}_0) \times \frac{\mathbf{U}_t}{\mathbf{Z} - \mathbf{Z}_t} \tag{3.110}$$

Figure 3.35 represents a single-mass rotor that was balanced at 1500 rpm by the standard influence method without the shaft bow considered in the balancing calculations. The rotor was balanced at 1800 rpm to zero amplitude. However, at the critical speed the rotor amplitude is 6 mils. In Fig. 3.36 the residual shaft bow vector was subtracted from the rotor response, and the rotor was balanced to the residual vector rather than to zero amplitude. The rotor amplitude goes to zero response at the critical speed. Balancing the rotor with slow-roll vector subtraction included results in a reduction of the balancing weight from 584 to 560 g and a shift in this phase angle from 261° to 241°.

There are currently several designs of synchronous digital vector tracking filters on the market with the capability of low-speed vector runout subtraction built in.

If possible, one should always measure the low-speed runout vector and subtract this vector from the rotor response obtained at speed.

Balancing the Bowed Rotor without Trial Weights

With the current generation of hand calculators and portable computers, it is possible to invert complex matrices of order 3 or 4 with little difficulty. It is thus
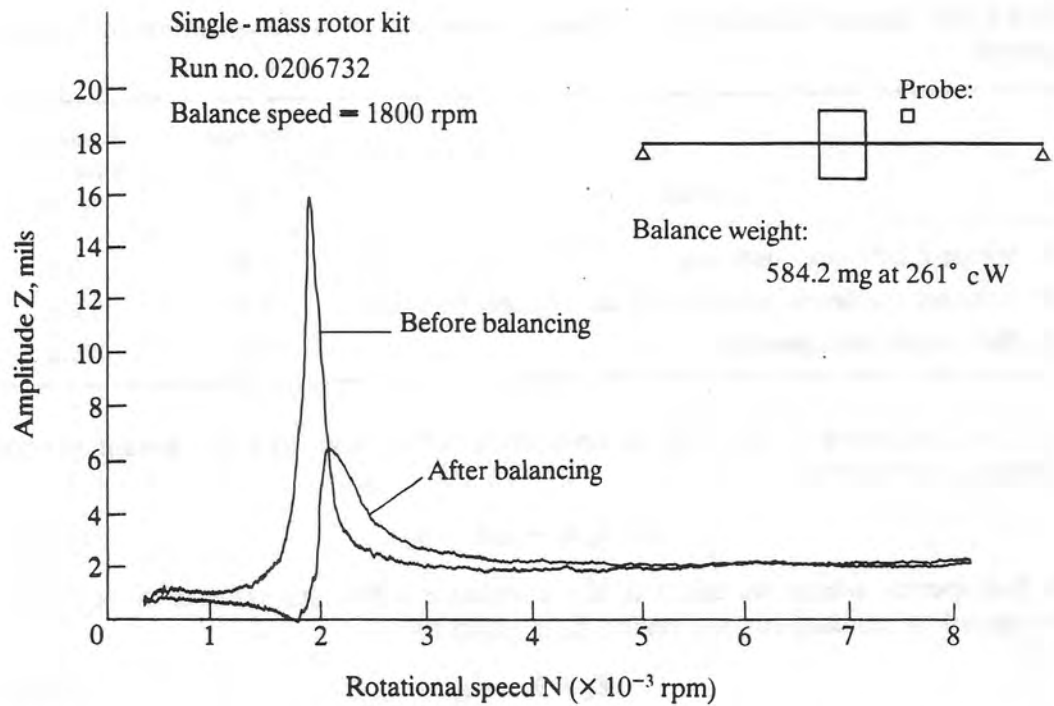
FIGURE 3.35 Unbalance response of a bowed rotor before and after balancing with residual bow neglected.
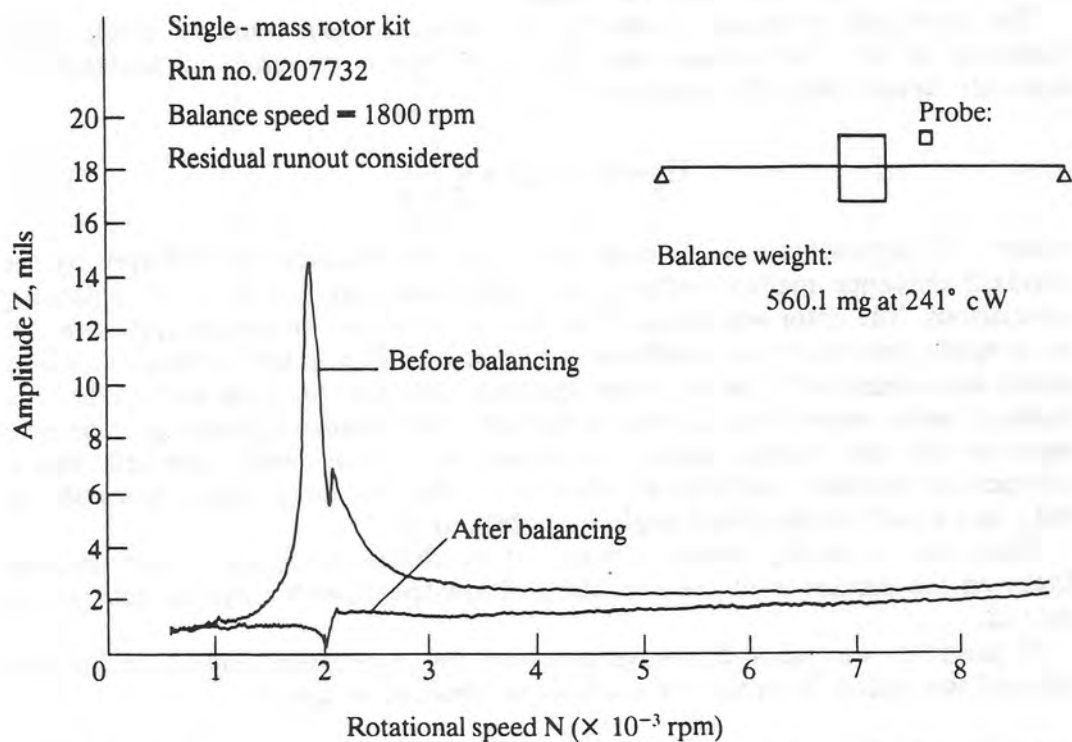
FIGURE 3.36 Unbalance response of a bowed rotor before and after balancing with residual bow considered.

Undamped critical speed of the single-mass Bently rotor
Symmetric bearings, K-1000 lb/in, 7 station model
14-in shaft with 12-in bearing span, 1.7-lb disk
Mode 1: frequency = 54.17 Hz (3250 rpm)
Mode is synchronous

Bearing 1

Bearing 2

0 1 2 3 4 5 6 7 8 9 10 11 12 13 14

Scale in inches
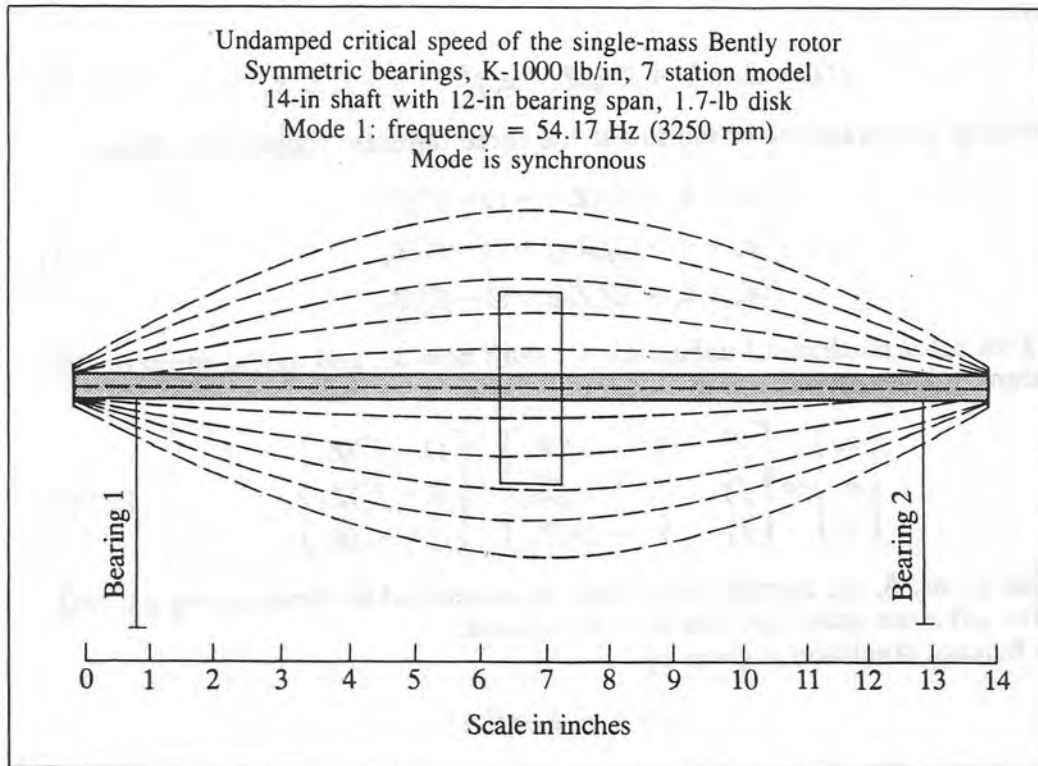
FIGURE 3.37 Single-mass rotor—animated mode shape of first critical speed.

possible to compute the initial balance of the rotor without the use of a trial weight. To do this, it is necessary to know the rotor critical speed, the rotor modal weight, and the axial location of the shaft probe along the shaft.

Figure 3.37 represents the rotor first critical speed mode shape. Normally the shaft probes are not located at the shaft center. The probes are located some distance z in from the end. At this distance z, the rotor dimensionless mode shape may be measured. The mode shape at the shaft center $\phi(L/2)$ is normalized to unity. For example, with the theoretical Jeffcott rotor with no bearing displacements, the mode shape $\phi(z)$ is given by

$$\phi(z) = \sin \frac{\pi z}{L} \tag{3.111}$$

The measurements at distance z along the shaft are corrected by the mode shape to arrive at the amplitude at the rotor center

$$\mathbf{Z}_{\text{center}} = \mathbf{Z} \times \frac{\phi(L/2)}{\phi(z)} \tag{3.112}$$

The rotor amplitude and phase are measured at three speeds. Since the critical speed is assumed known, the speed ratios $f_i = N_i/N_{\text{cr}}$ may be computed.

The rotor response at each speed is given by

$$M\ddot{\mathbf{Z}}_i + K(\mathbf{Z}_i - \mathbf{\delta}_r) + C\dot{\mathbf{Z}}_i = Me_u\omega^2 e^{i\omega t} \tag{3.113}$$

Assuming synchronous motion and normalizing the equation of motion by $M\omega_{\text{cr}}^2$;

we have

$$-f_i^2 \mathbf{Z}_i + \mathbf{Z}_i - \boldsymbol{\delta}_r + i2\xi f_i \mathbf{Z}_i = \mathbf{e}_u f_i^2 \qquad i = 1, 2, 3 \tag{3.114}$$

Rearranging the equations of motion at the three different speeds, we obtain

$$f_1^2 \mathbf{e}_u + \boldsymbol{\delta}_r - i2f_1 \mathbf{Z}_1 \xi = (1 - f_1^2)\mathbf{Z}_1$$
$$f_2^2 \mathbf{e}_u + \boldsymbol{\delta}_r - i2f_2 \mathbf{Z}_2 \xi = (1 - f_2^2)\mathbf{Z}_2 \tag{3.115}$$
$$f_3^2 \mathbf{e}_u + \boldsymbol{\delta}_r - i2f_3 \mathbf{Z}_3 \xi = (1 - f_3^2)\mathbf{Z}_3$$

Solving for rotor mechanical unbalance $\mathbf{e}_u$, shaft bow $\boldsymbol{\delta}_r$, and modal damping ξ as the system unknowns, we obtain

$$\begin{Bmatrix} \mathbf{e}_u \\ \boldsymbol{\delta}_r \\ \xi \end{Bmatrix} = \begin{bmatrix} f_1^2 & 1 & -2if_1\mathbf{Z}_1 \\ f_2^2 & 1 & -2if_2\mathbf{Z}_2 \\ f_3^2 & 1 & -2if_3\mathbf{Z}_3 \end{bmatrix}^{-1} \begin{Bmatrix} (1-f_1^2)\mathbf{Z}_1 \\ (1-f_2^2)\mathbf{Z}_2 \\ (1-f_3^2)\mathbf{Z}_3 \end{Bmatrix} \tag{3.116}$$

Note that $\mathbf{e}_u$ and $\boldsymbol{\delta}_r$ are complex (or vector) quantities while the damping ξ is real. Thus five unknown quantities are to be computed.

The balance condition is given by

$$\mathbf{e}_b + \mathbf{e}_u + \boldsymbol{\delta}_r = 0$$

and the balance correction weight is

$$\mathbf{W}_b = \frac{\mathbf{U}_b}{\mathbf{R}} = -\frac{W_{\text{modal}}(\mathbf{e}_u + \boldsymbol{\delta}_r)}{\mathbf{R}} \tag{3.117}$$

This procedure may be extended to multimass rotors and is referred to as *first mode balancing without trial weights*. The problem of balancing the first mode of a multimass rotor may often be reduced to the balancing of an equivalent signle-mass Jeffcott rotor in which the rotor modal weight is given by

$$W_{\text{modal}} = \int_0^L \rho \phi_1^2(x) \, dx = \sum W_i \phi_{i1}^2(x) $$

3.3.4 Balancing the Jeffcott Rotor by the Least-Squared-Error Method

Since it is difficult to distinguish between true shaft bow and a constant shaft residual runout vector, one may use a multispeed balancing method based on minimization of the rotor response over a speed range.

In the procedure, the rotor low-speed runout vector $\mathbf{Z}_0$ is measured. The rotor response $\mathbf{Z}_i$ is then measured at N_i speeds ($i = 1$ to n values). The rotor amplitude is assumed to be of the form

$$\mathbf{Z}_i = \mathbf{a}_i \mathbf{U} + \mathbf{Z}_0 \qquad i = 1, \ldots, n \tag{3.118}$$

A trial or calibration weight is next attached to the rotor, and the new response is measured at the same speeds.

$$\mathbf{Z}_{it} = \mathbf{a}_i(\mathbf{U} + \mathbf{U}_t) + \mathbf{Z}_0 \tag{3.119}$$

The influence coefficients $\mathbf{a}_i$ are then computed:

$$\frac{\mathbf{Z}_{it} - \mathbf{Z}_i}{\mathbf{U}_t} = \mathbf{a}_i \tag{3.120}$$

Let $\mathbf{Z}_{ic} = \mathbf{Z}_i - \mathbf{Z}_0$ represent the compensated rotor vibration with slow-roll runout subtraction. The compensated vibration readings at the various speeds may be expressed as

$$\mathbf{Z}_{ic} = \mathbf{a}_i \mathbf{U} + \epsilon_i \qquad i = 1, \dots, n \tag{3.121}$$

The error ϵ_i is given by

$$\epsilon_i = \mathbf{Z}_{ic} - \mathbf{a}_i \mathbf{U} \tag{3.122}$$

The error function ϵ_i is complex. Let ϵ_i^* be the complex conjugate error function.

A positive definite error function E_i may be constructed by multiplying the error function ϵ_i by its complex conjugate value ϵ_i^*:

$$E_i = \epsilon_i \epsilon_i^* = (\mathbf{Z}_{ic} - \mathbf{a}_i \mathbf{U})(\mathbf{Z}_{ic}^* - \mathbf{a}_i^* \mathbf{U}^*) \tag{3.123}$$

The total error function E is given by

$$E = \sum E_i = \sum (\mathbf{Z}_{ic} - \mathbf{a}_i \mathbf{U})(\mathbf{Z}_{ic}^* - \mathbf{a}_i^* \mathbf{U}^*) \tag{3.124}$$

Minimizing the total error function E with respect to U, we obtain the balancing conditions:

$$\mathbf{U}_b = -\mathbf{U} = \frac{-\sum \mathbf{a}_i^* \mathbf{Z}_{ic}}{\sum \mathbf{a}_i \mathbf{a}_i^*} \tag{3.125}$$

By taking vibration measurements at speeds both above and below the critical speed, excellent single-plane balancing may be achieved with a bowed rotor. This procedure also has the advantage that good balancing may be achieved by using the uncompensated vibration values $\mathbf{Z}_i$ corresponding to multiple speeds.

Example 3.10: Balancing a Bowed Rotor by the Least-Squared-Error Method. The rotor of Example 3.9 is to be balanced by measuring the vibration amplitude below and above the rotor critical speed, at 1800 and 2300 rpm.

The amplitude and phase at the three speeds are given by

$$\mathbf{Z}_{1800} = 4.69 \text{ mils } \angle -73° = \mathbf{Z}_1$$

$$\mathbf{Z}_{2080} = 13.77 \text{ mils } \angle -135° = \mathbf{Z}_{cr}$$

$$\mathbf{Z}_{2300} = 6.32 \text{ mils } \angle -192° = \mathbf{Z}_2$$

The compensated amplitude is given by subtracting the slow-roll vector $\mathbf{Z}_0$:

$$\mathbf{Z}_{1c} = 4.69 \angle -73° - 1.0 \angle -90° = 3.75 \angle -68°$$

$$\mathbf{Z}_{2c} = 6.32 \angle -192° - 1.0 \angle -90° = 6.6 \angle -201°$$

A trial weight of 0.576 g is placed at a radius of 1.5 in at 180° from the timing

mark

$$\mathbf{e}_t = 0.5 \text{ mil}$$

The new vibration readings after the application of the trial weight are

$$\mathbf{Z}_{1t} = 4.02 \angle -89°$$

$$\mathbf{Z}_{cr,t} = 10.9 \angle -153°$$

$$\mathbf{Z}_{2t} = 4.0 \angle -177°$$

The influence coefficients for 1800 and 2300 rpm are

$$\mathbf{a}_1 = 2.41 \text{ mils/g} \angle -20° \qquad \mathbf{a}_2 = 4.325 \text{ mils/g} \angle -152°$$

The complex conjugates of the influence coefficients $\mathbf{a}_1$ and $\mathbf{a}_2$ are

$$\mathbf{a}_1^* = 2.41 \angle 20° \qquad \mathbf{a}_2^* = 4.325 \angle 152°$$

The single-plane least-squared-error balancing procedure for the two speeds is

$$\mathbf{U}_b = -\frac{\mathbf{Z}_{1c}\mathbf{a}_1^* + \mathbf{Z}_{2c}\mathbf{a}_2^*}{\mathbf{a}_1\mathbf{a}_1^* + \mathbf{a}_2\mathbf{a}_2^*}$$

$$= \frac{-37.58 \angle -48.7°}{24.5} = 1.53 \angle -229° \text{ g} \qquad (3.126)$$

The balance correction computed with these two measurements is 1.53 g at a lag angle of 229° from the shaft reference mark.

Table 3.7 represents the Jeffcott rotor conditions before and after balancing using the vibration data at 1800 and 2300 rpm. In this table, the amplitude at the critical speed at 2080 rpm is shown as 13.8 mils at 135° lag.

In the bottom portion of the table, the initial readings, current vibration readings with trial weight, and predicted readings are given. The data indicates that if the computed balance correction of 1.53 g is placed on the rotor at 229°, then the response at the critical speed will drop from 13.8 to only 1.39 mils. The amplitude at the other low speeds is predicted to be only 1.0 mil at 80° lag. This is approximately the value of the low-speed runout vector. This situation represents an outstanding balanced condition.

Figure 3.38 represents the locations of the trial, trim, and total balance corrections. The mechanical unbalance of 1.15 g at 1.5 in is located at 0° which is at hole 1. The shaft bow of 1 mil radial is in the direction of hole 5 (90° lag angle). The trial weight of 0.58 g is shown at hole 9.

To balance the rotor, the trial weight of 0.58 g could be removed and 1.53 g could be placed in hole 11. If one did not wish to remove the trial weight (which is often the case), a trim weight of 1.23 g could be placed at hole 12. The trim and trial weight together would produce the same effect as the total balance correction of 1.53 g at 229°.

3.3.5 Single-Plane Balancing by the Three-Trial-Weight Method

One does not normally balance a lightly damped rotor at the critical speed by using the influence coefficient method because slight changes in speed cause

TABLE 3.7 Single-Plane Least-Squared-Error Balancing of Jeffcott Rotor with Shaft Bow Including Runout Compensation

Single-plane balancing of Jeffcott rotor with shaft bow, eu = 1.0 mil at 0°, shaft bow = 1.0 mil at 90° lag, two-speed balancing data taken below and above critical speed—critical speed data not included.

System influence coefficients: units = mils (g). All probe readings are in the lag convention.

| | Balance shot | | | | | | | | Influence coefficient | | |
| | | | | | | | | | | | Relative |
No.	Amplitude	Phase	Speed rpm	Predicted no.	Amplitude 1, mils	Phase 1, deg	Amplitude 2, mils	Phase 2, deg	Mag.	Deg	lag*
1	0.58	180	1800	1	4.700	73	4.020	89	2.410	20	160
1	0.58	180	2080	1	13.800	135	10.900	153	8.350	91	89
1	0.58	180	2300	1	6.320	192	4.700	212	4.325	152	28

Initial and current responses and predicted residual response†

| | | Initial | | Current | | Predicted | | Change in amplitude | |
Speed rpm	Probe no.	Amplitude mils	Phase deg	Amplitude mils	Phase deg	Amplitude mils	Phase deg	Predicted initial	Predicted current
1800	1	4.700	73	4.020	89	1.052	88	-3.648	-2.968
2080	1	13.800	135	10.900	153	1.392	93	-12.408	-9.508
2300	1	6.320	192	4.700	212	1.007	88	-5.313	-3.693

Balance correction weights

| | | Total balance | | | | Trim balance‡ | |
No.	Balance plane location	Mag, g	Phase lag	X	Y	Mag, g	Phase lag
1	Center plane	1.53	229	-1.0	-1.2	1.23	249

* Relative lag = amount the influence coefficient lags the trial weight.
† Sum of squared residuals = 4.060; rms residual = 1.163; max residual = 1.392.
‡ Note: Trim balance = (total balance) − (trial weight left in rotor).

3.81

Single plane balancing of Jeffcott rotor with shaft bow, Eu = mil at 0°
Shaft bow = 1.0 mil at 90° lag, 2 speed balancing data taken below and
above critical speed—slow roll compensation included—critical speed data not included

Balance plane 1: center plane

Trial weight (solid circle):
U_{trial} = 0.58 g
Phase = 180.00°

Total balance (solid line):
U_{total} = 1.53 g
Phase = 228.66°

Trim balance (dashed line):
U_{trim} = 1.23 g
Phase = 249.21°
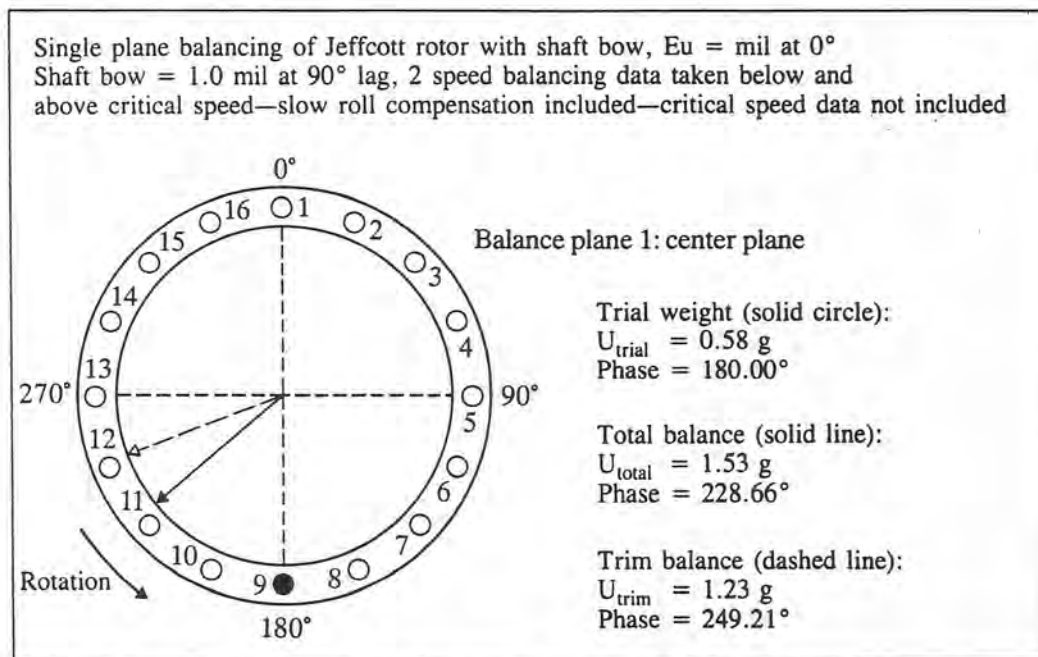
FIGURE 3.38 Single-plane balancing of Jeffcott rotor with shaft bow showing final and trim balance corrections.

considerable shifts in amplitude and phase. There is, however, a method that is ideally suited for balancing a lightly damped bowed rotor at the critical speed. This method is referred to as the *three-trial-weight or four-run* method, and it was first described by Blake (1967).

This method was first employed for balancing large fans under conditions where it was difficult to obtain a phase measurement. The procedure has the advantage that vibration can be recorded by a spectrum analyzer or fast Fourier transform (FFT) analyzer. The phase of the motion is not required. The basic procedure has been extended by Gunter, Springer, and Humphris (1982) to balance a multimass rotor through three critical speeds using modal balancing weight distributions.

The method has a fundamental drawback in that four runs of the rotor must be performed with trial weights moved in three different positions. It should not be used when thermal bowing is suspected.

As the first step in the three-trial-weight method, the initial rotor amplitude is recorded. Figure 3.39 represents the initial, trial, and final balance runs for the three-trial-weight method (Nicholas et al., 1976). The response Z_0 represents the original motion of a single-mass rotor with shaft bow. The amplitude of motion was plotted on an *XY* plotter to record the motion going through the critical speed. The peak motion passing through the critical speed Z_0 is recorded. A circle of radius 6.625 mils is drawn as shown in Fig. 3.40 to represent Z_0.

A trial weight of 0.34 g was selected and placed in hole 3 on the rotor disk. The rotor was rerun and the new amplitude of motion Z_1 was recorded. On the circumference of the circle Z_0, holes are labeled; Z_1 is drawn with a radius of 6.125 mils at hole 3 marked on circle Z_0.

The trial weight was then removed and placed in hole 8. The resulting vibration Z_2 was then recorded. A circle of diameter Z_2 was drawn with its origin at hole 8 marked on circle Z_0. The intersections of circles Z_1 and Z_2 represent possible balancing solutions.
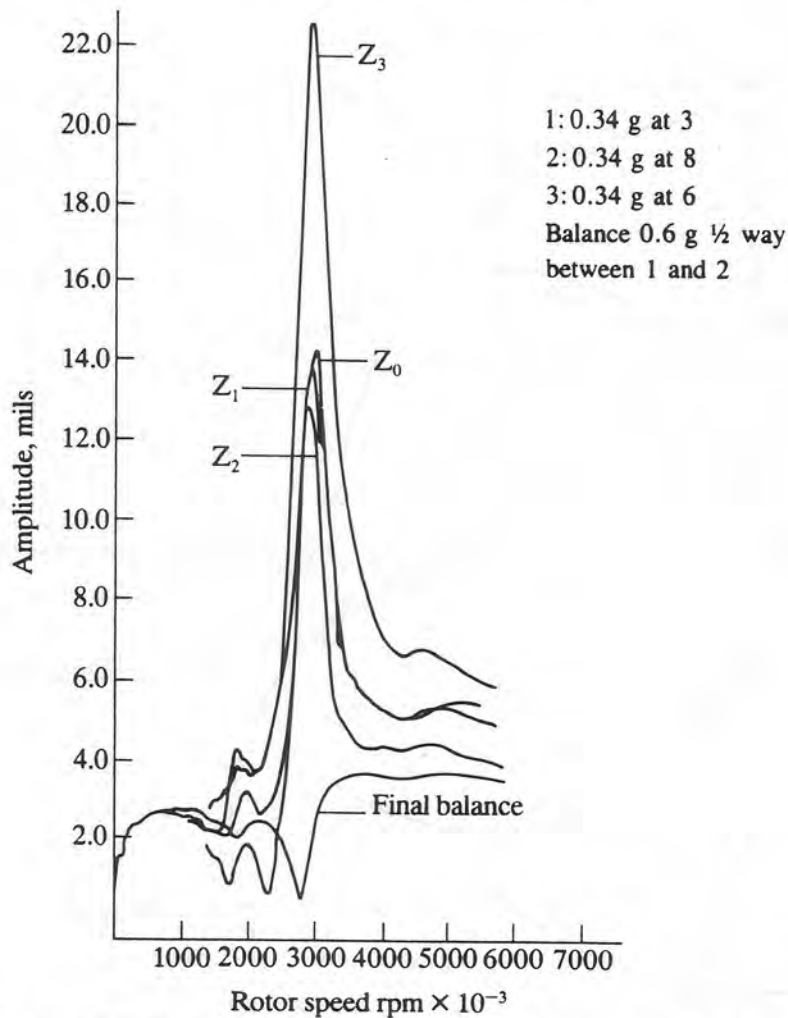
FIGURE 3.39 Initial, trial, and final balancing runs using the three-trial-weight method (Nicholas et al., 1976).

A third run is necessary to identify the final balance location and magnitude. The trial weight was next removed from hole 8 and placed in hole 6. The resulting amplitude Z_3 was recorded, and a circle was drawn with its origin at hole 6 on the circumference of Z_0.

Circles Z_1, Z_2, and Z_3 with origins lying on circle Z_0 represent the locus of points for various orientations of the unbalance vector $\mathbf{U}$ and the trial balance vector $\mathbf{U}_t$. The point, or vicinity, where all three circles intersect is the location of the balance correction weight, as shown in Fig. 3.40. A vector $\mathbf{e}_b$ is drawn from origin of Z_0 to the point of intersection of all three circles (or vicinity in case the circles do not exactly cross at a point). The line of action of $\mathbf{e}_b$ represents the balancing plane. The balance magnitude is given by

$$\mathbf{U}_b = \mathbf{U}_t \times \frac{\mathbf{Z}_0}{\mathbf{e}_b} \tag{3.127}$$

From Fig. 3.40, a balance correction of 0.6 g between holes 1 and 2 was computed. Figure 3.39 shows the final amplitude of motion after the required balance correction weight was placed on the shaft. Note the reduction in

Z₃ = 10.0 in at 6

$Z_1 = 6.125$ in at 3

$Z_1 = 6.125$

$Z_3 = 10.0$

$Z_0 = 6.625$

$e_b = 3.75$ in

Before → Z = 6.625

$Z_2 = 6.0$

$Z_2 = 6.0$ in at 8

$$U_B = U_t \left(\frac{z}{e_b}\right)$$

$$U_B = 0.34 \left(\frac{6.625}{3.75}\right) = 0.6 \text{ g}$$

$$U_B = 0.6 \text{ g}$$

$\frac{1}{2}$ way between
holes 1 and 2
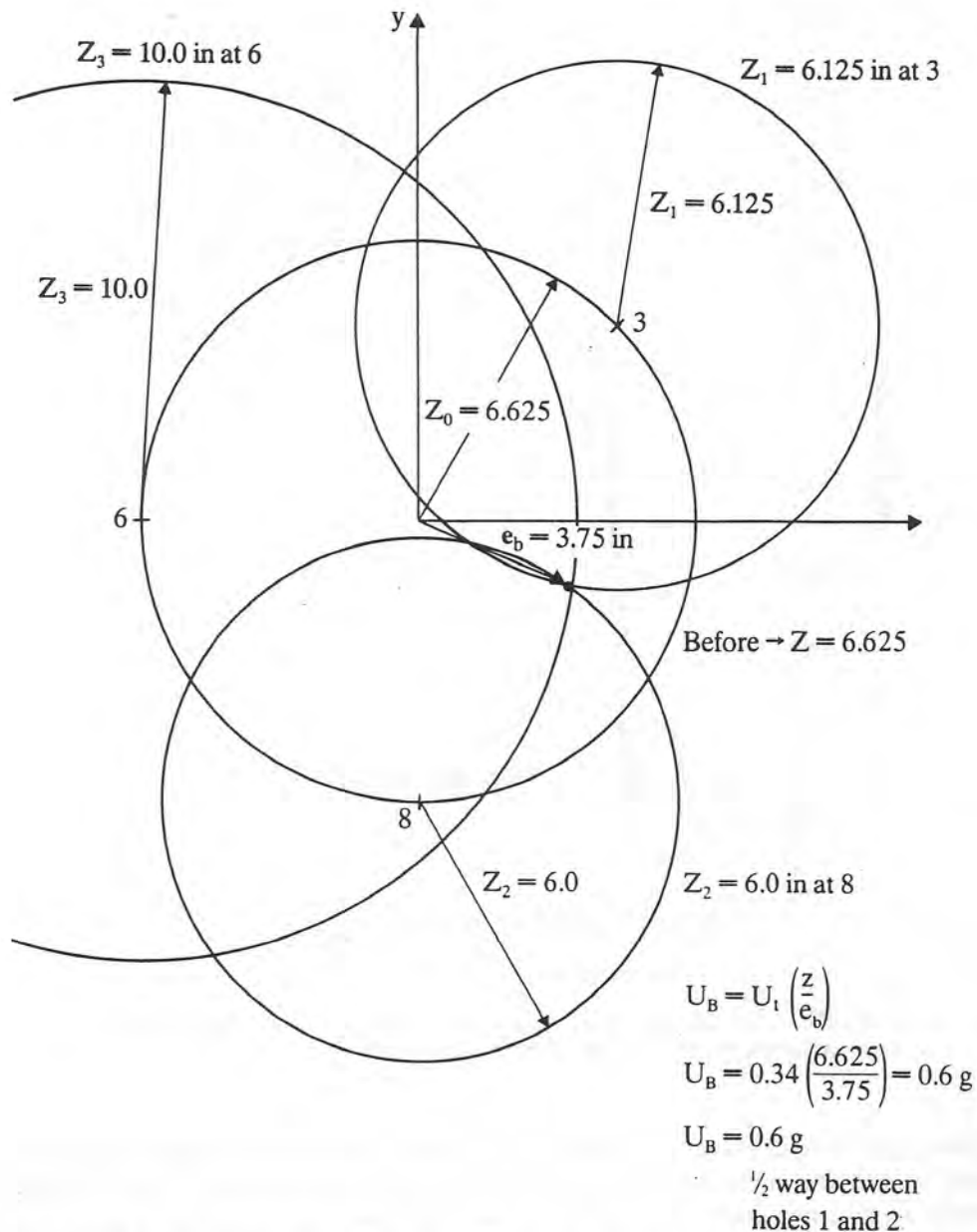
FIGURE 3.40 Graphical balancing solution using the three-trial-weight method (Nicholas et al., 1976).

amplitude near the critical speed. This is an indication that the rotor shaft bow and unbalance are of similar magnitudes and out of phase.

The three-trial-weight procedure is a very accurate method of single-plane balancing provided that one can easily attach and remove weights. The speed of the rotor does not have to be carefully controlled as in the influence coefficient method. One may use the peak hold capability of an analyzer and capture the maximum amplitude of motion while passing through the rotor critical speed. Since the influence coefficients, due to shaft bow and unbalance, are identical at the critical speed, a highly accurate balance is obtained. Therefore, it is not necessary to compensate for low-speed runout when this procedure is used.
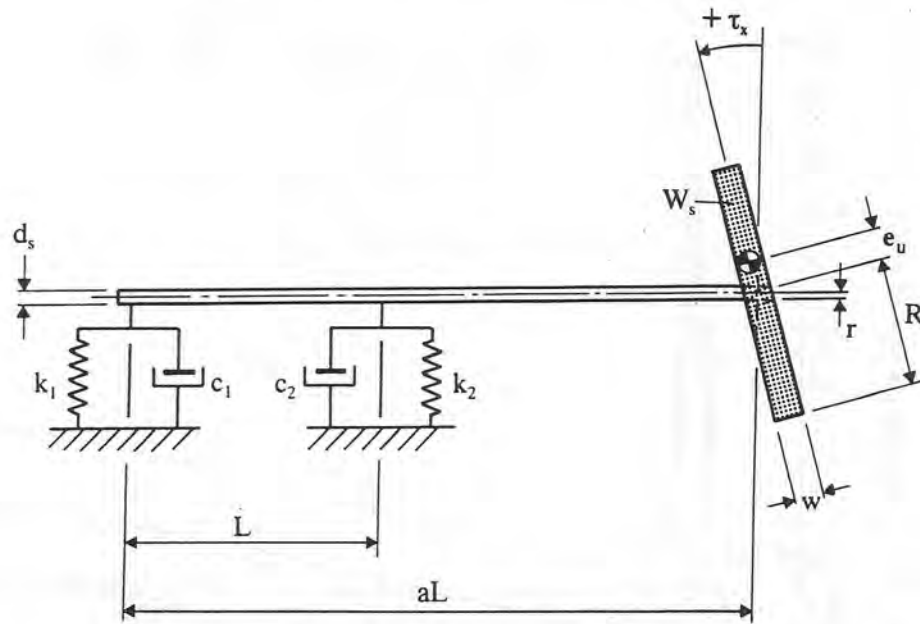
FIGURE 3.41 Overhung rotor with disk skew and unbalance (Benson, 1974).

3.3.6 Balancing the Overhung Rotor with Disk Skew

Figure 3.41 represents an overhung rotor with radial unbalance e_u and disk skew τ (Salamone and Gunter, 1978). The plane of the disk is inclined from the vertical by the small angle τ. The equations of motion of the overhung rotor with disk skew were extensively studied by Benson (1974). Balancing the overhung rotor with disk skew is considerably more complex than the conventional Jeffcott rotor which is symmetrically situated between the bearings.

The skew of the disk generates an unbalance moment with magnitude

$$M_{gyro} = \omega^2 \tau (I_p - I_t) \tag{3.128}$$

The sign of the moment is dependent on whether the polar moment of inertia I_p is larger than the transverse moment of inertia I_t. For $I_p > I_t$, which is the situation for a thin disk, there is normally only one synchronous critical speed due to the gyroscopic moment effects.

Figure 3.42 represents the response of an overhung disk as monitored at the near bearing for various combinations of rotor unbalance **U** and disk skew τ (Salamone and Gunter, 1978). If the disk skew is out of phase to the unbalance (case 4), the effects combine to increase the amplitude of motion at the critical speed. If, however, the disk skew is in phase to the disk unbalance, then the moment generated by the skewed disk will help to offset the radial unbalance force and the overall vibrational amplitude will be reduced.

If the disk skew is positive, as in case 5, there is a self-balancing speed at which zero amplitude of motion is achieved at the near bearing (the far bearing may have a very high amplitude of motion, however). It therefore can be readily demonstrated that for any given disk skew, one may choose a balance correction to reduce the rotor amplitude to zero for a particular speed. At any other speed, however, large amplitudes of motion may result.

Disk skew causes the rotor amplitude to increase with an increase in speed above the critical speed. This effect may often be confused with the approach of a
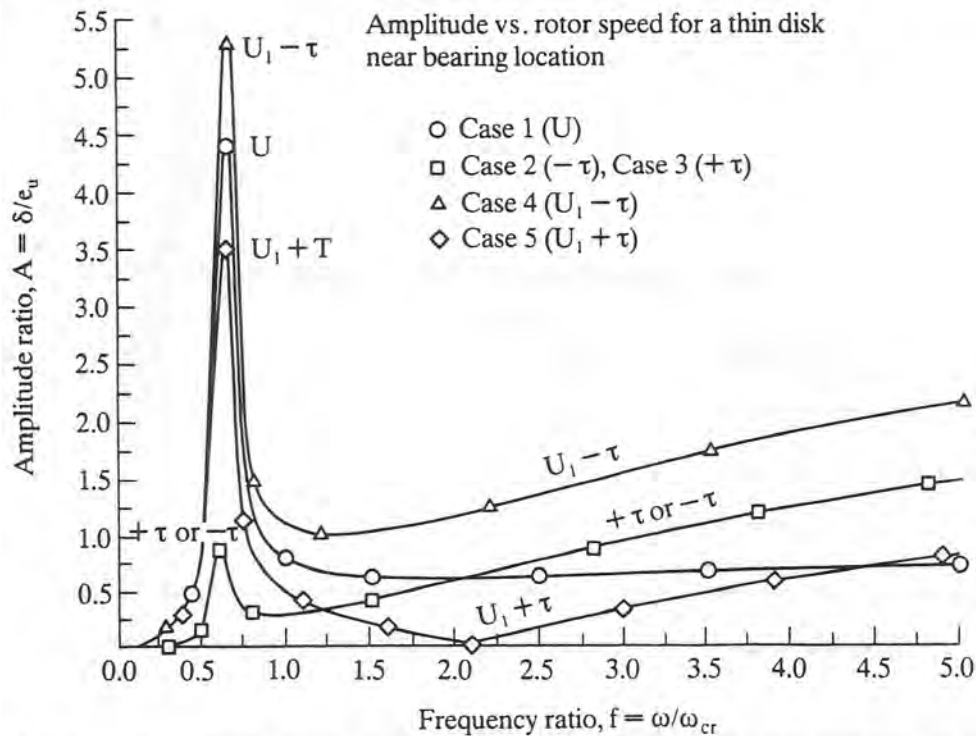
FIGURE 3.42 Amplitude versus rotor speed for a thin disk at the near-balancing location for various combinations of unbalance and disk skew τ (Salamone and Gunter, 1978).

second critical speed. It is often difficult to detect the presence of large disk skew by monitoring the motion at the near bearing.

When an overhung rotor is balanced, it is important to monitor the amplitude and phase at the far bearing as well as the near bearing. Figure 3.43 represents the phase-angle change observed at the far end bearing for an overhung rotor with various combinations of unbalance and disk skew. By observing the relative phase change at the far end bearing, it is very easy to distinguish between disk radial unbalance and disk skew effects. For the case of pure radial disk unbalance, a conventional 180° phase shift is observed while passing through the critical speed.

If, however, there is a substantial disk skew present in the rotor, then a phase reversal will be observed upon passing through the critical speed. If no phase reversal is observed at the far end bearing, then a single-plane balance correction on the disk will be sufficient to balance the rotor at all speeds. If the phase reversal is observed, then the single-plane correction cannot balance the rotor at all speeds. Attempts to precisely balance the near end bearing may result in large amplitudes at the far end bearing. In this case a compromise single-plane balancing may be achieved by using amplitude and phase readings obtained from both the near and far end bearings.

Figure 3.44 represents the near-bearing amplitude for an overhung rotor before and after various balancing procedures (Salamone and Gunter, 1978). In balance procedure 1, the rotor is balanced by a single-plane correction near the critical speed. Above the critical speed, the rotor amplitude increases rapidly. In balance run 3, the near plane is balanced to zero amplitude at $f = 3$, but large amplitudes result at the far bearing.
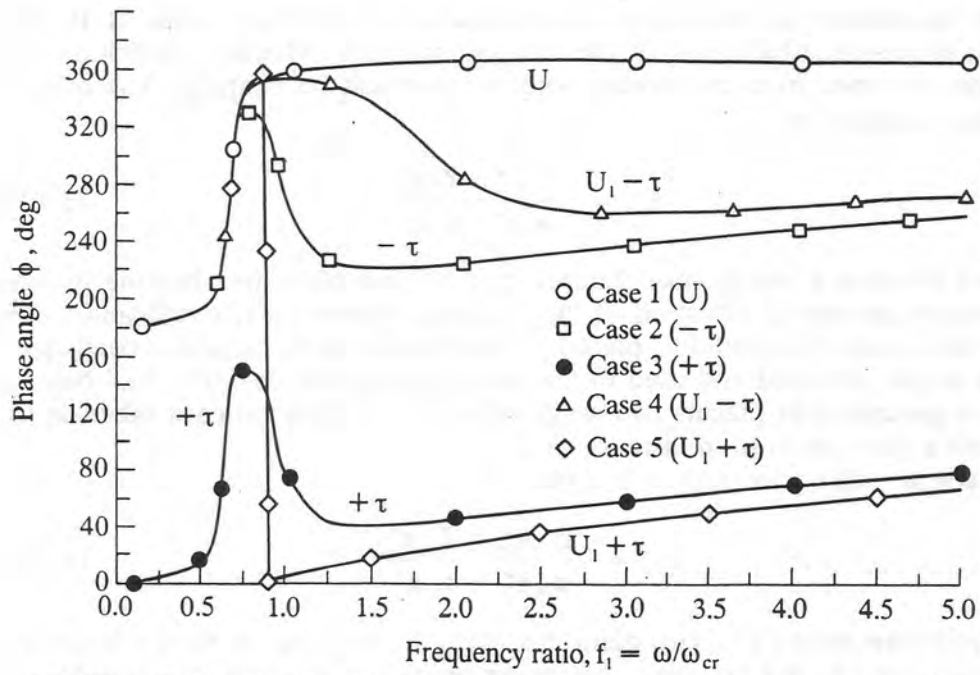
FIGURE 3.43 Phase angle versus rotor speed at the fan bearing for an overhung rotor for various combinations of rotor unbalance and disk skew (Salamone and Gunter, 1978).
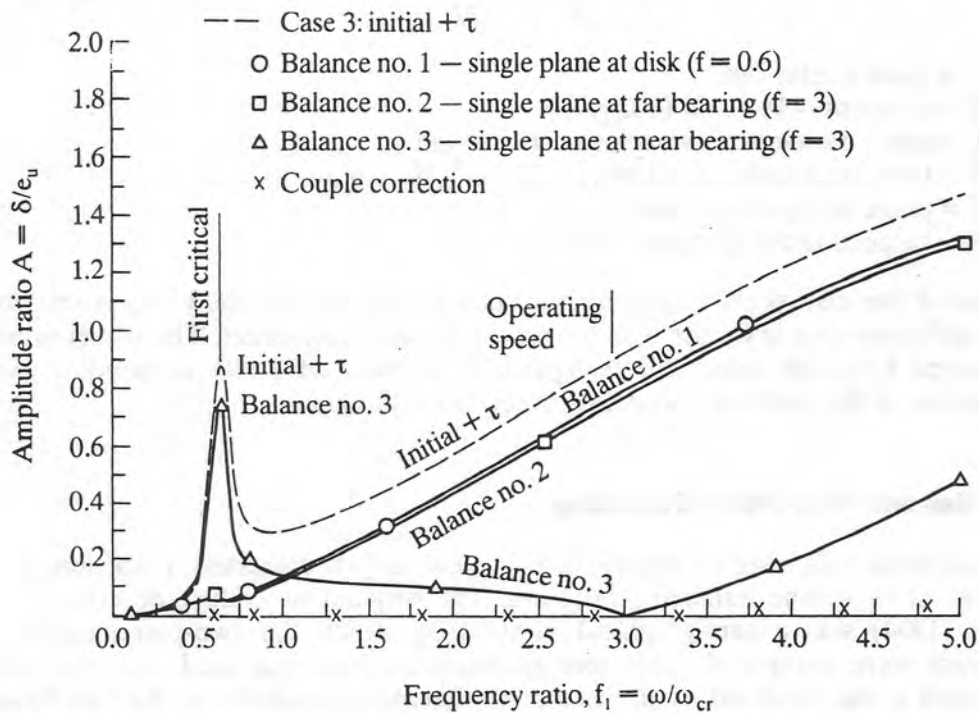
FIGURE 3.44 Near-bearing amplitude for an overhung rotor before and after various balancing procedures (Salamone and Gunter, 1978).

The recommended procedure for balancing an overhung rotor is to first attempt single-plane balancing of the disk by using the influence coefficients and vibrations obtained from monitoring both the near and far bearings. The balance correction is given by

$$\mathbf{U}_b = -\frac{\mathbf{Z}_n \mathbf{a}_n^* + \mathbf{Z}_f \mathbf{a}_f^*}{\mathbf{a}_n \mathbf{a}_n^* + \mathbf{a}_f \mathbf{a}_f^*} \tag{3.129}$$

This will produce a compromise balance that will not allow one bearing to have an excessive amount of vibration. If the resulting vibration is not sufficiently low, then a trial couple U_{tc} should be placed on the wheel and the influence coefficients for the couple obtained and used in the balancing calculations. The trial balance couple is generated by placing two weights 180° out of phase to each other on the disk with a plane separation distance of T.

The couple balance correction is given by

$$\mathbf{U}_{cb} = -\frac{\mathbf{Z}_{cn} \mathbf{a}_{cn}^* + \mathbf{Z}_{cg} \mathbf{a}_{cf}^*}{\mathbf{a}_{cn} \mathbf{a}_{cn}^* + \mathbf{a}_{cf} \mathbf{a}_{cf}^*} \tag{3.130}$$

This procedure results in a two-plane balancing of the disk. A similar balancing can be achieved by the two-plane balancing procedure in which trial weights are placed on the two planes of the disks and the vibrations for the near and far bearings recorded for the two trial runs. The solution of these balancing problems requires a computer to perform the necessary computations. The procedure presented here can be calculated by hand.

The required balance correction W_c (two weights 180° out of phase) for a given disk skew is given by

$$W_c = \frac{U_c}{TR} = \frac{\tau K(I_p - I_t)}{TR} \tag{3.131}$$

where τ = skew angle, rad
K = constant = 16 oz/lb (102 g/in)
I_p = polar moment of inertia, lb · in² (N · cm²)
I_t = transverse moment of inertia, lb · in² (N · cm²)
T = plane of axial separation, in (cm)
R = balance radial distance, in (cm)

Note that if the disk skew τ is excessive, then it may be physically impossible to place a sufficient couple on the disk to correct for the skew effect. The wheel must be removed from the rotor and realigned. It is often advisable to monitor the axial runout of the overhung wheel to check for disk skew.

3.3.7 General Two-Plane Balancing

The problem of balancing an overhung disk skew, as just discussed, is an example of a general two-plane balancing problem. The original procedure described by Thearle (1934) was a semigraphical method by which the two-plane balance corrections were computed. This semigraphical method was used into the late 1970s when it was replaced by the two-plane balancing solution on the handheld programmable calculators (see Jackson, 1979).

The vibration monitored at the near and far planes Z_n and Z_f is assumed to be

a function of the two unknown values of unbalance $\mathbf{U}_1$ and $\mathbf{U}_2$.

$$\mathbf{Z}_n = \mathbf{a}_{n1}\mathbf{U}_1 + \mathbf{a}_{n2}\mathbf{U}_2$$
$$\mathbf{Z}_f = \mathbf{a}_{f1}\mathbf{U}_1 + \mathbf{a}_{f2}\mathbf{U}_2 \qquad (3.132)$$

To compute the values of the two planes of unbalance, a total of four influence coefficients must be determined. To determine these influence coefficients, a trial balance is placed in each plane, and the new resulting amplitudes of motion are measured. For example, the placement of a trial weight in the first plane results in

$$\mathbf{Z}_{n1} = \mathbf{a}_{n1}(\mathbf{U}_1 + \mathbf{U}_{1t}) + \mathbf{a}_{n2}\mathbf{U}_2$$
$$\mathbf{Z}_{f1} = \mathbf{a}_{f1}(\mathbf{U}_1 + \mathbf{U}_{1t}) + \mathbf{a}_{f2}\mathbf{U}_2 \qquad (3.133)$$

The influence coefficients $\mathbf{a}_{n1}$ and $\mathbf{a}_{f1}$ may now be determined as follows:

$$\mathbf{a}_{n1} = \frac{\mathbf{Z}_{n1} - \mathbf{Z}_n}{\mathbf{U}_{1t}}$$

$$\mathbf{a}_{f1} = \frac{\mathbf{Z}_{f1} - \mathbf{Z}_f}{\mathbf{U}_{1t}} \qquad (3.134)$$

The trial balance weight $\mathbf{U}_{1t}$ is now removed, and a trial balance weight $\mathbf{U}_{2t}$ is placed in the second balance plane. Note that it is not necessary to remove the first trial balancing weight. If the first balancing weight has caused a substantial reduction in the rotor response, then it is desirable to keep the trial weight in place. For example, removing a trial weight from the hot section of a gas turbine may require an extra day for the unit to cool down. Also complications may arise when an attempt is made to remove the balancing weight from the hot section, such as breaking the extraction tool or dropping the weight into the turbine passageway. When this occurs, the unit must be disassembled to remove the weight to prevent blade damage.

If the first trial weight $\mathbf{U}_{1t}$ is assumed to be left in place, and a second trial balance weight $\mathbf{U}_{2t}$ is placed in the second balance plane, the resulting vibration is given by

$$\mathbf{Z}_{n2} = \mathbf{a}_{n1}(\mathbf{U}_1 + \mathbf{U}_{1t}) + a_{n2}(\mathbf{U}_2 + \mathbf{U}_{2t})$$
$$\mathbf{Z}_{f2} = \mathbf{a}_{f1}(\mathbf{U}_1 + \mathbf{U}_{1t}) + \mathbf{a}_{f2}(\mathbf{U}_2 + \mathbf{U}_{2t}) \qquad (3.135)$$

The influence coefficients $\mathbf{a}_{n2}$ and $\mathbf{a}_{f2}$ are obtained by subtracting the vibration readings after the application of the first trial weight as follows (if $\mathbf{U}_{1t}$ is left in):

$$\mathbf{a}_{n2} = \frac{\mathbf{Z}_{n2} - \mathbf{Z}_{n1}}{\mathbf{U}_{2t}}$$

$$\mathbf{a}_{f2} = \frac{\mathbf{Z}_{f2} - \mathbf{Z}_{f1}}{\mathbf{U}_{2t}} \qquad (3.136)$$

If the first trial weight $\mathbf{U}_{1t}$ is removed, then replace $\mathbf{Z}_{n1}$ and $\mathbf{Z}_{f1}$ by the original vibration readings $\mathbf{Z}_n$ and $\mathbf{Z}_f$.

The balance corrections $\mathbf{U}_{b1}$ and $\mathbf{U}_{b2}$ are given by

$$\begin{Bmatrix} \mathbf{U}_{b1} \\ \mathbf{U}_{b2} \end{Bmatrix} = - \begin{vmatrix} \mathbf{U}_1 + \mathbf{U}_{1t} \\ \mathbf{U}_2 + \mathbf{U}_{2t} \end{vmatrix} = - \begin{vmatrix} \mathbf{a}_{n1} & \mathbf{a}_{n2} \\ \mathbf{a}_{f1} & \mathbf{a}_{f2} \end{vmatrix}^{-1} \begin{Bmatrix} \mathbf{Z}_{n2} \\ \mathbf{Z}_{f2} \end{Bmatrix} \qquad (3.137)$$

Solving for the final balance correction values gives

$$U_{b1} = \frac{a_{n2}Z_{f2} - a_{f2}Z_{n2}}{a_{n1}a_{f2} - a_{f1}a_{n2}}$$

$$U_{b2} = \frac{a_{f1}Z_{n2} - a_{n1}Z_{f2}}{a_{n1}a_{f2} - a_{f1}a_{n2}}$$

(3.138)

The values of U_{b1} and U_{b2} represent the values of trim balance correction required if both trial balance weights are left in place. If the balance computations are performed using the original vibration readings for the near and far planes Z_n and Z_f, then the computed balances will correspond to the total original balance correction required on the rotor.

Example 3.11: Two-Plane Balancing Using the Influence Coefficient Method Including Runout Compensation, Rotor 99DM-1. Table 3.8 represents the initial and final vibration readings after trial weights were placed on a rotor at the near and far planes (Jackson, 1979). Shown on the table are the computed near and far plane balance corrections. In this calculation, a positive sign convention represents lag angles for both vibration and balance weights measures against rotation from the vibration data probe.

The compensated near and far amplitudes are first determined by subtracting the slow-roll vectors measured at the two ends:

$$Z_{nc} = 1.8\angle148° - 0.5\angle272° = 2.12\angle137°$$

$$Z_{fc} = 3.6\angle115° - 0.4\angle123° = 3.2\angle114°$$

The four influence coefficients are

$$a_{n1} = 0.206\angle175° \qquad a_{f1} = 0.364\angle194°$$

$$a_{n2} = 0.341\angle182° \qquad a_{f2} = 0.170\angle165°$$

Let

$$\Delta = a_{n1}a_{f2} - a_{f1}a_{n2} = 0.0986\angle208°$$

Let $[R] = -[a]^{-1}$ be the negative of the inverse of the influence coefficient matrix.

$$R_{11} = -\frac{a_{f2}}{\Delta} = -\frac{0.170\angle165°}{0.0986\angle208°} = 1.724\angle137°$$

$$R_{12} = \frac{a_{n2}}{\Delta} = 3.458\angle334°$$
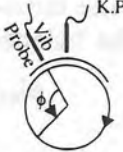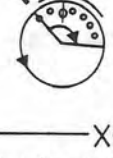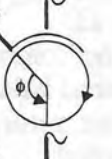
$$R_{21} = \frac{a_{f1}}{\Delta} = 3.69\angle346°$$

$$R_{22} = -\frac{a_{n1}}{\Delta} = 2.09\angle147°$$

The balancing solution for U_{b1} and U_{b2} is given in terms of the R matrix and compensated vibration readings as follows:

$$U_{b1} = R_{11}Z_{nc} + R_{12}Z_{fc}$$

$$U_{b2} = R_{21}Z_{nc} + R_{22}Z_{fc}$$

(3.139)

TABLE 3.8 Two-Plane Balance and Trim correction of Rotor Including Runout Compensations

Rotation counter-clockwise		Rotation clockwise

Machine identification __99DM-1__ DATE __7/78__
Run-out recorded @ __300__ R.P.M.; "at-speed" data @ __31,000__ RMP
Key phasor probe is @ __0°__ ; Probes @ __90__ N& __90°__ F

- H.P. 67 in "run" press [f][Program]... read mag. card sides 1 & 2
- Press [f][a]

	Near plane			Far plane		
	Angle	Amount		Angle	Amount	
Enter run-out data	1	272 R/S	2	0.5 R/S	3	123 R/S	4	0.4 R/S

- Press [f] [b] and enter "at speed" data

		Angle		Amount			Angle		Amount
Orig. data	5	48 R/S	6	1.8 R/S	11	115 R/S	12	3.6 R/S
T.W. @ near plane	7	178 R/S	8	1.1 R/S	13	98 R/S	14	2.0 R/S
T.W. @ far plane	9	98 R/S	10	2.1 R/S	15	102 R/S	16	3.7 R/S

T.W. locations	17	120 °	18	4.9 gms	Units	19	220 °	20	4.9 gms	Units

- Press [A,B,C,D] to read out wt. add locations

	A	B		C	D
Corr. weight + location	7.49	84 .96 °		5.32	179.73 °
	Amt	Loc		Amt	Loc

- Press [E] Enter trim data

	Near plane			Far plane		
	Angle	Amount		Angle	Amount	
	1	268 R/S	2	6.6 R/S	3	0.85 R/S	4	0.5 R/S

- Press [A,B,C,D] to read out trim corrections

	A	B		C	D
	2.79	-47.11 312.89 °		1.55	135.54. °
	Amt	Loc		Amt	Loc

Note: At pts.(3) marked (X →) in left margin. System para-meters may be recorded in run by [r] [w/data] and mag. card.

Notes
- Phase angles (all) taken against rotation from vib. data probe (sensor).
- Trial wts. (T.W.) are also placed against rotation from vib. data probe.
- Correction wts. & angles hold same logic.

3.91

Coefficients $\mathbf{R}_{11}$ and $\mathbf{R}_{22}$ are the direct or principal balancing coefficients, while coefficients $\mathbf{R}_{12}$ and $\mathbf{R}_{21}$ are the cross-coupling balancing coefficients. Note that both the cross-coupling coefficients $\mathbf{R}_{12}$ and $\mathbf{R}_{21}$ are greater than the principal balancing coefficients $\mathbf{R}_{11}$ and $\mathbf{R}_{22}$. When this occurs, it is difficult to balance the rotor by single-plane balancing using each plane in turn. This approach is only valid if the principal balancing coefficients (or influence coefficients) are larger than the cross-coupling coefficients.

The balance values are given by

$$\mathbf{U}_{b1} = 1.724\angle137° \times 2.12\angle137° + 3.458\angle334° \times 3.2\angle114°$$

$$= 3.65\angle274° + 11.06\angle88° = 7.49\angle85° \text{ (against rotation)}$$

$$\mathbf{U}_{b2} = 3.69\angle346° \times 2.12\angle137° + 2.09\angle147° \times 3.2\angle114°$$

$$= 7.822\angle123° + 6.68\angle261° = 5.3\angle180° \text{ (against rotation)}$$

Figure 3.45 represents the locations of the trial and final balance weights on the near and far balancing planes. On the near balancing plane, the direction of rotation, looking at the end of the rotor, is counterclockwise. The near balancing plane is shown labeled with 36 balancing holes. The trial weight of 4.9 g is placed in hole 13. The final balance weight is shown as being situated between holes 9 and 10. A vector split of the weight between holes 9 and 10 results in the computation of 3.79 g for hole 9 and 3.726 g for hole 10.

When the far balancing plane is viewed from the other end of the rotor, the direction of rotation is shown to be clockwise. In both balance planes, however, the holes are always labeled against rotation. The initial trial weight is shown located at hole 23, and the final balance should be 5.32 g located at hole 18. If the trial weight is left in hole 23, then a trim balance of 3.54 g is computed. This trim balance may be split between holes 12 and 13 with 1.32 g in hole 12 and 2.23 g in hole 13.

The combination of the trim plus the trial is equivalent to the predicted total required balance weight of 5.3 g in hole 18. After the balance weights were placed on the rotor, the resulting amplitudes $\mathbf{Z}_{nb} = 0.6\angle268°$ and $\mathbf{Z}_b = 0.5\angle0.85°$ are recorded.

A refined trim balance based on the $[R]$ balance matrix and the current-compensated vibration readings may be computed as follows:

$$\mathbf{U}_{n,\text{trim}} = \mathbf{R}_{11}\mathbf{Z}_{nbc} + \mathbf{R}_{12}\mathbf{Z}_{fbc} = 2.79\angle313°$$

$$\mathbf{U}_{f,\text{trim}} = \mathbf{R}_{21}\mathbf{Z}_{nbc} + \mathbf{R}_{22}\mathbf{Z}_{fbc} = 1.55\angle135.5°$$

This additional balance correction would reduce the final uncompensated rotor response to

$$\mathbf{U}_{n,\text{final}} = 0.5 \text{ mil} \angle272°$$

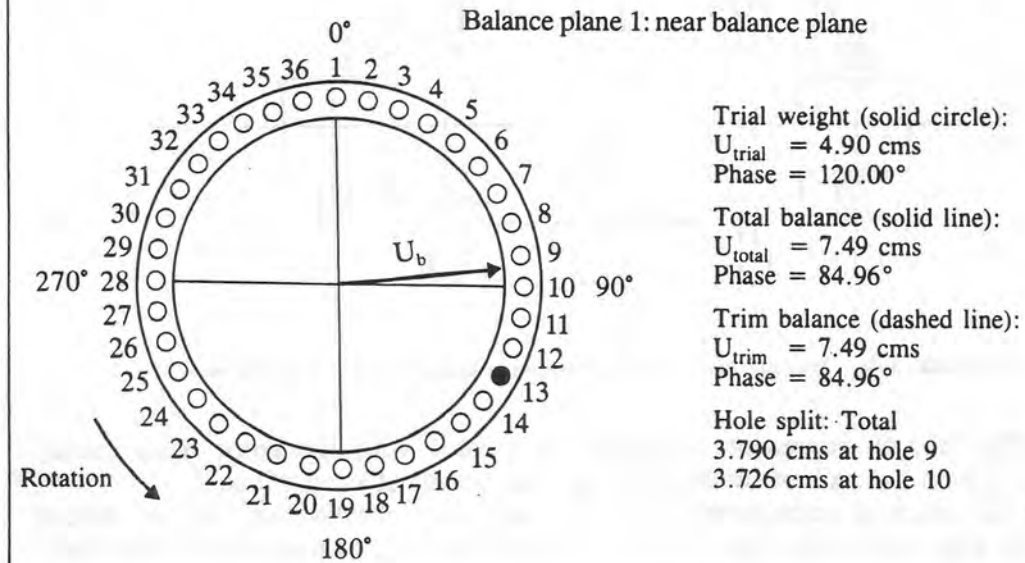$$\mathbf{U}_{f,\text{final}} = 0.40 \text{ mil} \angle123°$$

The above values are identical to the initial slow-roll vectors.
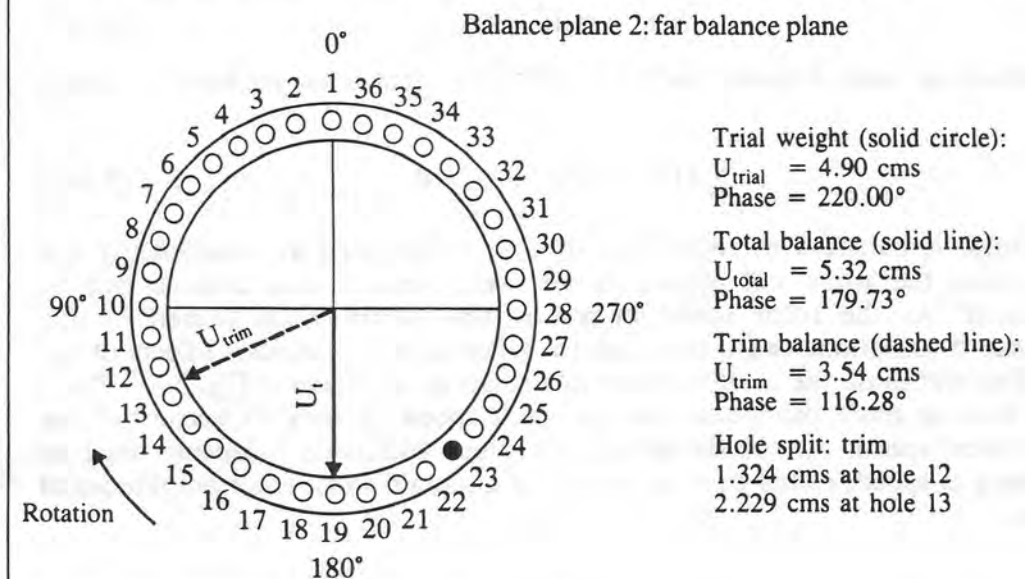
3.4 MULTIPLANE FLEXIBLE ROTOR BALANCING

3.4.1 Introduction

All rotating shafts exhibit flexibility effects when spinning. A rotor is called *flexible* if the shaft does not appear to hold balance after being balanced as a rigid

Two plane balancing of 99DX-1 — (Jackson — *Practical Vibration Prixer*, pp. 103)
H = 3600 rpm, run-out recorded at 300 rpm, non-contact displacement probes
phase angles and trial weights measured against rotation from data probe

Balance plane 1: near balance plane

Trial weight (solid circle):
U_{trial} = 4.90 cms
Phase = 120.00°

Total balance (solid line):
U_{total} = 7.49 cms
Phase = 84.96°

Trim balance (dashed line):
U_{trim} = 7.49 cms
Phase = 84.96°

Hole split: Total
3.790 cms at hole 9
3.726 cms at hole 10

Two plane balancing of 99DX-1 — (Jackson — *Practical Vibration Prixer*, pp. 103)
H = 3600 rpm, run-out recorded at 300 rpm, non-contact displacement probes
phase angles and trial weights measured against rotation from data probe

Balance plane 2: far balance plane

Trial weight (solid circle):
U_{trial} = 4.90 cms
Phase = 220.00°

Total balance (solid line):
U_{total} = 5.32 cms
Phase = 179.73°

Trim balance (dashed line):
U_{trim} = 3.54 cms
Phase = 116.28°

Hole split: trim
1.324 cms at hole 12
2.229 cms at hole 13

FIGURE 3.45 Location of trial, final, and trim balance weights on near and far balance planes.
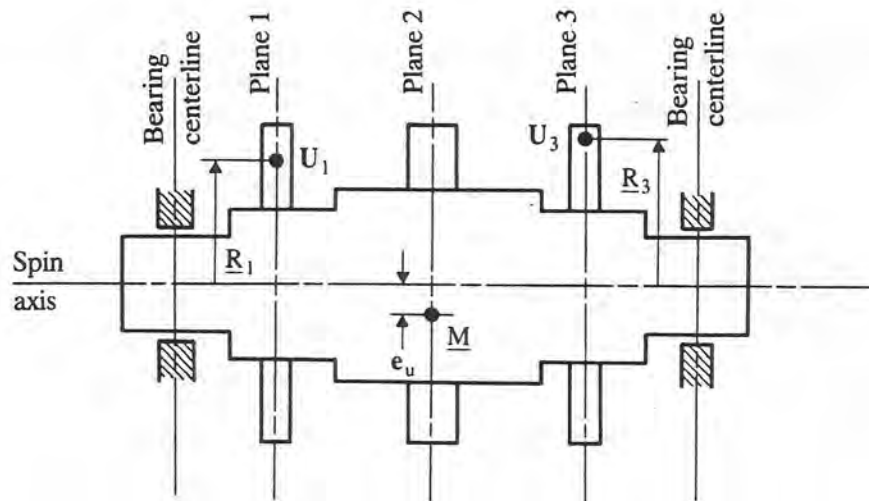
FIGURE 3.46 Multimass rotor with two-plane static balance correction.

body. Figure 3.46 represents a multistation rotor with the rotor mass center displaced from the axis of rotation by the distance e_u at rotor plane 2.

For this class of unbalance, the rotor rigid-body inertia axis will be shifted from the spin axis by the distance of e_u. When this rotor is placed in a rigid-body balancing machine, either the hard or soft bearing type, the balance machine will indicate a two-plane correction in which the left and right planes will be in phase and of similar magnitude.

Correction weights of w_1 and w_3 are placed at planes 1 and 3, respectively, at radii R_1 and R_3. As a rigid body, the multistage rotor now appears to be perfectly balanced. The original rotor unbalance may be represented by

$$M e_u = m_2 \mathbf{R}_2 = \mathbf{U}_2 \qquad (3.140)$$

The rotor is in static balance since it satisfies the rigid rotor balance conditions that

$$\sum \mathbf{U} = \mathbf{U}_1 + \mathbf{U}_2 + \mathbf{U}_3 = 0 \qquad (3.141)$$

If the rotor is balanced as shown in Fig. 3.47 is operated at a sufficiently low speed, then the rotor will appear to be well behaved and balance will be maintained. As the rotor speed increases, the inertia loads caused by the unbalance distributions cause the shaft to deflect due to elasticity effects of the shaft. This will cause the shaft to bow while rotating, as shown in Fig. 3.48. These effects become more pronounced as the shaft speed exceeds 70 percent of the rotor critical speed. At speeds above this value, additional balancing must be performed at speed, called *trim balancing*, to maintain small rotor amplitudes of motion.

3.4.2 Types of Unbalance

The multimass flexible rotor may have a variety of unbalance distributions. Figure 3.49 represents four basic types of unbalance distributions encountered with a multimass rotor. There are many instances in which all four types of unbalance are encountered.
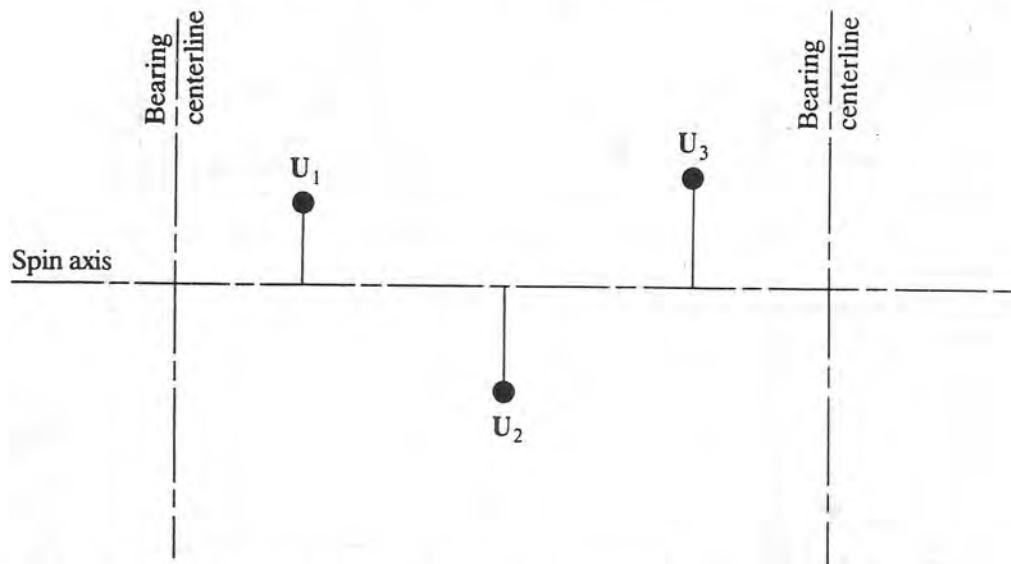
**FIGURE 3.47** Equivalent multiplane unbalance distribution.

Figure 3.49*a* represents a continuous unbalance distribution along the shaft due to machining a concentric shaft with radial eccentricity. The second distribution, shown in Fig. 3.49*b,* includes radial unbalances such as encountered by assembled compressor turbine stages on a shaft. It is often desirable to individually balance each wheel before assembly on a shaft to minimize radial wheel unbalance.

Figure 3.49*c* represents a shaft with bow. In a bowed rotor, the mass-elastic centerline does not lie along the shaft axis of rotation. Bows may be introduced by nonuniform shrink fits, thermal effects, permanent sag due to gravitational effects, or excessive vibration. The initial bow may change with operating conditions, as is the case with all generator rotors. Excessive shaft bow is difficult to correct by simple balancing because it may require large correction weights.

The last case shown is the disk skew. The influence of disk skew is the most pronounced with overhung impellers and wheels. Disk skew may be induced by
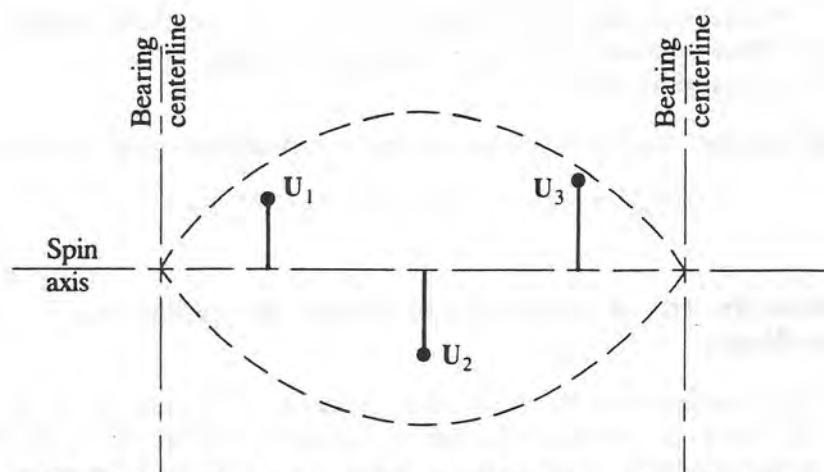
FIGURE 3.48 Shaft deflection with speed for rotor balanced as a rigid body.
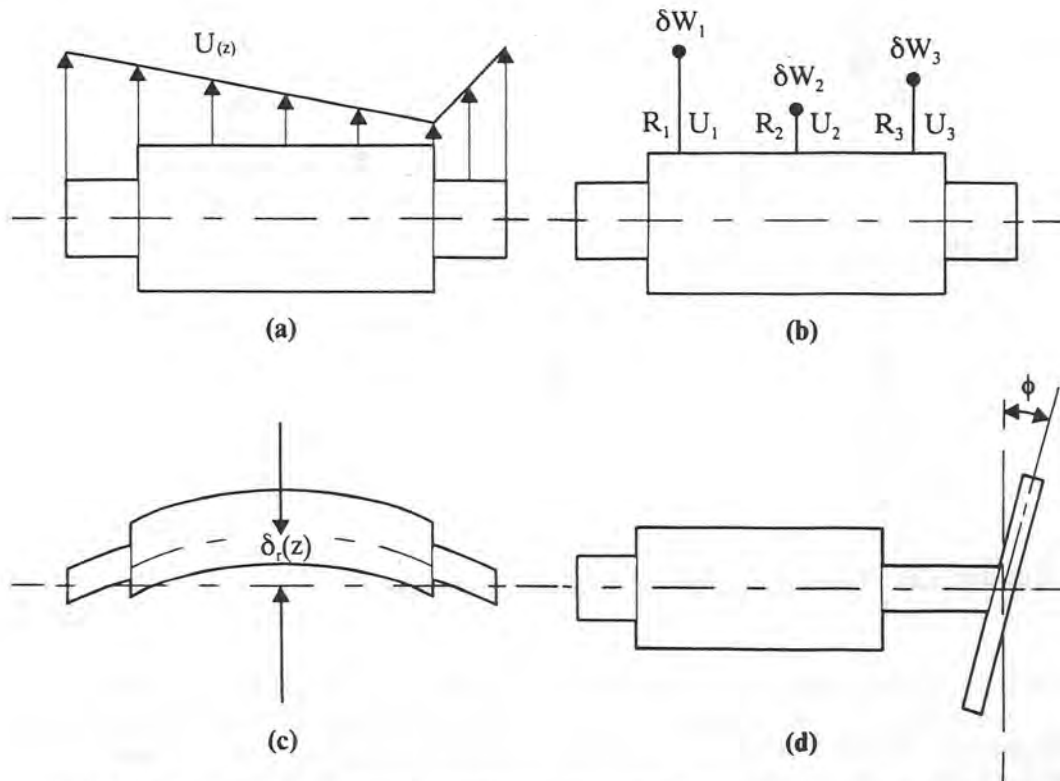
FIGURE 3.49 Types of unbalance distribution in a multimass flexible rotor: (*a*) continuous unbalance; (*b*) distributed radial point mass unbalance; (*c*) rotor row unbalance; (*d*) moment unbalance.

improper filtering of the impeller to the shaft. A shaft bow will also induce a disk skew effect in an overhung rotor.

The general rotor equations of motion may be expressed in matrix form as

$$[M]\{\ddot{Z}\} + [G]\{\dot{Z}\} + [C]\{\dot{Z}\} + ([K][\{Z\} - \{Z_0\}]) = \{F(t)\} \qquad (3.142)$$

where $\{Z\}' = [\{X\}, \{Y\}, \{\Theta_x\}, \{\Theta_y\}]'$
$\qquad$ = horizontal and vertical displacements and rotations of shaft
$\qquad [G]$ = skew symmetric gyroscopic damping matrix
$\qquad \{Z_0\}$ = initial shaft bow

The forcing function due to radial unbalance and disk skew is of the form:

$$\{F(t)\}' = [\{Ue^{-i\phi_m{}'}\}, \{\tau(I_p - I_t)e^{-i\phi_d{}'}\}]\omega^2 e^{i\omega t} \qquad (3.143)$$

3.4.3 Critical Speeds of a Uniform Shaft and Reduction to a Point-Mass Model

To more fully understand some of the concepts of balancing a multistation flexible rotor with a discrete number of balance planes, it is necessary to introduce some concepts of continuum theory of shafts and the reduction of a continuum to a discrete point or lumped-mass stiffness rotor model.

Figure 3.50*a* represents a uniform beam of length L and diameter D. The
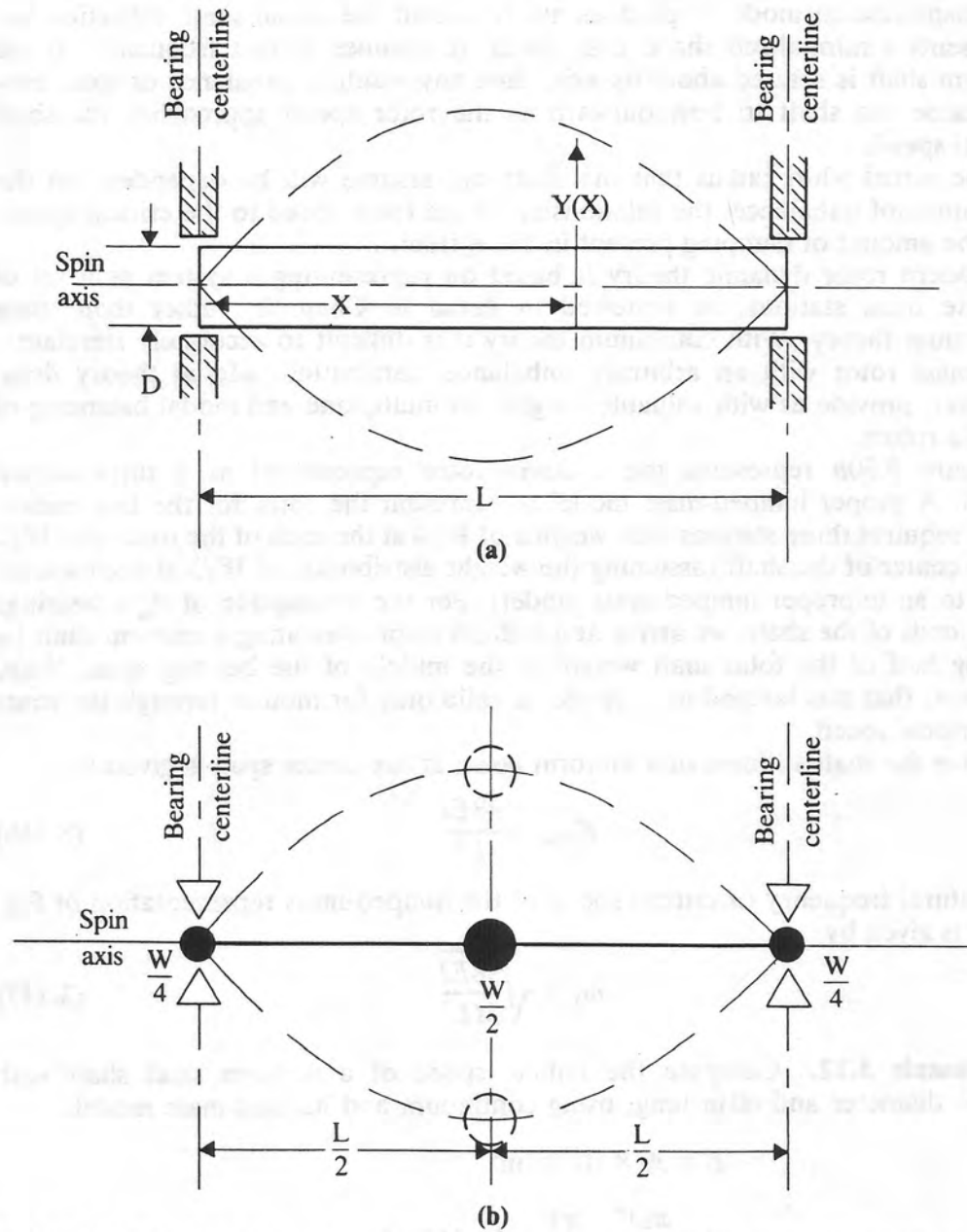
FIGURE 3.50 (a) First mode of a uniform beam; (b) uniform beam represented as a three-station lumped-mass model.

beam natural frequencies (considering ideal rigid supports) are given by

$$\omega_n = (n\pi)^2 \sqrt{\frac{EI}{ML^3}} \quad \text{rad/s} \tag{3.144}$$

where $\omega_n = n$th natural frequency. Corresponding to each natural frequency (or eigenvalue) is a mode shape or eigenvector. The eigenvectors for a uniform beam are given by

$$\phi(x) = \sin \frac{n\pi x}{L} \tag{3.145}$$

The displacement mode shape does not represent the actual shaft deflection but represents a normalized shape that the shaft assumes at that frequency. If the uniform shaft is rotated about its axis, then any residual unbalance or shaft bow will cause the shaft to bow outward as the rotor speed approaches the shaft critical speed.

The actual whirl radius that the shaft will assume will be dependent on the magnitude of unbalance, the relationship of the rotor speed to the critical speed, and the amount of damping present in the system.

Modern rotor dynamic theory is based on representing a system as a set of discrete mass stations, as reviewed in detail in Chap. 2, rather than using continuum theory. With continuum theory it is difficult to accurately simulate a multimass rotor with an arbitrary unbalance distribution. Modal theory does, however, provide us with valuable insights on multiplane and modal balancing of flexible rotors.

Figure 3.50b represents the uniform rotor represented as a three-station model. A proper lumped-mass model to represent the rotor for the first critical speed requires three stations with weights of $W/4$ at the ends of the rotor and $W/2$ at the center of the shaft (assuming the weight distribution of $W/3$ at each station leads to an improper lumped-mass model). For the assumption of rigid bearings at the ends of the shaft, we arrive at a Jeffcott rotor simulating a uniform shaft by placing half of the total shaft weight at the middle of the bearing span. Note, however, that this lumped-mass model is valid only for motion through the rotor first critical speed.

Since the shaft stiffness of a uniform beam at the center span is given by

$$K_{\text{shaft}} = \frac{48EI}{L^3} \tag{3.146}$$

the natural frequency or critical speed of the lumped-mass representation of Fig. 3.50b is given by

$$\omega_1 = \sqrt{\frac{98EI}{ML^3}} \tag{3.147}$$

Example 3.12. Compute the critical speed of a uniform steel shaft with 4.00-in diameter and 60 in long, using continuum and lumped-mass models.

$$E = 30 \times 10^6 \, \text{lb/in}^2$$

$$I = \frac{\pi D^4}{64} = \frac{\pi 4^2}{64} = 12.566 \, \text{in}^2$$

$$M = \rho AL = \frac{0.283 \, \text{lb/in}^3}{386 \, \text{in/s}^2} \times \frac{\pi 4^2}{2} \times 60$$

$$= 1.106 \, \frac{\text{lb} \cdot \text{s}}{\text{in}^2} \text{ total shaft mass (426.75 lb)}$$

$$K = \frac{48EI}{L^3} = 83,773 \, \text{lb/in}$$

$$\omega_{1,\text{uniform shaft}} = (3.142)^2 \sqrt{\frac{30.0 \times 10^6 \times 12.566}{1.106 \times 60^3}}$$

$$= 392.06 \, \text{rad/s} = 3744 \, \text{rpm}$$

$$\omega_{1,\text{lumped mass}} = \sqrt{\frac{83,773}{\left(\frac{1.106}{2}\right)}}$$

$$= 389.2 \text{ rad/s} = 3717 \text{ rpm}$$

From the above example, we see that the three-station lumped-mass rotor represents the uniform beam first critical speed with a deviation of less than 0.7 percent. It has been found that any continuous unbalance distribution along a rotor may be represented by a set of three discrete balance stations located along the shaft to simulate rotor bowing over the first critical speed.

To approximate the characteristics of the uniform beam for the second mode, five mass stations are required, as shown in Fig. 3.51. The ends have lumped weights of $W/8$, and the center sections have lumped weights of $W/4$. This results in a lumped-mass model which approximates the second rotor critical speed, also to less than 0.7 percent error. Note that a lumped-mass model in which each
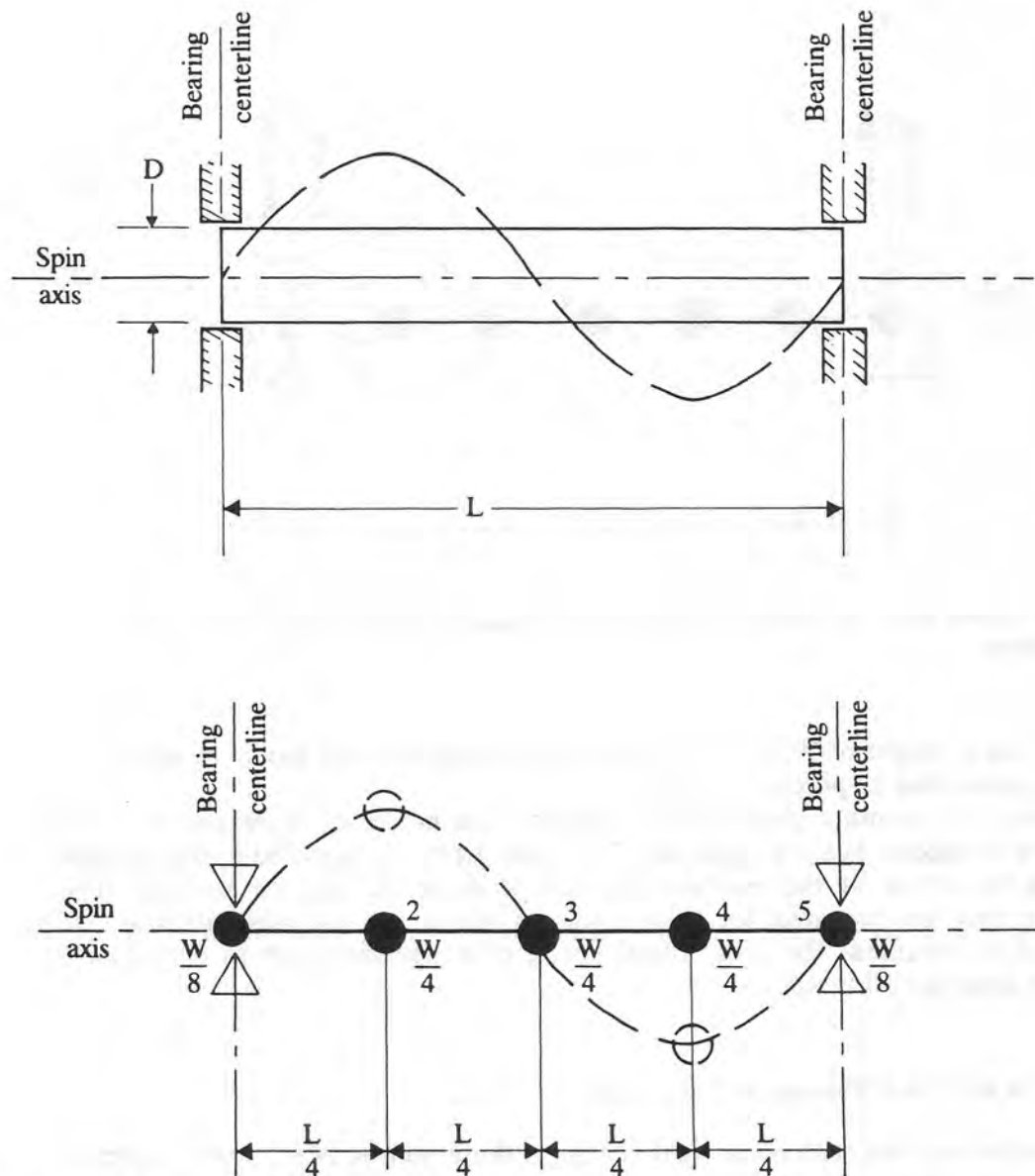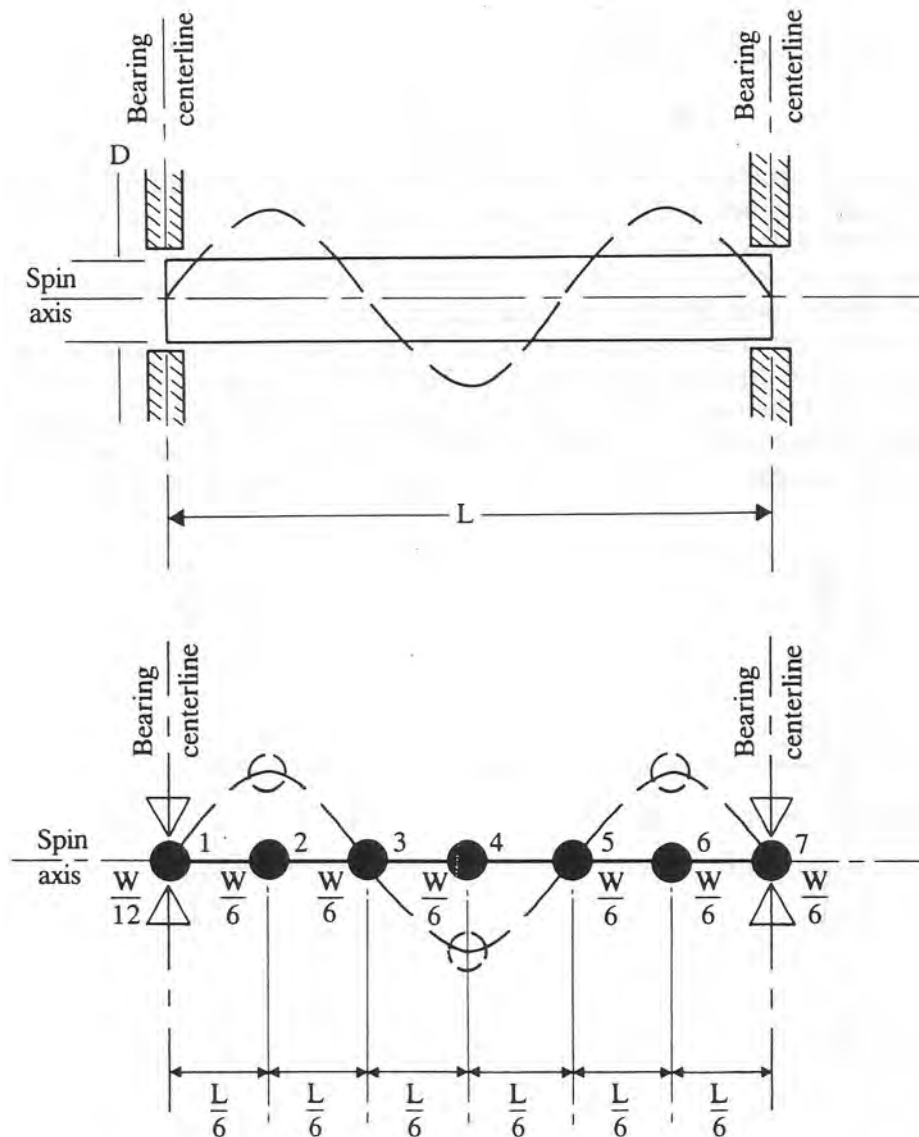

FIGURE 3.51 Lumped-mass model for second mode representation of a uniform beam.

FIGURE 3.52 Lumped-mass model for third mode representation of a uniform beam.

station has a weight of $W/5$ would produce an incorrect rotor model in which the critical speed was 12 percent too high.

Figure 3.52 shows a seven-station lumped-mass model to represent the third mode of a uniform beam to less than 1 percent error. In this model, the lumped weights are $W/12$ at the end stations and $W/6$ at the interior stations. The analogy may be repeated for higher modes. Only $2N+1$ mass stations are required to represent the Nth critical speed of a uniform shaft to less than 1 percent error for all modes.

3.4.4 *N* or *N* + 2 Planes of Balancing

For a uniform rotor with ideal rigid bearings, there will be $N+1$ node points at which zero motion occurs. If a rotor has a point along the shaft at which zero displacement occurs for a particular critical speed, it is called a *nodal point*. The

placement of a balance weight at this nodal point will have no effect on the rotor balancing for speeds within 20 percent of this particular critical speed.

Hence, the number of active balance planes required for the idealized uniform rotor to balance the Nth critical speed is given by the number of required mass stations minus the zero-displacement nodal points as follows:

$$N_{\text{balance planes}} = (2N + 1)_{\text{total nodes}} - (N + 1)_{\text{zero disp. nodes}} = N \qquad (3.148)$$

Thus for the first mode or critical speed ($N = 1$), only one balance plane is required. Two balance planes are required to balance the second mode, and three planes are required to balance the third mode. This is referred to as the *N-plane method* of balancing. Long turbogenerators usually follow this rule. There has been considerable discussion in the literature as to whether N or $N + 2$ balance planes are required for balancing a flexible rotor (e.g., Kellenberger, 1972; Bishop and Parkinson, 1965, 1972).

For a highly flexible rotor with little displacement at the bearing locations, only N balance planes are required. If the rotor is to operate near or above the third rotor critical speed, rigid-body balancing may actually result in higher vibrations near the third critical speed. Under these circumstances three-plane modal balancing must be employed.

A great deal of information, as to the required number of balancing planes and their most effective location, may be obtained by examining the critical speed map and corresponding mode shapes for a particular rotor.

Figure 2.36 represents a typical critical speed map of a uniform shaft for various bearing stiffness values, as shown by Rieger (1986). The first three critical speeds are plotted in log-log format as a function of bearing stiffness. From the chart we see that for bearing stiffness stress below 2×10^5 lb/in, the rotor first and second critical speeds are effectively straight lines on the log-log plot.

If the rotor speed is kept below the rotor third critical speed and the bearing stiffness is below 2×10^5 lb/in, then the rotor will operate essentially as a rigid body. The modes shown on the chart for this region represent rigid-body conical and cylindrical modes of motion. The rotor may be balanced as a rigid body in any two arbitrary planes.

As the rotor speed is increased, assuming that the bearing stiffness values do not change, the rotor third critical speed is encountered. The bearing stiffness has little influence on the third critical speed until stiffness values of over 0.5×10^6 are encountered. This third mode is referred to as the *free-free mode*. Gas bearing supported rotors have the characteristics of rigid-body behavior at the first two modes due to their low bearing stiffness values. The rotor will behave as if it is badly out of balance as it approaches the third or free-free critical speed. This will be particularly true if the original balance weights have been placed at the node points of the third mode. Three additional balance planes will be required to balance the third mode so as not to upset the first two modes. A modal balancing procedure will be required to balance this mode that uses three simultaneous balance weights.

The other extreme range of operation is the situation of high bearing stiffness relative to the shaft stiffness. For bearing stiffness values of above 5×10^6 lb/in, the bearings begin to approach nodal points of zero vibration. Under these circumstances, rigid-body balancing may not be beneficial. If, e.g., the rigid-body correction weights are placed in the rotor end planes, there is no improvement in the balance condition. A single balancing plane at the rotor center is required to balance the rotor for the first mode. To balance the second mode, two balance planes are required for the case of high bearing stiffness. These balance planes

should not be placed at node points of the second mode, but rather at the locations corresponding to maximum amplitude.

3.4.5 Rotor Modal Equations of Motion and Modal Unbalance Distribution

The generalized equations of motion of a rotor bearing system (neglecting shaft bow) may be written in terms of the rotor mass, damping, and stiffness matrices as follows:

$$[M]\{\ddot{\mathbf{Z}}\} + [C]\{\dot{\mathbf{Z}}\} + [K]\{\mathbf{Z}\} = \omega^2\{\mathbf{U}\}e^{i\omega t} \qquad (3.149)$$

where $\{\mathbf{Z}\}$ represents the complex rotor displacements at the various n stations along the shaft.

The undamped system critical speeds are determined by setting the damping and external forcing functions to zero. This results in the standard eigenvalue problem for the determination of the rotor critical speeds:

$$[-\omega^2[M] + [K]]\{\mathbf{Z}\} = 0 \qquad (3.150)$$

where

$$\{\mathbf{Z}\} = \sum_{i=1}^{m} q_i\{\phi\}_i = [\Phi]\{q\} \qquad (3.151)$$

$$q_i = \text{modal coefficient for } i\text{th mode}$$

Since $[M]$ and $[K]$ are symmetric $n \times n$ matrices, there are only n natural frequencies associated with the system as compared to an infinity of solutions for a continuum such as our uniform beam example. From the standpoint of flexible rotor balancing, only the first several critical speeds are of interest.

By using only the first m modes (where $m < n$ stations), the rotor equations of motion are reduced further:

$$\left[\underbrace{\Phi}_{n \times m}\right] = \left[\underbrace{\{\phi\}_1}_{n \times 1} \underbrace{\{\phi\}_2}_{n \times 1} \underbrace{\{\phi\}_m}_{n \times 1}\right]\Big\} n \text{ stations} \qquad (3.152)$$

$$\underbrace{}_{m \text{ modes}}$$

In a typical multiplane balancing problem, $m = 2$ or 3 modes should be sufficient. Large turbine-generators, however, may require 4 to 5 modes for accurate multiplane balancing.

Assuming that three modes of motion will be sufficient to represent the rotor balancing problem, the modal properties are given by

$$\left[\underbrace{\phi_1 \quad \phi_2 \quad \phi_3}_{m \times n}\right]^T \left[\underbrace{M}_{n \times n}\right] \left[\underbrace{\phi_1 \quad \phi_2 \quad \phi_3}_{n \times m}\right] = \begin{bmatrix} M_1 & & \\ & M_2 & \\ & & M_3 \end{bmatrix}_{m \times m}$$

$$\left[\underbrace{\Phi}_{m \times n}\right]^T \left[\underbrace{C}_{n \times n}\right] \left[\underbrace{\Phi}_{n \times m}\right] = \begin{bmatrix} C_{11} & C_{12} & C_{13} \\ C_{21} & C_{22} & C_{23} \\ C_{31} & C_{32} & C_{33} \end{bmatrix}_{m \times m} \qquad (3.153)$$

$$\left[\underbrace{\Phi}_{m \times n}\right]^T \left[\underbrace{K}_{n \times n}\right] \left[\underbrace{\Phi}_{n \times m}\right] = \begin{bmatrix} K_1 & & \\ & K_2 & \\ & & K_3 \end{bmatrix}_{m \times m}$$

Note that in the reduced modal $[M]$, $[C]$, and $[K]$ matrices, the mass and stiffness matrices are diagonal matrices because of the properties of orthogonality. In general, with discrete bearings providing the damping, the damping modal matrix is never diagonal. The damping matrix is diagonal only if it is proportional to the mass and stiffness matrix as follows:

$$[C]_{\text{diag}} = \alpha[K] + \beta[M] \tag{3.154}$$

This idealized assumption, called *proportional damping*, does not occur in real-life rotor systems. The concept of proportional damping is often used in structural damping but is not exact when applied to turborotors with substantial damping at the bearings. With symmetric rotors such as the uniform beam, the model cross-coupling between the first and the second modes C_{12} and C_{21} may be ignored, along with the cross-coupling between the second and third modes C_{23} and C_{32}. However, the modal cross-coupling coefficients between the first and third modes C_{13} and C_{31} are never zero as is true for the modal cross-coupling coefficients C_{24} and C_{42} between the second and fourth modes.

The oversimplification and neglect of these modal cross-coupling coefficients have caused much confusion and led to numerous misconceptions concerning modal balancing as compared to the influence coefficient method.

The reduced modal equations of motion using three modes only for a turborotor are of the form

$$M_1\ddot{q}_1 + C_{11}\dot{q}_1 + C_{13}\dot{q}_3 + K_1 q_1 = \omega^2 \phi_1^T U e^{i\omega t}$$

$$M_2\ddot{q}_2 + C_{22}\dot{q}_2 + K_2 q_2 = \omega^2 \phi_2^T U e^{i\omega t} \tag{3.155}$$

$$M_3\ddot{q}_3 + C_{31}\dot{q}_1 + C_{33}\dot{q}_3 + K_3 q_3 = \omega^2 \phi_3^T U e^{i\omega t}$$

By dividing by modal mass, the generalized equations become

$$\ddot{q}_1 + 2\xi_{11}\omega_1\dot{q}_1 + 2\xi_{13}\omega_3\dot{q}_3 + \omega_1^2 q_1 = \omega^2 e_1 e^{i\omega t}$$

$$\ddot{q} + 2\xi_{22}\omega_2\dot{q}_2 + \omega_2^2 q_2 = \omega^2 e_2 e^{i\omega t} \tag{3.156}$$

$$\ddot{q}_3 + 2\xi_{31}\omega_1\dot{q}_1 + 2\xi_{33}\dot{q}_3 + \omega_3^2 q_3 = \omega^2 e_3 e^{i\omega t}$$

where e_i are the complex modal unbalance eccentricity vectors

$$e_i = \frac{\phi_i^T}{M_i} U \tag{3.157}$$

It is of interest that the second modal equation is essentially uncoupled from the first and third modal equations for most symmetric 2-bearing rotor systems. The second mode balancing follows identically the procedure used for balancing the single-mass Jeffcott rotor except that a second mode distribution of weights is applied. These two weights are usually taken as equal and are placed on the rotor out of phase to each other.

The first and third equations are modally coupled through the modal cross-coupling coefficients C_{13} and C_{31}. Only for the case where the bearing amplitudes of motion approach nodal points of zero motion do these coefficients disappear. This situation is approximated by long generators in which modal uncoupling may be approximated. The assumption of modal uncoupling leads to the general theory of modal balancing. The modal cross-coupling coefficients cause the rotor to form a nonplanar mode shape or corkscrew in space.

Example 3.13. For the uniform rotor of Example 3.12, assume unbalance components of $U_1 = 100$ g · in, $U_2 = -200$ g · in, and $U_3 = 100$ g · in. Compute the modal unbalance eccentricity vectors e_i for the system.

Assuming that the balance weights are placed at $x_1 = L/4$, $x_2 = L/2$, and $x_3 = 3L/4$, the mode shapes for these positions for the three modes are given by

$$\{\phi\}_1^T = [0.707 \ 1.00 \ 0.707]$$

$$\{\phi\}_2^T = [1.00 \ 0.0 \ -1.00]$$

$$\{\phi\}_3^T = [0.707 \ -1.0 \ 0.707]$$

The modal weight for the uniform beam for the three modes is $W_1 = W_2 = W_3 = W_{tot/2} = 213.4$ lb $= 97{,}000$ g.

The modal unbalance eccentricities e_i in mils are given by

$$e_1 = \frac{1}{97{,}000 \text{ g}} [0.707 \ 1 \ 0.707] \left\{ \begin{array}{c} 100 \\ -200 \\ 100 \end{array} \right\} \text{g} \cdot \text{in}$$

$$= \frac{70.7 - 200 + 70.7}{97{,}000} = -0.0006 \text{ in} = -0.6 \text{ mil} < 0°$$

$$e_2 = \frac{1}{97{,}000 \text{ g}} [1.0 \ 0 \ -1.0] \left\{ \begin{array}{c} 100 \\ -200 \\ 100 \end{array} \right\} \text{g} \cdot \text{in} = 0$$

$$e_3 = \frac{1}{97{,}000 \text{ g}} [0.707 \ -1.0 \ 0.707] \left\{ \begin{array}{c} 100 \\ -200 \\ 100 \end{array} \right\} \text{g} \cdot \text{in}$$

$$= \frac{70.7 + 200.0 + 70.7}{97{,}000} = 0.00352 \text{ in} = 3.52 \text{ mils} < 0°$$

In Example 3.13 we see that the modal unbalance eccentricity for the first mode $e_1 = -0.6$ mil while the modal unbalance eccentricity for the third mode is $e_3 = 3.52$ mils. The rotor response at the third critical speed may be considerable. Since its modal unbalance eccentricity is 3.52/0.6, or 5.8, times that at the first critical speed.

If it is assumed that the modes are uncoupled (all the modal cross-coupling coefficients are assumed negligible), then the rotor response Z is a function of the rotor modal amplification factors and the modal unbalance eccentricities:

$$\{Z\} = \sum_{i=1}^{m \text{ modes}} Q_i(\omega) e_i \{\phi_i\} e^{i(\omega t - \phi_m)} \tag{3.158}$$

where

$$Q_i(\omega) = \frac{(\omega/\omega_i)^2}{\sqrt{[1 - (\omega/\omega_i)^2]^2 + (2\xi_i(\omega/\omega_i))^2}}$$

At the critical speed where $\omega = \omega_i$, the rotor amplification factor is given by

$$Q_i(\omega)\big|_{\omega=\omega_i} = A_{ci} = \frac{1}{2\xi_i} \tag{3.159}$$

Neglecting the small influences of the other modes, the rotor response at the ith critical speed is given approximately by

$$\{Z\}\big|_{\omega=\omega_i} = \frac{e_i}{2\xi_i}\{\phi_i(x)\}e^{i(\omega t - 90)} \tag{3.160}$$

The rotor motion at the critical speed (for modal uncoupling only) is equal to the products of the rotor modal unbalance eccentricity vector e_i times the modal amplification factor multiplied by the mode shape.

From Eq. 3.160 the displacements of the shaft are lagging the unbalance eccentricity vector e by 90° at the critical speed.

Example 3.14. Compute the rotor motions at the center of the shaft at the first and third critical speeds, assuming rotor amplification factors of $A_1 = 10$ and $A_3 = 8$ for the two modes.

At the first critical speed of $N_1 = 3717$ rpm, the rotor amplitude at the center (peak-to-peak motion) is given by

$$\{Z\}\big|_{x=L/2} = 2A_1 e_1\{\phi\}_1 \angle -90°$$

$$= 20(-0.6 \text{ mil})\left\{\phi\left(x = \frac{L}{2}\right)\right\}_1 \angle -90°$$

$$= 12 \text{ mils } \angle -270° \text{ peak to peak}$$

At the third critical speed of $N_3 = 33{,}453$ rpm the rotor amplitude at the center ($x = L/2$) is given by

$$\{Z\} = 2A_3 e_3 \phi \angle -90°$$

$$= 16(3.52 \text{ mils})\phi_3 \angle -90°$$

$$= 56.3 \text{ mils } \angle -90° \text{ peak to peak}$$

It is thus obvious that the rigid-body balancing procedure of Example 3.13 has created a set of unbalance weights which will have a substantial effect on the rotor at the first critical speed (12 mils peak to peak) and a catastrophic effect on the third critical speed (56 mils peak to peak). Without the rigid-body balancing, the rotor would have an amplitude of 32 mils peak to peak at the third critical speed but would have an amplitude of 41 mils at the first critical speed.
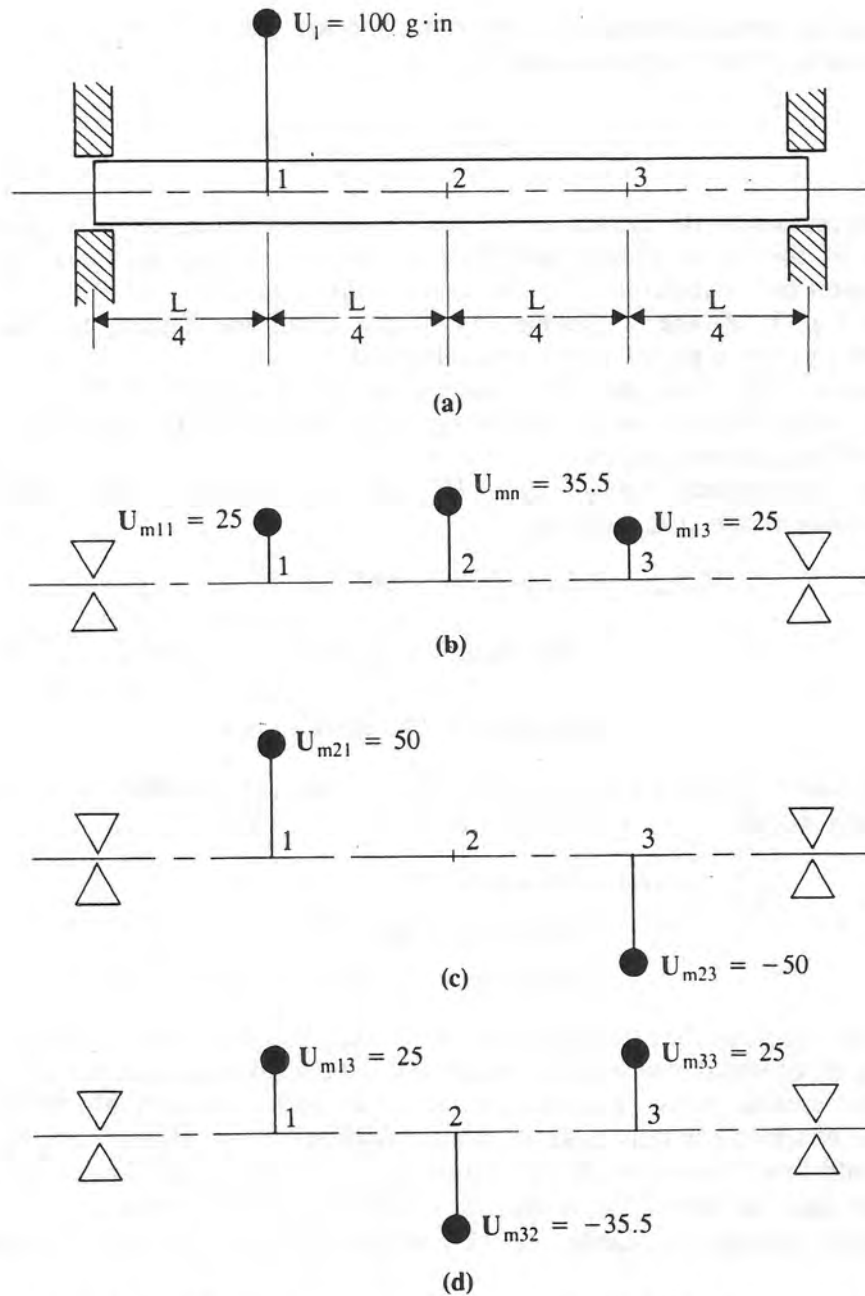
The rotor unbalance distribution $\{U\}$ may be expressed in modal components as

$$\{U\} = U_{m1}\{\phi\}_1 + U_{m2}\{\phi\}_2 + U_{m3}\{\phi\}_3 \tag{3.161}$$

Example 3.15. For the uniform rotor of Example 3.12, determine the modal unbalance components U_{m1} for an unbalance of $100\,\text{g}\cdot\text{in}$ at $L/4$ and $L/2$ along the shaft, as shown in Fig. 3.53.

Case 1:

$$\{U\} = 100\,\text{g}\cdot\text{in} < 0° \qquad \text{at } x = \frac{L}{4}$$

$$\{U\} = \left\{\begin{array}{c} 100 \\ 0 \\ 0 \end{array}\right\} = U_{m1}\left\{\begin{array}{c} 0.707 \\ 1 \\ 0.707 \end{array}\right\} + U_{m2}\left\{\begin{array}{c} -1 \\ 0 \\ 1 \end{array}\right\} + U_{m3}\left\{\begin{array}{c} -0.707 \\ 1 \\ -0.707 \end{array}\right\}$$

FIGURE 3.53 Single-plane unbalance of a flexible shaft represented as modal distributions: (a) uniform rotor with $100\,g \cdot in$ at station $L/4$; (b) equivalent first mode unbalance distribution; (c) equivalent second mode unbalance distribution; (d) equivalent third mode unbalance distribution.

$$\begin{Bmatrix} 100 \\ 0 \\ 0 \end{Bmatrix} = \begin{bmatrix} 0.707 & -1 & -0.707 \\ 1 & 0 & 1 \\ 0.707 & 1 & -0.707 \end{bmatrix} \begin{Bmatrix} \mathbf{U}_{m1} \\ \mathbf{U}_{m2} \\ \mathbf{U}_{m3} \end{Bmatrix}$$

Solving for the components $\mathbf{U}_{mi}$ gives

$$\mathbf{U}_{m1} = 35.5\,g \cdot in \qquad \mathbf{U}_{m2} = -50\,g \cdot in \qquad \mathbf{U}_{m3} = 35.5\,g \cdot in$$

The corresponding modal unbalance eccentricities are given by

$$e_1 = 0.73 \text{ mils} \qquad e_2 = -1.03 \text{ mils} \qquad e_3 = -0.707 \text{ mil}$$

The relationship between the modal unbalance is

$$\mathbf{U}_{mi} = 4\mathbf{e}_i \mathbf{M}_i \qquad (3.162)$$

For the unbalance of $100\,\text{g}\cdot\text{in}$, placed at the quarter span along the shaft, all three critical speeds of the rotor will be excited.

Case 2:

$$\mathbf{U} = 100 \text{ g in} \qquad \text{at } x = \frac{L}{2}$$

$$\mathbf{U} = \left\{ \begin{array}{c} 0 \\ 100 \\ 0 \end{array} \right\} = \mathbf{U}_{m1}\{\phi\}_1 + \mathbf{U}_{m2}\{\phi\}_2 + \mathbf{U}_{m3}\{\phi\}_3$$

Solving for the modal unbalances $\mathbf{U}_{mi}$ gives

$$\mathbf{U}_{m1} = 50 \text{ g} \cdot \text{in} \qquad \mathbf{U}_{m2} = 0 \text{ g} \cdot \text{in} \qquad \mathbf{U}_{m3} = 50 \text{ g} \cdot \text{in} < 0°$$

From case 2 an unbalance located at the shaft center will cause an excitation of both the first and the third modes.

Modal Balancing of the Uniform Rotor

Figure 3.53 represents a uniform shaft with $100\,\text{g}\cdot\text{in}$ of unbalance at $x = L/4$. The single plane of unbalance may be represented as modal distributions located at three planes. Each modal unbalance distribution has the property that it has little or no effect on the excitation of the other modes. For example, with the balance distributions shown in Fig. 3.53a for the first mode, no rotor excitation will be experienced at the second or third modes. If the unbalances are doubled but the ratio of balance values is maintained, then only the response at the first critical speed will be doubled. No influence will be experienced at the higher modes.

To modally balance a flexible rotor such as given in Example 3.13, the balance weights should be selected as a modal distribution. The requirement for balancing a particular mode is that the modal unbalance eccentricity e_i be zero. Thus a rotor may be modally balanced for other modes. Modal balancing usually upsets the rigid rotor balancing.

The condition for modally balancing a rotor at the first mode is given by

$$\{\phi\}_1^T \left[\{\mathbf{U}\} + \sum_{bj}^m \mathbf{U}_{bj}\{\phi\}_j \right] = \mathbf{M}_1 \mathbf{e}_1 = 0 \qquad (3.163)$$

Expanding the above gives

$$\mathbf{U}_{m1}\phi_1^T\phi_1 + \mathbf{U}_{m2}\phi_1^T\phi_2 + \mathbf{U}_{m3}\phi_1^T\phi_3 + \mathbf{U}_{b1}\phi_1^T\phi_1 + \mathbf{U}_{b2}\phi_1^T\phi_2 + \mathbf{U}_{b3}\phi_1^T\phi_3 = 0$$

For the uniform beam, the displacement modes are orthogonal. (For rotors with unsymmetric axial mass distributions, this is not the case.) The first mode balance condition reduces to

$$\phi_1^T\phi_1[\{\mathbf{U}\}_{m1} + \{\mathbf{U}\}_{b1}] + \epsilon = 0$$

or

$$\{U_b\}_1 = U_{b1}\{\phi\}_1 = -U_{m1}\{\phi_1\}_1 \qquad (3.164)$$

Example 3.16. For the flexible rotor of Example 3.13 which was balanced as a rigid rotor, determine the first and third mode balancing components.

The first mode balancing components are given by

$$\phi_1^T[\{U\} + U_{b1}\phi_1] = 0$$

$$[0.707 \ 1 \ 0.707]\left[\left\{\begin{array}{c} 100 \\ -200 \\ 100 \end{array}\right\} + U_{b1}\left\{\begin{array}{c} 0.707 \\ 1.0 \\ 0.707 \end{array}\right\}\right] = 0$$

$$-58.6 + 2U_{b1} = 0 \qquad U_{b1} = 29.3 \text{ g} \cdot \text{in} < 0°$$

The first mode balancing distribution to place on the shaft to balance out the rotor through the first critical speed is

$$\{U_b\}_1 = 29.3\{\phi\}_1 = \{20.7 \ \ 29.3 \ \ 20.7\}^T \qquad \text{g} \cdot \text{in}$$

After first mode balancing, the unbalance distribution is now

$$\{U\}_{\text{current}} = \left\{\begin{array}{c} 100 \\ -200 \\ 100 \end{array}\right\} + \left\{\begin{array}{c} 20.7 \\ 29.3 \\ 20.7 \end{array}\right\} = \left\{\begin{array}{c} 120.9 \\ -170.7 \\ 120.90 \end{array}\right\}$$

The current rotor is no longer balanced as a rigid rotor, but is perfectly balanced to operate through the first two flexible critical speeds. At this point, further rigid-body balancing would destroy the modal balancing of the rotor.

To operate the rotor through the third critical speed, the rotor must be now modally balanced for the third mode. The third mode balancing component U_{b3} is given by

$$\phi_3^T[\{U\} + U_{b3}\phi_3] = 0$$

$$[-0.707 \ 1 \ -0.707]\left[\left\{\begin{array}{c} 120.9 \\ -170.9 \\ 120.90 \end{array}\right\} + U_{b3}\left\{\begin{array}{c} -0.707 \\ 1.00 \\ -0.707 \end{array}\right\}\right] = 0$$

$$-341.90 + 2U_{b3} = 0 \qquad U_{b3} = 170.9 \text{ g} \cdot \text{in} < 0°$$

The third mode balancing component is given by

$$\{U_b\}_3 = 170.9\left\{\begin{array}{c} -0.707 \\ 1.00 \\ -0.707 \end{array}\right\} = \left\{\begin{array}{c} -120.9 \\ 170.9 \\ -120.9 \end{array}\right\}$$

The final balance is now

$$\{U_b\}_{\text{final}} = \left[\{U\} + \left\{\begin{array}{c} -120.9 \\ 170.9 \\ -120.9 \end{array}\right\}\right] = \{0\}$$

Hence after the third mode balancing has been performed, the rotor is perfectly

balanced. For very flexible rotors, the rotor is best balanced by using a modal procedure.

In actual balancing of a flexible rotor using the modal method, one must determine the modal balance components by using a modified form of the influence coefficient method in a procedure similar to that used with the single-mass Jeffcott rotor. Instead of applying only a single trial weight, a modal distribution of weights is applied to the shaft. The modal influence coefficients should be obtained by taking vibration measurements near the critical speed to be balanced. It is not necessary or desirable to take data at higher speeds near another critical speed if one is using a modal distribution of weights.

Figure 3.54 represents the experimental data obtained on a flexible three-mass rotor after modal balancing through two critical speeds. Initially the rotor had a high response while passing through the first critical speed. A set of modal weights was placed in phase at the three rotor stations. These modal weights were treated as if they were a single balance component. The first mode was balanced by using the single-plane influence coefficient method.

3.4.6 Multiplane Balancing by the Influence Coefficient Method

General Influence Coefficient Method of Balancing—Exact-Point Method
The two-plane method of balancing derived from Thearle's earlier work (1934) may be readily expanded to N planes of balancing. This method is referred to as
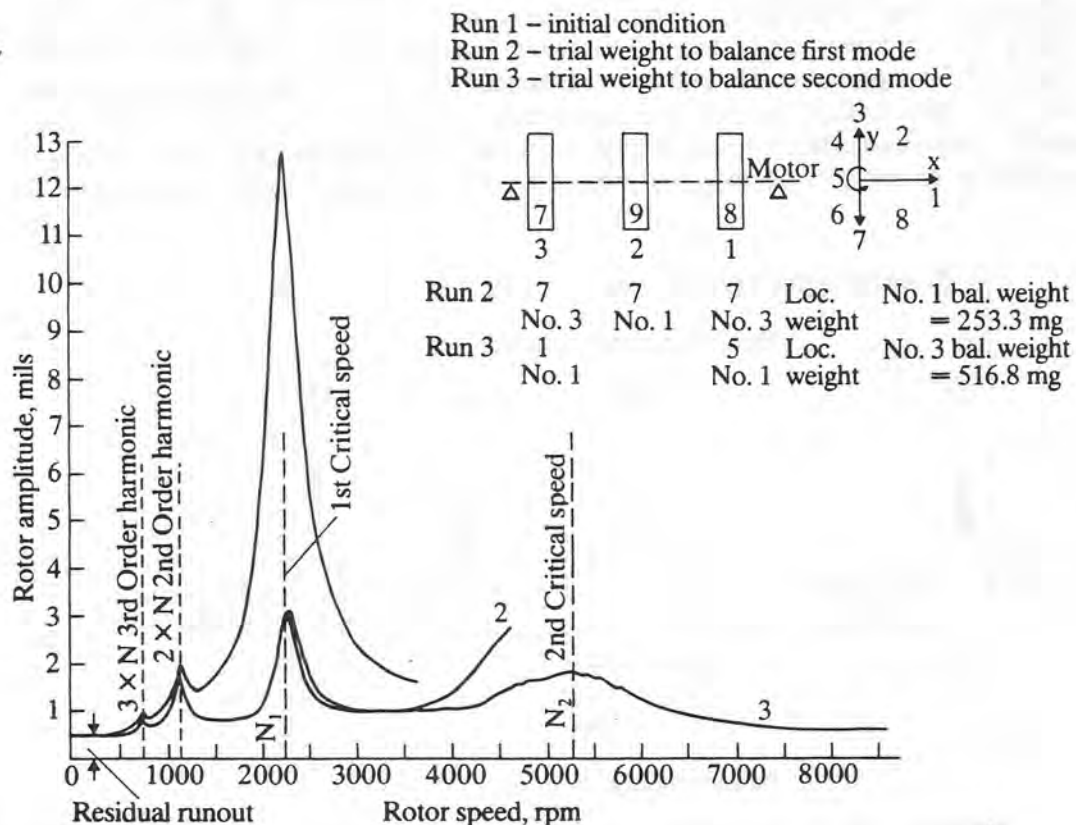

FIGURE 3.54 Modal balancing of a three-mass rotor (Gunter et al., 1976).

the *exact-point speed method* of balancing and was presented in detail by Tessarzik (1970).

In the exact-point speed method, the number of probes corresponds to the number of balance planes. The measurements are made at only one speed.

The vibration is assumed to be of the form

$$Z_1 = a_{11}U_1 + a_{12}U_2 + a_{13}U_3$$

$$Z_2 = a_{21}U_1 + a_{22}U_2 + a_{23}U_3 \qquad (3.165)$$

$$Z_3 = a_{31}U_1 + a_{32}U_2 + a_{33}U_3$$

In general matrix form, the equations of vibration are

$$\{Z\}_n = [a]_{n \times n}\{U\}_n \qquad (3.166)$$

where $[a]$ is a square $n \times n$ matrix of influence coefficients. Since $[a]$ is a square complex matrix, its complex inverse may be computed. The balance solution is given by

$$\{U\}_b = -\{U\}_n = -[a]_{n \times n}^{-1}\{Z\}_n \qquad (3.167)$$

A total of n^2 influence coefficients must be determined to use this procedure.

The influence coefficients a_{ij} must be determined for a particular speed by placing a trial balance weight at the ith balance plane and recording the resulting amplitudes at the jth probe. For N planes of balancing, a total of $N + 1$ runs must be made to establish the coefficients for a given speed.

The exact-point and the least-squared-error procedures for flexible rotor balancing were investigated experimentally by Tessarzik and Badgley (1973). Figure 3.55 represents the test rig showing balance planes and probe locations. (Figure 3.56 represents the rotor mode shapes for the first three critical speeds. The first two critical speeds are essentially rigid-body cylindrical and conical modes. The third critical speed is equivalent to a free-free flexible mode with zero amplitude of motion at the bearings. The first two rigid-body modes may be
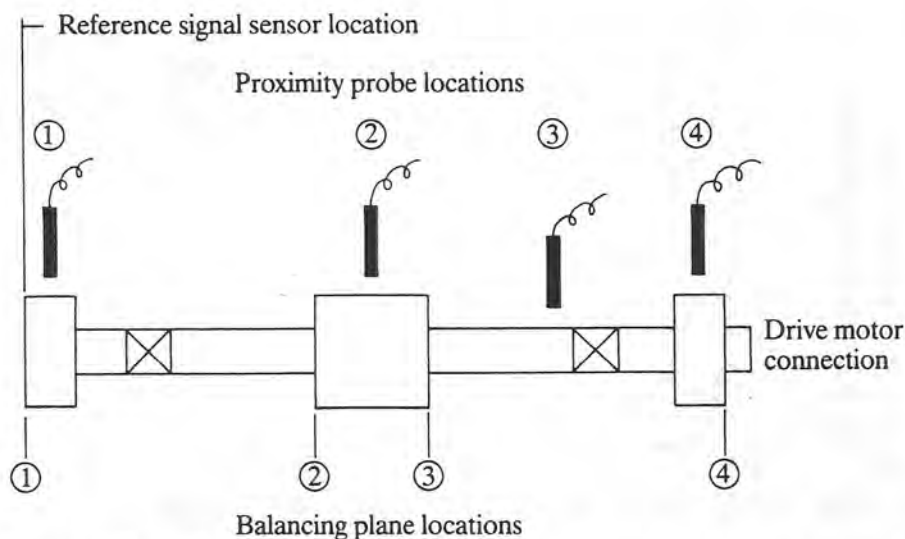

FIGURE 3.55 Tessarzik–Badgley (1973) test rig showing balance planes and probe locations.
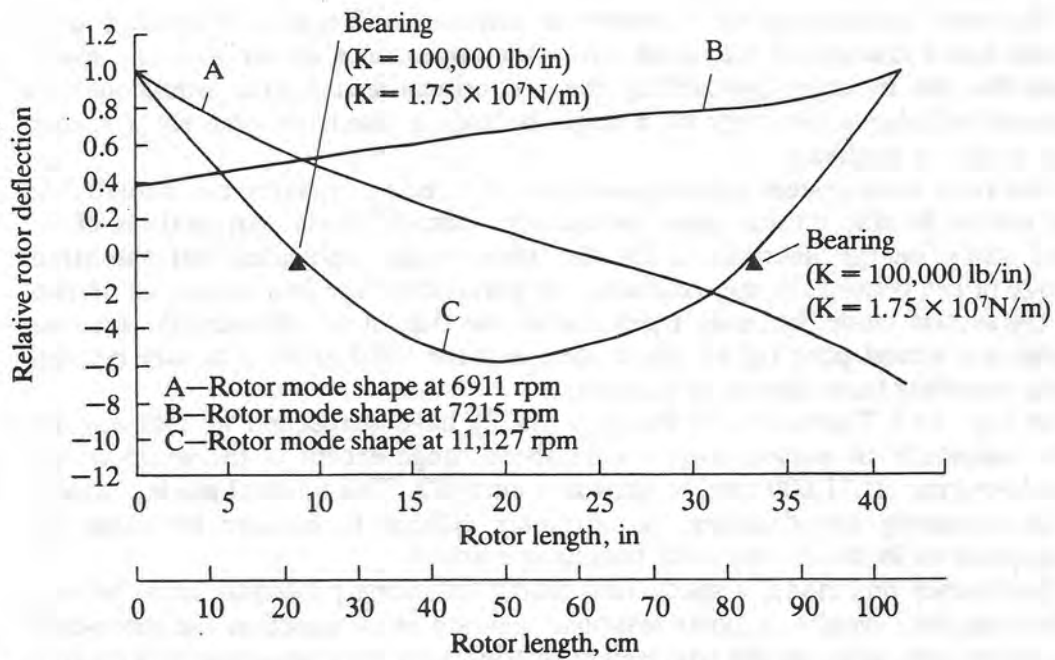
FIGURE 3.56 Critical-speed mode shapes for Tessarzik–Badgley (1973) test rig.

readily balanced, but the third free-free critical speed is extremely difficult to balance because of the high rotor sensitivity for this mode.

Figure 3.57 represents the rotor response of the Tessarzik and Badgley (1973) test rotor before and after three consecutive balancing runs by the exact-point speed influence coefficient method. Curve A represents the initial response of the rotor with a spiral or corkscrew unbalance distribution. The rotor rigid-body critical speeds at 6911 and 7215 rpm in the initial run A are not apparent due to the unbalance distribution used and the bearing damping.
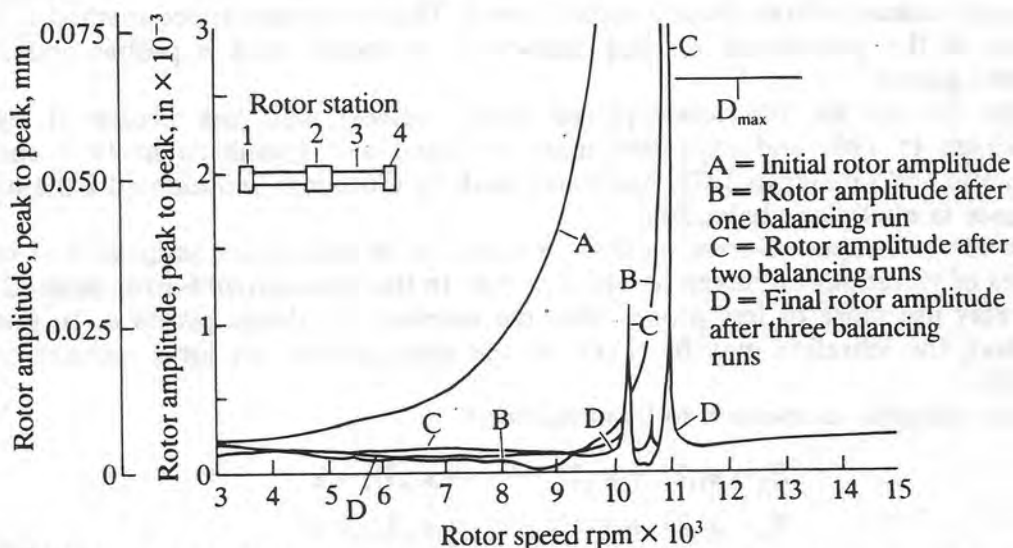
FIGURE 3.57 Vertical amplitudes at station 2 before and after three consecutive balancing runs by the exact-point speed influence coefficient method; rotor with corkscrew unbalance (Tessarzik and Badgley, 1973).

The rotor initial amplitude appears to increase with speed. Without a prior critical speed analysis of this rotor, from the appearance of curve A one would think that the rotor is approaching the first critical speed. One would then be tempted to balance the rotor by a single balancing plane near the rotor center. This would be incorrect.

The rotor third system critical speed encountered at 11,000 rpm is actually the first system flexible critical speed or free-free flexible mode. An analysis of the rotor strain energy distribution for the three modes indicates that the strain energy in the bearings is approximately 90 percent for the first mode, 96 percent for the second mode, but only 1 percent for the third mode. Hence, the first two modes are almost pure rigid-body modes, and the third mode is a pure bending mode requiring three planes of balance.

In Fig. 3.57 Tessarzik and Badgley (1973) have succeeded in reducing the rotor amplitude of motion over a wide speed range except at the sharp critical speed response at 11,000 rpm, as shown in curve D. This unusual mode, because of its extremely low damping, is extremely difficult to balance by either the exact-point or least-squared error balancing method.

To balance this mode, a specialized modal balancing procedure must be used employing the Nyquist or polar response diagram in conjunction the three-trial-weight method, using modal trial weight distributions with measurements taken at the critical speed.

Least-Squared-Error Multiplane Balancing Procedure

In the exact-point method of balancing using influence coefficients, one is limited to the computation of n planes of balance corresponding to one speed only. In a very flexible rotor, the rotor response is dictated by the modal distribution of the unbalances. If one measures the vibrations at speeds far removed from the critical speed, then an accurate estimation of the modal unbalance component cannot be predicted.

By taking measurements at a number of speeds, a best fit of the balance weights may be computed. The use of least-squared-error method with the data taken at multiple speeds will ensure that you do not overbalance at one speed, causing excessive vibrations at a second speed. The exact-point speed method is a subset of the generalized least-squared-error procedure with n probes and n balance planes.

The theory for the least-squared error method was first presented by Goodman in 1964 and expanded upon by Lund and Jonnessen in 1972 and Palazzolo and Gunter in 1977. The early work by Goodman represented a major advance in multiplane balancing.

In the least-squared-error method, n planes of balancing are assumed and m values of vibrations are taken in which $m > n$. In the least-squared-error method, one may use more or less probes than the number of balance planes n. In this method, the vibration may be taken on the same probes but for a number of speeds.

The vibration is assumed to be of the form

$$
\begin{aligned}
\mathbf{Z}_1 &= \mathbf{a}_{11}\mathbf{U}_1 + \mathbf{a}_{12}\mathbf{U}_2 + \cdots + \mathbf{a}_{1n}\mathbf{U}_n + \epsilon_1 \\
\mathbf{Z}_2 &= \mathbf{a}_{21}\mathbf{U}_1 + \mathbf{a}_{22}\mathbf{U}_2 + \cdots + \mathbf{a}_{2n}\mathbf{U}_n + \epsilon_2 \\
&\ \vdots \\
\mathbf{Z}_m &= \mathbf{a}_{n1}\mathbf{U}_1 + \mathbf{a}_{m2}\mathbf{U}_2 + \cdots + \mathbf{a}_{mn}\mathbf{U}_n + \epsilon_m
\end{aligned}
\tag{3.168}
$$

The measurements $\mathbf{Z}_1 - \mathbf{Z}_m$ may be a combination of only several probes but measured over a number of speeds. If measurements are not taken near a particular critical speed, then calculations of that particular nodal distribution may not necessarily be accurately performed.

The vibration in matrix form is given by

$$\{\mathbf{Z}\}_m = [a]_{m \times n}\{\mathbf{U}\}_n + \{\epsilon\}_m \tag{3.169}$$

where $m \geq n$ ($m = n$ is exact-point method).

The problem of least-squared-error analysis is identical to the problem of computing a pseudoinverse of unknowns with m equations. The procedure here is somewhat different since we are dealing with complex vectors and matrices.

The influence coefficient matrix must first be generated by the application of trial weights on the rotor. The resulting rotor responses due to the application of the trial weights must be computed at the same speeds as the initial readings. Also the slow-roll vector $\{\mathbf{Z}\}_0$ should be recorded before and after application of all weights to ensure that the shaft runout or bow is not substantially changing.

The transpose of the complex conjugate of the set of influence coefficients is computed next:

$$[\mathbf{T}]_{n \times m} = [\mathbf{a}]^{*t}_{m \times n}$$

Multiplying Eq. 3.168, we obtain

$$[\mathbf{T}]_{n \times m}\{\mathbf{Z}\}_m = [\mathbf{T}]_{n \times m}[\mathbf{a}]_{m \times n}\{\mathbf{U}\}_n + [\mathbf{T}]_{n \times m}\{\epsilon\}_m$$

The product of $[\mathbf{T}]_{n \times m} \times [\mathbf{a}_1]_{m \times n}$ is a square matrix of order n which may be inverted. Let

$$[\mathbf{D}]^{-1}_{n \times n} = [[\mathbf{T}]_{n \times m} \times [\mathbf{a}]_{m \times n}]^{-1}$$

The least-squared-error balancing matrix is given by

$$\{\mathbf{U}_b\}_n = [\mathbf{B}]_{n \times m}\{\mathbf{Z}\}_m \tag{3.170}$$

where

$$[\mathbf{B}]_{n \times m} = -[\mathbf{D}]^{-1}_{n \times n} \cdot [\mathbf{T}]_{n \times m}$$

For balancing by using runout compensation, the least-squared-error equation is given by

$$\{\mathbf{U}_b\}_n = [\mathbf{B}]_{n \times m}[\{\mathbf{Z}\}_m - \{\mathbf{Z}_0\}_m] \tag{3.171}$$

The procedure as outlined above may also be modified to include a weighting function to emphasize certain vibrations. The least-squared-error method is preferred to the exact-point method. Previously, this procedure required a mainframe computer to perform the complex calculations and matrix inversion. However, with current handheld calculators and portable computers, this procedure may be quickly accomplished in the field.

The application of the least-squared-error method for multiplane balancing of a bowed flexible rotor was extensively investigated by Palazzolo and Gunter in 1977. The synchronous amplitudes of motion for three stations along the rotor are shown in Fig. 3.58. The rotor has an initial shaft bow of 4 mils near the rotor center. With the original rotor unbalance distribution, the rotor amplitude at the first mode was almost 20 mils, and the rotor could not operate through the second critical speed because of excessive vibrations.
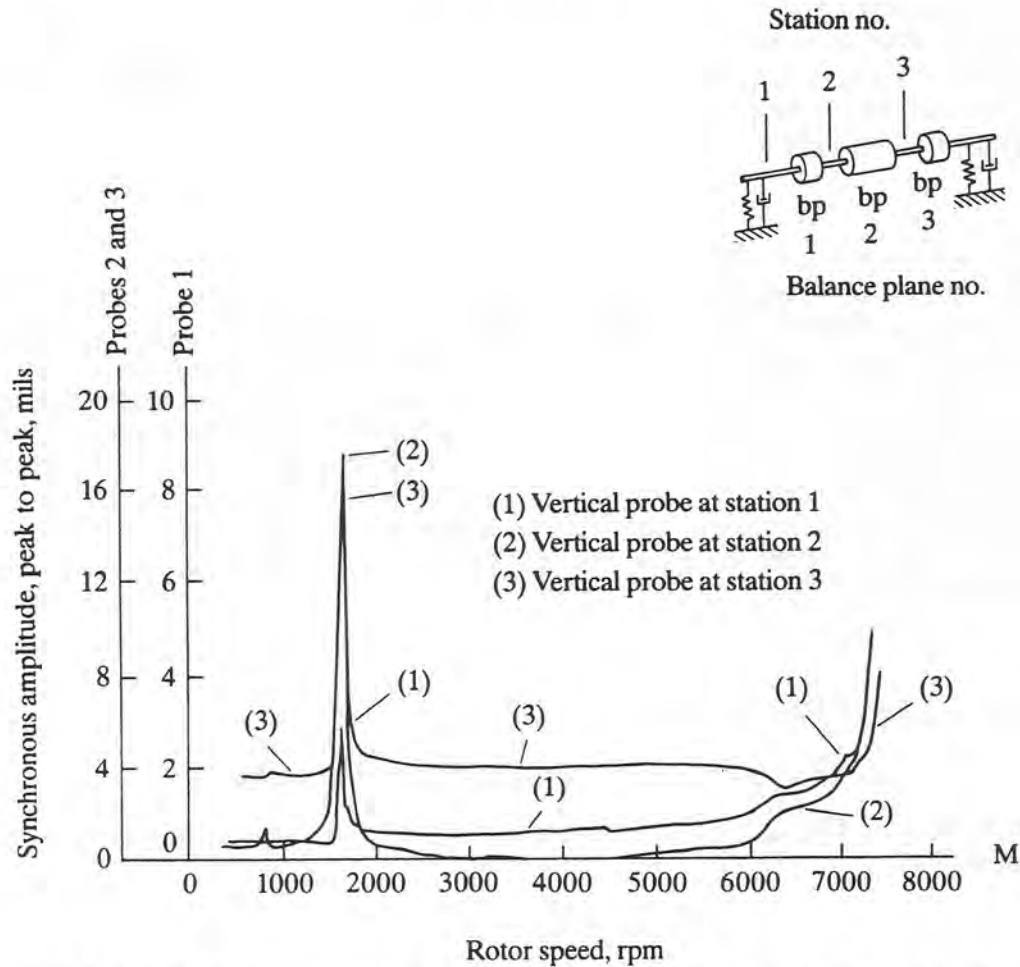
FIGURE 3.58 Synchronous unbalance response of a Bently three-mass rotor before least-squared-error balancing (Palazzolo and Gunter, 1977).

The least-squared-error method was used to compute the balance distribution in the rotor. Table 3.9 represents the calculated rotor three-plane balance values by the least-squared-error method for various combinations of speed data. Case 1, e.g., represents the balance distribution at 1200 rpm. This distribution of balance correction weights would give excellent balance at 1200 rpm, but the rotor would still be badly out of balance at the first critical speed and would not be able to traverse the second critical-speed region.

Case 5 represents the rotor balance computed in with five speed cases from 1200 to 1900 rpm. This represents speed cases taken below and above the first critical speed. This distribution represents an excellent balance for the first mode. If one were to apply this balance distribution to the rotor for first mode balancing, then the second mode could be balanced by the influence coefficient method using second-mode distributions of trial weights. This would represent a combined modal–influence coefficient method. Case 8 represents the best compromise balance set determined with eight speed cases from 200 to 7500 rpm. Figure 3.58 represents the motion of a three-mass rotor with shaft bow. The rotor has critical speeds at 1700 and 7500 rpm. It is impossible to operate the rotor above 7200 rpm because of the unbalance level.

TABLE 3.9 Calculated Rotor Three Plane Balance Values by the Least Squares Method for Various Combinations of Speed Data

| Case	Speeds (rpm) N	BP1 g·in,	BP1 deg	BP2 g·in,	BP2 deg	BP3 g·in,	BP3 deg
		Correction unbalances					
1	1200	0.683	207.045	0.110	121.33	0.811	60.75
2	1200, 1400	0.673	224.5	0.094	128.32	0.925	70.78
3	1200, 1400, 1500	0.855	185.9	0.161	119.9	0.705	35.73
4	1200, 1400, 1500, 1800	0.56	134.7	0.193	96.46	0.113	63.80
5	1200, 1400, 1500, 1800, 1900	0.513	117.45	0.172	91.15	0.134	94.27
6	1200, 1400, 1500, 1800, 1900, 6500	0.263	79.52	0.114	84.72	0.393	116.86
7	1200, 1400, 1500, 1800, 1900, 6500, 7000	0.178	87.73	0.106	97.7	0.419	106.6
8	1200, 1400, 1500, 1800, 1900, 6500, 7000, 7500	0.092	122.57	0.112	106.4	0.374	100.38
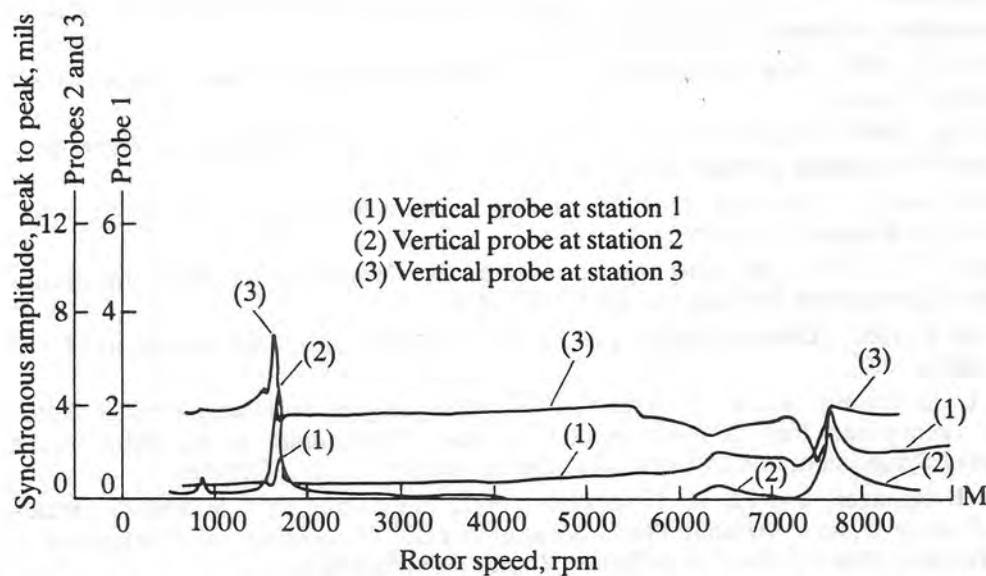
FIGURE 3.59 Synchronous unbalance response of a Bently three-mass rotor after least-squared-error balancing (Palazzolo and Gunter, 1977).

Figure 3.59 represents the motion of the bowed rotor after balancing with the weight distribution given in case 8 using eight speed cases. The rotor second mode has been completely balanced with some residual vibration remaining at the first mode. Note that Table 3.9 shows that the use of additional vibration data will, in general, constrain the values of the balance weights computed.

Thus, one will normally be on the conservative side with the use of the least-squared-error balancing procedure. The exact-point method should not be used to calculate balancing for flexible rotors operating through several critical speeds. The use of the exact-point method will lead to the calculation of excessive balance weights. The least-squared-error balancing method has been demonstrated by Gunter and Humphris (1986) to be highly effective for field balancing of gas turbine-generator systems with load-dependent thermal bows.

3.5 REFERENCES

Badgley, R. H., 1974, "Recent Developments in MultiPlane-Multispeed Balancing of Flexible Rotors in the United States," International Union of Theoretical and Applied Mechanics, Lyngby, Denmark.

Benson, R. C., 1974, "Dynamic Response of an Overhung, Unbalanced Skewed Rotor in Fluid Film Bearings," M.S. thesis, University of Virginia, Charlottesville.

Bently, D. E. 1982, *Polar Plotting Applications for Rotating Machinery*, Vibrations Institute, Clarendon Hills, Ill.

Bently-Nevada Co., 1984a, *ADRE Multi-Plane Balance Package*, Minden, Nev.

——, 1984b, *Automated Diagnostics for Rotating Machinery—ADRE Operators' Guide*, Minden, Nev.

Bishop, R. E. D., and A. G. Parkinson, 1963, "On the Isolation of Modes in the Balancing of Flexible Shafts," *Proceedings of the Institute of Mechanical Engineers*, 177: 407–423.

—— and ——, 1966, "Second-Order Vibration of Flexible Shafts," *Proceedings Royal Society of London*, 259: 1–31.

—— and ——, 1972, "On the Use of Balancing Machines for Flexible Rotors," *Journal of Engineering for Industry*, 94(2): 561–576.

Blake, M. P., 1967, "Use Phase Measuring to Balance Rotors in Place," *Hydrocarbon Processing*, August.

Darlow, M., 1989, "Flexible Rotor Balancing by the Unified Balancing Approach," Rensselaer Polytechnic Institute, Troy, N.Y.

Foiles, W., and E. J. Gunter, 1982, "Balancing a Three Mass Rotor with Shaft Bow," University of Virginia, Charlottesville.

Goodman, T. P., 1964, "A Least-Squares Method for Computing Balance Corrections," *Journal of Engineering for Industry*, 86(3): 273–279.

Gunter, E. J., 1966, "Dynamic Stability of Rotor-Bearing Systems," NASA Report SP-113, Washington, D.C.

——, L. E. Barrett, and P. E. Allaire, 1976, "Balancing of Multimass Flexible Rotors Part I Theory and Part II Experimental Results," Proceedings of the Fifth Turbomachinery Symposium, A & M University, College Station, Texas, October.

——, H. Springer, and H. H. Humphries, 1982, "Balancing of a Multimass Flexible Rotor-Bearing System Without Phase Measurements," Proceedings of Conference on Rotordynamics Problems in Power Plants, Rome, Italy, September.

—— and R. Humphris, 1986, "Field Balancing of 70 MW Gas Turbine Generators," Proceedings International Conference on Rotordynamics, JSME, (Tokyo), pp. 135–143.

International Standards Organization, 1973, *Balance Quality of Rotating Rigid Bodies,* ISO Document 1940, Geneva, Switzerland.

Jackson, C., 1971, "Using the Orbit to Balance," *Mechanical Engineering,* pp. 28–32, February.

———, 1979, *Practical Vibration Primer,* Guef Publishing Co., Houston.

Jeffcott, H. H., 1919, "The Lateral Vibration of Loaded Shafts in the Neighborhood of a Whirling Speed—The Effect of Want of Balance," *Phil. Mag.,* 37: 304.

Kellenberger, W., 1972, "Should a Flexible Rotor Be Balanced in N or $(N+2)$ Planes?" *Journal of Engineering for Industry,* 94: 548–560.

Kirk, R. G., and E. J. Gunter, 1973, "Nonlinear Transient Analysis of Multimass Flexible Rotors—Theory and Applications," NASA CR-2300, Washington, D.C.

Little, R. M., 1971, "Current State of the Art of Flexible Rotor Balancing Technology," Ph.D. thesis, University of Virginia, Charlottesville.

Lund, J. W., and J. Tonnesen, 1972, "Analysis and Experiments on Multi-Plane Balancing of Flexible Rotors," *Journal of Engineering for Industry,* 94(1): 233.

Mechanalysis Inc., "Vector Calculations for Two Plane Balancing," Applications Report 327, IRD, Columbus, Ohio.

Nicholas, J. C., E. J. Gunter, and P. E. Allaire, 1976, "Effect of Residual Shaft Bow on Unbalance Response and Balancing of a Single Mass Flexible Rotor: Part I—Unbalance Response; Part II—Balancing," *Journal of Engineering for Power,* 98(2): 171–189.

Palazzolo, A. B., and E. J. Gunter, 1977, "Multimass Flexible Rotor Balancing by the Least Squares Error Method," Vibration Institute, Clarendon Hills, Ill.

———, 1982, "Modal Balancing of a Multimass Flexible Rotor Without Trial Weights," *A.S.M.E.,* Gas Turbine Paper 82-GT-267.

Rieger, N., 1986, *Balancing of Rigid and Flexible Rotors,* SVN 12, The Shock and Vibration Center.

Salamone, D. J., and E. J. Gunter, 1978, "Effect of Shaft Warp and Disc Skew on Synchronous Unbalance Response of a Multi-Mass Rotor in Fluid Film Bearings," *Topics in Fluid Film Bearings and Rotor Bearing Systems Design and Optimization,* ASME, New York, pp. 79–107.

Schenek Trebel Corp., 1980, "Fundamentals of Balancing," Deer Park, Long Island, New York.

Tessarzik, J. M., 1970, "Flexible Rotor Balancing by the Exact Point-Speed Influence Coefficient Method," NASA, Cleveland, Ohio, CR-72774, October.

——— and R. H. Badgley, 1973, "Experimental Evaluation of the Exact Point-Speed and Least Squares Procedures for Flexible Rotor Balancing by the Influence Coefficient Method," ASME 73-DET-115, New York.

Thearle, E. L., 1934, "Dynamic Balancing of Rotating Machinery in the Field," *Transactions of ASME,* 56: 745-753.

Thomson, W. T., 1965, *Vibration Theory and Applications,* Prentice-Hall, Englewood Cliffs, N.J.

Winkler. A. F., 1983, "High Speed Rotating Unbalance, Coupling or Rotor," *Proceedings Vibration Institute,* Nassau Bay Conference, Vibration Institute, Clarendon Hills, Ill.

CHAPTER 3 ROTOR BALANCING
Nomenclature

A	Amplification factor , *Dim*
A_c	Amplification factor at critical speed
a	Influence coefficient
a	Acceleration vector , *in/sec²* , *(M/sec²)*
a_t	Tangential acceleration , *in/sec²* , *(M/sec²)*
a_n	Normal acceleration , *in/sec²* , *(M/sec²)*
C_c	Critical damping , *Lb-sec/in* , *(N - sec/M²)*
D	Shaft diameter , *in* , *(M)*
e_u	Unbalance eccentricity vector , *in* , *(M)*
e_r	Unit vector in radial direction - rotating with angular velocity ω
e_t	Unit vector in tangential direction - rotating with angular ω
F_b	Bearing reaction , *Lb* , *(N)*
F_u	Rotating unbalance force , *Lb* , *(N)*
f	Frequency ratio , *Dim*
g	Gravity , *in/sec²*
I	Shaft second moment of area , *in⁴*
I_{ij}	Moment of inertia matrix
I_p	Polar moment of inertia , *Lb-in* , *sec²* , *(Kg - M²)*
I_t	Transverse moment of inertia , *Lb-in* , *sec²* , *(Kg - M²)*
[I]	Moment of inertia matrix
K	Bearing or shaft spring rate , *Lb/in* , *(N/M²)*
L	Length , *in* , *(M)*
L_b	Bearing span , *in* , *(M)*
M	Rotor mass , *Lb-sec²/in* , *(Kg)*

m_b	Small rotor balancing mass , *Lb-sec²/in* , *(Kg)*
m_i	Unbalance masses , *Lb-sec²/in* , *(Kg)*
m_u	Effective unbalance mass , *Lb-sec²/in* , *(Kg)*
M_u	Unbalance moment , *Lb-in* , *(N - M)*
n	Number of unbalance weights
N	Rotor speed , *RPM*
N	Number of balance planes
P	Position vector
R	Shaft radius or radius of motion
t	Disk thickness , *in* , *(M)*
U	Unbalance vector , *gram-in, oz-in, Lb-sec²* , *(Kg - M)*, *(gram-mm)*
U_b	Rotor radial balance correction , *gram-in.* , *oz-in.* , *Lb-sec²* , *(Kg - m)* , *(gram - mm)*
V	Velocity Vector , *in/sec, m/sec*
V	Velocity of motion , *in/sec, m/sec*
W	Total rotor weight , *Lb, (Kg)*
W_u	Unbalance weight , *Lb, (Kg)*
X , Y	Absolute Cartesian coordinates of rotor motion
X_i , Y_i	Relative Cartesian locations of unbalance weight W_i
x , y , z	Cartesian coordinate system fixed in shaft with z along spin axis Z
X´,Y´,Z´	Principal coordinates fixed in disc or cylinder
Z	Rotor spin axis or axial distance , *in*
Z	Complex displacement

α	Angular acceleration ,	rad/sec^2
α_{ij}	Influence coefficient matrix	
β	Relative mass-displacement phase angle ,	deg
δ	Shaft deflection ,	in , (M)
ϕ	Phase angle ,	deg
ρ	Material density ,	Lb - sec^2/in^4 , (Kg/M)
θ	Cylindrical coordinate ,	deg
τ	Disk skew ,	deg or rad
ω	Angular velocity ,	rad/sec
ω_{cr}	Rotor critical speed on rigid supports ,	rad/sec